EURASIAN PHYSICAL TECHNICAL JOURNAL

p - ISSN 1811-1165
e - ISSN 2413-2179

Volume 13, No. 2(26), 2016

Quarterly Journal of the International Higher Education Academy of Sciences

1st issue – March, 2004

Journal Founders:

THE INTERNATIONAL HIGHER EDUCATION ACADEMY OF SCIENCES

ХАЛЫҚАРАЛЫҚ ЖОҒАРҒЫ БІЛІМ АКАДЕМИЯСЫ

KARAGANDA STATE UNIVERSITY NAMED AFTER E.A.BUKETOV

Е.А.БӨКЕТОВ АТЫНДАҒЫ ҚАРАҒАНДЫ МЕМЛЕКЕТТІК УНИВЕРСИТЕТІ

INSTITUTE OF TECHNICAL PHYSICS AND PROBLEMS OF ECOLOGY

ТЕХНИКАЛЫҚ ФИЗИКА ЖӘНЕ ЭКОЛОГИЯ МӘСЕЛЕЛЕРІ ИНСТИТУТЫ

Contact information:

Editorial board of EPhTJ (Build. 2, room 221)
Karaganda State University named after E.A.Buketov
Universitetskaya Str.28, Karaganda, Kazakhstan, 100028
Subscription index: 75240
Tel: +7(7212)77-04-03
Fax: +7(7212)77-03-84
e-mail: ephtj@mail.ru

Signed to print on 08**.12.2016**.
Format 60x84 1/8. Offset paper.
Volume 16,25 p.sh. Circulation 300 copies.
Agreed price. Order No. 474.

Басуға **08.12.2016** ж. қол қойылды.
Пішімі 60×84 1/8. Офсеттік қағазы.
Көлемі 16,25 ес. -б.т. Таралымы 300 дана.
Бағасы келісім бойынша. Тапсырыс № 474.

Printed in the Publishing House
of the KarSU named after E.A.Buketov

Е.А. Бөкетов атындағы ҚарМУ баспасының
баспаханасында басылып шықты

Registered by the Ministry of Culture, Information and Public Adjustment of the Republic of Kazakhstan.
Қазақстан Республикасы мәдениет, ақпарат және қоғамдық келісім министрлігімен тіркелді
Registration Certificate No. 4382-Zh from November, 7, 2003.

Eurasian Physical Technical Journal

Vol. 13, No. 2(26) **2016**

CONTENTS

THERMOPHYSICS. HYDRODYNAMICS. ENERGETICS.

Dear Authors and Readers! Honourable colleagues!

The editorial board of «Eurasian Physical Technical Journal» wishes you a Happy New 2017 Year!

As a rule, at the close of a calendar year, results of the past year are reviewed and plans for the future are set out. As we have earlier reported, according to the results of the international examination of «Eurasian Physical Technical Journal» in 2015, its ISSN 1811-1165 for printed version was confirmed and ISSN 2413-2179 of on line version of the journal was assigned. Currently, the work on updating the website of the journal is going on.

Taking into account the recommendations of experts and professionals, in order to promote scientific publications and to involve a wide academic audience, along with scientific articles we are going to publish review articles, as well as to introduce autobiographical information and scientific achievements of leading scientists, the members of the editorial board and others to the authors and readers. At present, the editorial board and the expert group of Eurasian Physical Technical Journal has been changed.

In this issue, the research objects of the authors' articles are physical and technical processes and phenomena in a very wide range of micro and nano size to mega cosmic distances. The research at the nanoscale is presented in the article of Belarusian scientists, which analyzes "the processes of formation of nanodiamonds ...". New findings of investigation of nanostructured films and nanoparticles obtained using the equipment of the Institute of Molecular Nanophotonics, led by Professor Ibraev N.H., are of great interest. The article by Almaty scientists presents the data on the studied spectra of "photoluminescence of carbon-nano-structured objects." In the works of Uzbek scientists on the basis of the simulation "the condition of the Faraday effect intensification in multilayer nano-structures" is found.

In practice, problems of maintenance of technical equipment reliable operation, as well as others, do not depend on geography and state. In the paper of Kemerovo scientists, an «analysis of roof fall risk assessment method in underground workings» is made. The article of Zaporozhye researchers presents a methodology for the study of the regularities of the system of coupled vibrations of component parts of an aircraft engine turbine for the examination of rotor blades wear-out.

The articles about solving various heat and mass transfer problems, and in particular, the use of renewable energy sources, are supposed to be of interest. Review articles on «Theory of corrosion and thermal destruction of metals materials» and «Analysis of developing wind power apparatus in Kazakhstan» are useful to young researchers.

We hope that in this issue both scientific and review articles addressing the most urgent problems of modern physics and engineering, will be interesting and useful to readers. But special attention should be paid to the paper of the academician A.A. Potapov, concerned with the development and the description "of fractal dimensions of lightning discharges in the ionosphere," and "... the analysis and synthesis of … complex tasks of radio engineering and radiolocation."

We are pleased to introduce this author, Doctor of physical and mathematical sciences, Professor of V.A. Kotelnikov Institute of Radio Engineering and Electronics of the Russian Academy of Sciences, the academician of A.M. Prokhorov Academy of Engineering Sciences and the academician of Academy of Natural Sciences, A.A. Potapov as a new member of the editorial board of EAPhTJ.

Alexander Alekseevich is a prominent scientist in the field of radio physics and radiolocation, detecting and processing of images and signals, fractal analysis, fractional operators and deterministic chaos. Since 1981, the main research area of A.A. Potapov has been the application of the theory of fractals, fractional operators, scaling and deterministic chaos in radio physics, radiolocation, radio electronics, antenna theory, electrodynamics, the theory of management for the creation and development of breakthrough information technologies. A.A. Potapov was the initiator and organizer of the earliest research and development work on radiophysical application of the fractal theory, scaling effects and fractional operators in radio systems in Russia.

The results of the scientific activity of A.A. Potapov. on fractal processing of information in the high-intensity noise and on fractal radio systems and fractal radio elements were published in more than 800 scientific papers, 23 monographs and 6 textbooks published in Russia and abroad.

The outstanding scientific knowledge, hard work, integrity, commitment, and a great sense of responsibility for the dealt-with matter won him well-deserved prestige and international fame. Professor A.A. Potapov was awarded many state medals and honorary signs of Russia for his outstanding achievements in the development of radio electronics and communication.

In March 2011, A.A. Potapov was awarded the title of Honorary Professor of the University of Dzhinan (Honorary Professor of Jinan University, Guangzhou city, China). He is the President of the joint Chinese-Russian laboratory of information technologies and fractal processing of signals (2011). In April 2015, at the international scientific competition in Beijing, A.A. Potapov won the Government grant of China "Leading Talents" for fractal methods of signals and images processing.

A.A. Potapov is the editor in chief of the journal "Nonlinear World" (2003), a member of the editorial boards of international journals "Electromagnetic Phenomena" (2005) and "Materials Sciences and Applications" (USA, New York, 2009), a member of the editorial boards of "Achievements of modern radioelectronics" (2009) "Nano-technologies: development, application - XXI century" (2009), "Radioelectronics. Nanosystems. Information technology " (RANS, 2009),"Complex Systems "(Moscow State University, 2011)," "The Sky" (Azerbaijan, Baku, 2012),"Bulletin of Kharkiv National University. Radio Physics and Electronics" (Kharkiv, KhNU, 2012) and "Proceedings of Russian higher educational institutions. Radioelectronics "(SPbETU "LETI", 2015).

On May 4, 2016 Alexander Alekseevich Potapov was 65 years of age!

On behalf of the editorial board of the «Eurasian Physical Technical Journal» and on behalf of all our readers our congratulations on the anniversary! We wish you health, prosperity and success in scientific work!

We hope that the international prestige of Professor A.A. Potapov, as a scientist and a high-class professional, will make for establishing closer international scientific contacts, which beneficially will affect not only the quality of our journal, but it will contribute to the development of physical and engineering science as a whole!

We wish all our authors and readers good health, success and good luck in the research work!

We will be very glad to see you among authors in future issues, and gladly publish and present the results of your research to the international scientific community.

Respectfully, Chief Editor Saule Sakipova

Karaganda, December, 2016

UDC 550.388.2

ON FRACTAL DIMENSION SPECTRUM OF NEW LIGHTNING DISCHARGE TYPES IN IONOSPHERE: ELVES, JETS AND SPRITES

Potapov A.A.

V.A. Kotelnikov Intstitute of Radio Engineering and Electronics of RAS, Moscow, Russia,
Chinese-Russian laboratory of informational technologies and signals fractal processing
of JNU-IREE RAS, JiNan University (JNU), Guangzhou, China, potapov@cplire.ru

Starting from the middle of nineties of XX a new phenomenon became the focus of physicists' interest – lightning electric discharge in the middle atmosphere at attitudes from 20 to 100 kilometers which are above the absolute majority of clouds. It results in rise of absolutely new classes of discharge phenomena. Physical properties of elves, jets and sprites which are the most interesting types of the high-attitude discharges in the atmosphere are considered in the work. The results of researches of its fractal characteristics are presented. The obtained results give grounds for a deeper insight of development, relaxation of such atmosphere processes and taking into account of action of such kind of strays on functioning of radio systems.

Keywords: fractal dimension, lightning discharge, ionosphere, noise

Introduction

Since the mid 90-ies of XX century a new phenomenon has become the focus of physicists' interest. It is a lightning electrical discharge in the middle atmosphere at altitudes from 20 to 100 km, lying above the absolute majority of the clouds. This leads to a few completely new classes of discharge phenomena called elves, jets and sprites.

Physical models of sprites, elves and jets are still a subject of intense debate [1, 2]. Although the data accumulation phase, characterizing the morphology of these phenomena is not completed, it is already possible go to the study of finer features of the structure and dynamics of high-altitude discharges and their role in the global electric circuit and the balance of minor components of the atmosphere. Methods of study of nonlinear dynamics of high-altitude lightning discharge rely mainly on classical statistical processing of the obtained data. However, the rapid development of fractal scaling methods of signal and image processing makes it possible to expand and refine the obtained data. In particular, the fractal processing provides an opportunity to study topology of the discharges in space and time.

The paper presents the results of experimental studies of fractal characteristics of the new types of atmospheric disturbances such as high-altitude lightning discharges. The concept of a global atmospheric electrical circuit is defined. The obtained data may be of interest when considering the problems of immunity space radiocommunication and radiolocation to interferences, as well as in the evaluation of potential threats to the existing spacecraft and probes.

1. A global atmospheric electric circuit

A global electric circuit or GEC (Fig. 1) is a current distribution loop, which is "closed" by electrically conductive atmosphere [1, 2]. GEC consists of a combination of solid and plasma gas shells united by the continuity of the electric current density, with lightning generators as the main sources of electromotive forces and undisturbed regions of the free atmosphere as return current areas. The physical reason for the formation of GEC in the atmosphere is a sharp increase in the conductivity of the air with increasing altitude.

Near the Earth's surface the conductivity of the air is very low and amounts to $(2\div3)\times10^{-14}$ cm/m, which corresponds to the concentration of light ions of about 10^3 cm^{-3}. With increasing altitude, due to rise in ionization level, which up to 40 km altitude results from galactic cosmic rays, and above – from ultraviolet and X-ray radiation of the Sun, the conductivity increases almost exponentially with a characteristic scale of 6 km. As high as at the altitude H of the ionosphere layer (about 80 km), it increases by more than 10 orders of magnitude compared to the troposphere. The conductivity of the earth in the surface layer (and particularly that of ocean water) is also higher than the conductivity of the atmospheric boundary layer by 10 ... 12 orders.

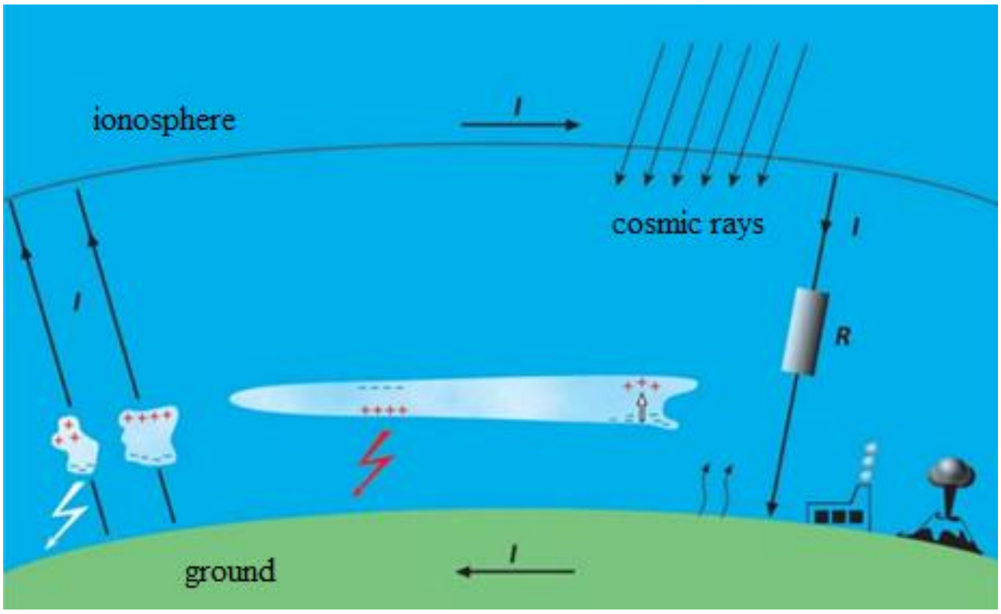

Fig.1. Diagram of the global atmospheric electrical circuit.

To simplify the GEC description, the earth surface and the lower boundary of the ionosphere (about 60-70 km) are often considered as coatings of a giant spherical capacitor, which discharges in areas of fair weather and charges in areas of thunderstorm activity. In these conditions, quasi-stationary charging currents are not completely closed to the ground near thunderclouds, but partly "dragged" into the overlying area of high conductivity and spread over the ionosphere. It is believed that primarily quasi-stationary currents, "bear responsibility" for the maintenance of the potential difference ≈350 kV between the ionosphere and the ground. Since the upper part of most thunderstorm clouds has a positive charge, the potential of the ionosphere is also positive, and in the areas of fair weather the electric field is directed downward, in that way causing conduction currents, closing GEC. If the action of the generators stopped, the potential difference between the Earth surface and the ionosphere would disappear in about 8 minutes.

According to the hypothesis of Wilson, tropospheric lightning generators provide charging the spherical Earth-ionosphere capacitor and determine the quasi-stationary electric state of the undisturbed atmospheric regions [3]. The potential difference between the huge plates of the spherical capacitor is 300...400 kV. Under this voltage, electric current of about 1,000 amperes passes through the air to the ground. This figure may seem huge, but the current is distributed over the entire surface of the planet, so that only a couple of microamps is accounted for by every square kilometer of water or land, and the entire power of the atmospheric circuit is comparable to a turbine of a large hydroelectric power plant. That's why the idea (which goes back to Nikola Tesla) to use atmospheric potential differences to produce energy is untenable.

2. A brief history of the discovery of new dynamic natural structures in the ionosphere and a their brief characteristics

Every twenty-four hours the sky is traced by 4 million lightnings, about 50 ones per every second. And over the gunmetal grey thunderstorm fronts, in the upper layers of the atmosphere a light show of "spectral lightnings" is set: blue jets, red-purple sprites, red rings of elves soaring in the sky. Those are very high energy discharges, which are not directed to the ground but to the ionosphere. Thus, high-altitude electrical discharges (20...100 km) are divided into several basic types: elves, jets, sprites, halos, etc. – Fig. 2.

The story of their discovery was as follows. On the night of 5 July 1989, an important event happened in the history of the study of the Earth. John Randolph Winkler, a retired professor, 73-year-old NASA veteran focused a high-sensitivity camera on thunderstorm clouds. Then, thoroughly looking through the record, he found two bright flashes, which, unlike the lightning did not go down to the ground but went up, to the ionosphere. In that way *sprites*, the largest of high-altitude discharges in the Earth's atmosphere, were discovered. They clearly confirmed the existence of GEC on the planet and gave new opportunities for its research. His articles literally caused a shock among experts on astronomy, atmospheric electricity, radio physics, atmospheric acoustics, gas discharge physics and aerospace safety.

The shortest-lived high-altitude discharges, *elves* occur in the lower ionosphere at heights of 80...100 km. Having originated in the center, the glow expands to 300...400 km in less than a millisecond, and then quenches. Elves emerge in 300 microseconds after a strong lightning having stricken the ground from a thunderstorm cloud. The channel of the lightning becomes a "transmitting antenna", from which a powerful spherical electromagnetic wave of very low frequency rate "starts" at light speed. In 300 microseconds it reaches a height of 100 km, where it "sets in" a red glow of nitrogen molecules.

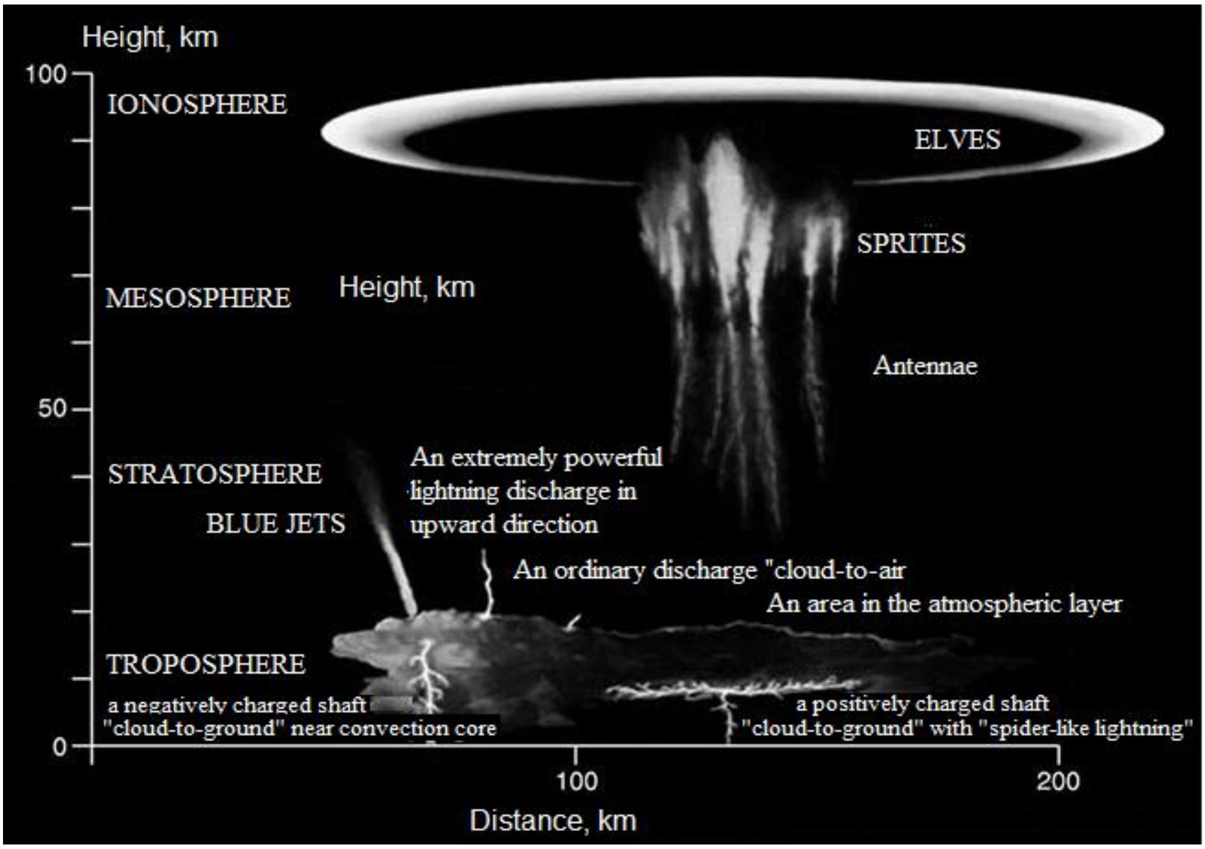

Fig.2. Dynamic fractal structures in the atmosphere.

The most mysterious high-altitude discharges are blue jets; they are also a glow of nitrogen molecules in the ultraviolet-blue spectrum. They look like a narrow blue inverted cone, "starting" from the upper boundary of a thundercloud. Sometimes jets reach a height of 40 km, their extension rate is 10 to 100 km/s. Their emergency is not always caused by lightning discharges. Besides blue jets, "blue starters" (they extend to a height of ≤ 25 km) and the "gigantic jets" (extending to the lower ionosphere heights of about 70 km) are differed.

Sprites are very bright three-dimensional flashes with duration on the order of milliseconds, occurring at an altitude of 70-90 km and descend down to 30-40 km. Their top width reaches tens of kilometers. Sprites flare up in the mesosphere in about a hundredth of a second after the discharge of powerful lightning "cloud-to-ground", sometimes at a distance of several tens of kilometers horizontally from the lightning channel.

The red-purple color of sprites, as well as that of elves, is attributed to atmospheric nitrogen. The frequency of sprites occurrence is on the order of several thousands of events per day around the globe. The fine structure of the bottom of sprites is characterized by a plurality of luminous channels with transverse dimensions ranging from tens to hundreds of meters – Fig.1. The emergence of sprites is associated with the formation of a high dipole moment of the uncompensated charge, after particularly powerful lightning discharges cloud-to-ground, usually of positive polarity.

Halo is a uniform reddish-purple glow at an altitude of about 80 kilometers. Halo is a luminous disc in the mesosphere just above the area of tropospheric discharge. The reason for the discharge is probably the same as that of the top of sprites, but unlike them, halo always originates just above the "cloud-to-ground" flash of lightning.

It is a mystery for scientists that discharges in the ionosphere are fairly numerous; they appear not only where there are thunderstorm clouds occur, and not over the entire surface of the Earth. They are not visible above Siberia, oceans and deserts. But a large number of them are recorded over Australia, Africa and Latin America. It is difficult to register high-altitude discharges and diagnose their characteristics due to their short lifetime.

3. Some approaches to the modeling of ionospheric structures

Development of physical and mathematical models of sprites, elves and jets is an urgent task of researchers. Dynamic spatiotemporal characteristics and morphology of sprites may be explained, in particular, by fractal geometry of discharges and percolation. [1, 2, 4 – 14].We have here another example of self-organized criticality when the dynamics of the system (in this case, of a high-altitude discharge) results from reaching the threshold of the so-called directed percolation, which features the formation of branched (fractal) conducting channels that cover the entire length of the sprite.

4. The results of fractal processing of a sprite and a jet in the ionosphere

The situation is quite different with the matters of statistical data processing. In this case, classical methods are traditionally used. They *do not make it possible* to obtain all the information about these new atmospheric structures. In other words, in [6-16] the author shows that the use of the mathematical theory of fractional measure and fractals opens up a whole range of new methodological principles for physicists and experimenters – for examples, see Fig. 3 and Fig. 4. There are clearly visible numerous branches and channels in the structures of sprites and jets.

Apropos, these are *the first in the world* results of fractal processing of such structures (the initial processing was carried out at the beginning of 2013, the final processing – in 2014). In such cases it is possible to apply simulation based on fractal mazes, which reflect the physics and morphology of those ionospheric structures quite well [14, 15].

a) b)

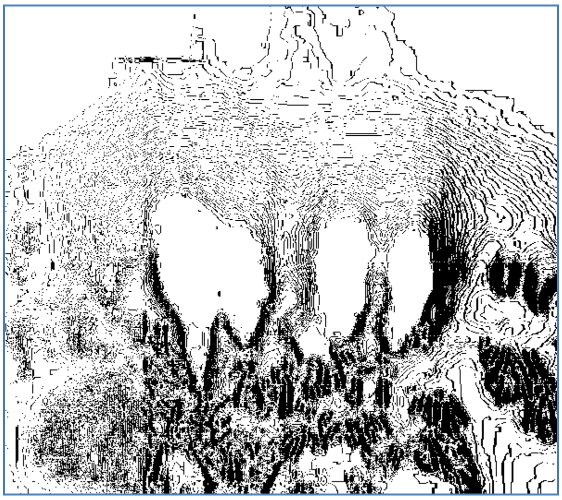

c)

Fig. 3. The results of fractal filtering of a sprite image:
(*a*) – an initial sprite image (US, NASA [17]),
(*b*) – a fractal dimension estimate chart with the average value of the fractal dimension $D = 2.43$,
(*c*) – the section of the chart on the value of $D = D - 0.05$.
(External, basic and hyperfine sprite structures clearly differ).

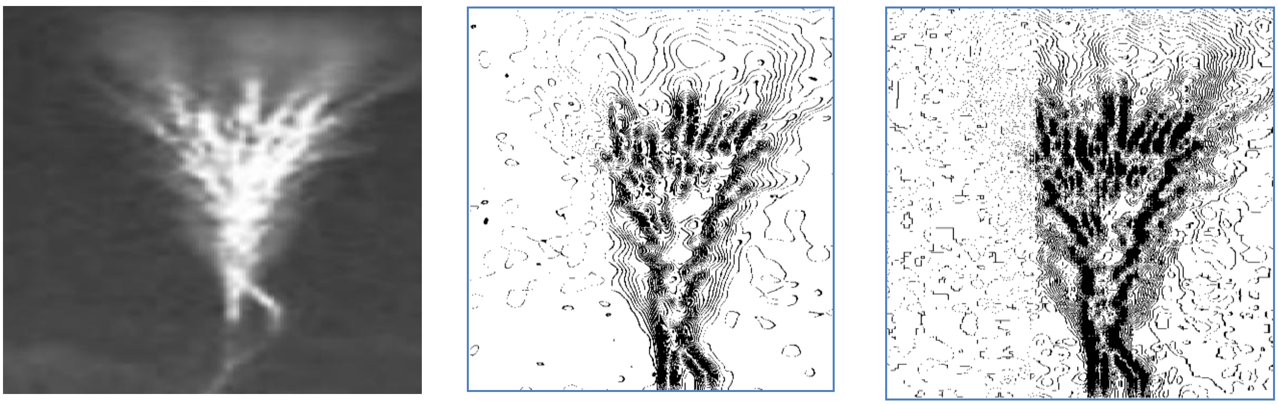

a) b) c)

Fig. 4. The results of the fractal filtering of a gigantic jet image (photographed in China, 12 August 2010): (a) –the jet image [18], (b) and (c) – the sections of D fractal dimension

A complete series of fractal filtering results of an instant frame sprite image based on initial data from [17] is shown in Fig. 5.

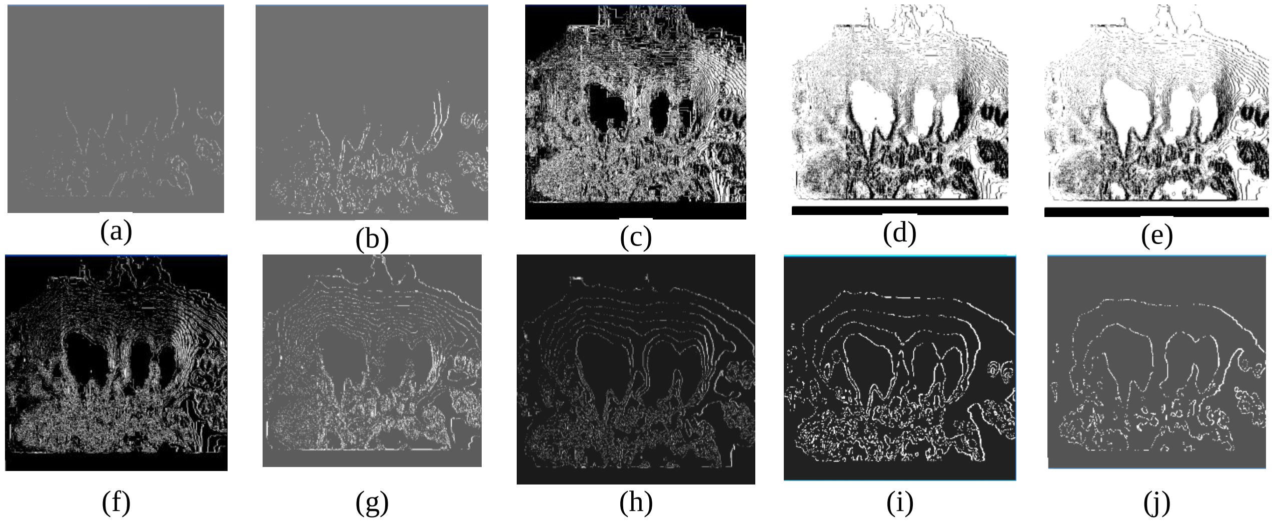

Fig. 5. A complete series of the results of the sprite image fractal filtering:
(a) – a chart of the fractal dimension with the mean value of D = 2.1; (b) – 2.2;
(c) – 2.3; (d) – 2.4; e) – 2.5; (f) – 2.6; (g) – 2.7; (h) – 2.8; (i) – 2.9; (j) – 3.0.

Conclusion

One of new types of high-power pulse interferences are recently discovered specific discharges of atmospheric electricity. Fractal scaling methodology applied to describe the morphology of jets, sprites and elves can be successfully used to evaluate their performance and development dynamics. This evaluation will be overall and objective as it is based on quantitative estimates of *D* fractal dimensions at contouring of related structures; and it is operational since the data processing is easily performed by computers. Then problems of mathematical physics are solved.

The results obtained in this work provide a basis for more profound effect of interferences of this kind on the functioning of modern ground and space radio systems. Here are some characteristics of sprites [4, 5]: typical space $30\times30\times30$ km; the spatial extent of irregularities – the external structure on the order of 10 km, the basic structures on the order of 1 km, the hyperfine structure less than 100 m; the electron density N_e~10^4 cm^{-3}, the flash duration τ_s ~10 ms; relaxation time of the electron density τ_r ~1...10s; the electron temperature T_e~2 eV at the flash and T_e~0.02eV during the relaxation period; total current momentum in the discharge p_s~100 $kA\times km$.

The obtained results in this paper confirm that the common point of nonlinear electrodynamics of GEC and the developed global fractal-scaling method has been found [6-16, 19].

Acknowledgment

Supported by the leading talents of Guangdong province Program (No. 00201502);
JNU-IREE RAS, JiNan University (JNU), Guangzhou, China

REFERENCES

1 Mareyev E.A., Trahtengerts V. Mysteries of atmospheric electricity. *Nature*, 2007, No. 3, pp. 24 – 33.

2 Anisimov S.V. The global electric circuit of geospher shells. *Proceedings of the All-Russian Conf. "The global electric circuit".* Yaroslavl: SO "Borok" IPE RAS, 2013, pp. 6 – 7.

3 Wilson C.T.R. Investigations on lightning discharges and on the electric field of thunderstorms. *Phil. Trans. Roy. Soc. A*, 1920, Vol. 221, pp. 73 – 115.

4 Mareyev, E.A., Klimenko V.V. Nonlinear dynamics of high-altitude lightning discharge. *Proceedings "Nonlinear Waves-2006"*. Nizhny Novgorod, IAP RAS, 2007, pp. 337 – 359.

5 Fullekrug M., Mareev E., Rycroft M. *Sprites, Elves and Intense Lightning Discharges*. NATO Science Series. Springer, Dordrecht, 2006, Vol. 225, pp. 211 – 235.

6 Potapov A.A. Fractal-scaling method of processing of data on the global electric circuit: elves, jets, sprites. *Proceedings of the All-Russian Conf. "The global electric circuit"*. Yaroslavl, SO "Borok" IPE RAS, 2013, p. 70.

7 Potapov A.A. On fractal scaling characteristics of the troposphere and ionosphere. // *Proceedings of the Int. Conf. "Aerosol and Atmospheric Optics"*. Moscow, IAP RAS, 2014. Available: http://ifaran.ru/science/conferences/Rozenberg2014.html.

8 Potapov A.A. Research of the fractal and scaling properties of tropospheric and ionospheric turbulence with artificial perturbations. *Proceedings of the Int. Conf. "Transformation of waves, coherent structures and turbulence: MSS-14"*. Moscow, 2014, pp. 334 – 339.

9 Potapov A.A. Features of multifractal structure of high-altitude lightning discharges in the ionosphere: elves, jets, sprites. *Proceedings of the 8th All-Russian Scientific and Technical Conf. "Radiolocation and radiocommunication"*. Moscow, V.A. Kotelnikov IRE RAS, 2014, pp. 316 – 320.

10 Potapov A.A. *Fractal Radar: Towards 1980 – 2015. Proceedings of the Int. Conf.* “CHAOS 2015”. - Paris: Henri Poincaré Institute, 2015, pp. 559 – 573.

11 Herman V.A., Potapov A.A. On measuring fractal characteristics and structures of atmospheric elves, jets and sprites. *Proceedings of the 8th All-Russian Conf. "Irreversible processes in nature and technology"*. Part I. Moscow, N.E. Bauman MSTU, 2015, pp. 112 – 115.

12 Potapov A.A. Elements of the global atmospheric electric circuit (elves, jets, sprites) as fractals. *Proceedings of the 8th All-Russian Conf. "Irreversible processes in nature and technology"*. Part I. Moscow, N.E. Bauman MSTU, 2015, pp. 116 -121.

13 Potapov A.A. *Chaos Theory, Fractals and Scaling in the Radar: A Look from 2015.* Edit. Ch. Skiadas., *C.* - Switzerland, Basel, Springer Int. Publ., 2016, pp. 195 – 218.

14 Potapov A.A. Oscillations, waves, structures and systems illustrated by examples of the global fractal-scaling method (measure zero sets, singularity, scaling, sample topology, sprites, jets, elves, memristors, oscillators, fractal mazes, robust antenna arrays and fractal detectors). *The non-linear world*, 2014, Vol. 12, No. 4, pp. 3 – 38.

15 Potapov A.A. *Fractal method and fractal paradigm in the modern natural science*. Voronezh, 2012, 108 p.

16 Potapov A.A. *Chaos Theory, Fractals and Scaling in the Radar: A Look from 2015*. Chapter 12 in book: *The Foundations of Chaos Revisited: From Poincaré to Recent Advancements*. Ed. Skiadas, C.- Switzerland, Basel: Springer Int. Publ., 2016, pp. 195 – 218.

17 *The Foundations of Chaos Revisited: From Poincaré to Recent Advancements*. Edit. Ch. Skiadas (el. book). Available: http://science.compulenta.ru/701264/

18 Yang Jing, Feng Gui Li. A gigantic jet event observed over a thunderstorm in mainland China. *Chinese Science Bulletin*, 2012, Vol. 57, No. 36, pp. 4791 – 4800.

19 Potapov A.A. *Fractals in radiophysics and radiolocation: Sample topology*. Moscow, 2005, 848 p.

Article accepted for publication 11.11. 2016

UDC 550.388.2

ANALYSIS AND SYNTHESIS OF TOPOLOGICAL RADAR DETECTORS OF LOW-CONTRAST TARGETS AGAINST THE BACKGROUND OF HIGH INTENSITY NOISE AS A NEW BRANCH OF RADIOLOCATION AND THE THEORY OF STATISTICAL SOLUTIONS

Potapov A.A.

V.A. Kotelnikov Institute of Radio Engineering and Electronics of RAS, Moscow, Russia, potapov@cplire.ru

The new kind and approach of up-to-date radiolocation: fractal-scaling or scale-invariant radiolocation has been proposed. The main ideas and strategic directions in synthesis of fundamentally new topological radar detectors of low-contrast objects have been considered. The objects detection is conducted against the background of reflections from the ground, sea and precipitations. The new topologic signs and methods of detection of low-contrast objects against the background of high-intensity noise are presented. The methods are based on the textural and fractal analysis and also on the theory of deterministic chaos. The main purpose of the work is to interpret the main directions of radio physics, radio engineering and radio location in "fractal" language that makes new ways and generalizations promising radio systems in future.

Keywords: texture, fractal, lacunarity, Hurst exponent, signals detector, low-contrast target, radar, fractal - frequency MIMO – Systems.

Introduction

Radar detection of low observable and small objects near the surface of the earth and the sea, as well as at meteorological precipitation is an extremely difficult problem [1, 2]. In addition, sea and vegetation clutters are of non-stationary and multiscale character, especially at ϑ shallow angles. A variety of underlying coverings, radar observation conditions and following the above mentioned objects very often lead to the fact that the signal to noise ratio q_0^2 for such problems almost always fills the area of negative values(in decibels), i.e., q_0^2<1 dB [1,2]. This makes classical radar detection methods and detection algorithms inapplicable in most cases, that is, use of energy detectors (when the likelihood ratio is determined solely and only by the received signal energy) becomes essentially impossible.

What is to be done? There is a way! Detection of low-contrast targets against the background of mentioned above high-intense natural noise inevitably requires to offer, and then calculate some fundamentally new characteristic that is different from the functional related to noise and signal energy, and is determined by the topology and the dimension of the received signal.

Introduction of the concepts "texture", "deterministic or dynamic chaos", "fractal" and "fractal dimension" to the scientific use in radio physics and radiolocation, enabled the author to be the first to offer and then apply new dimension and topological (not energy!) characteristics (invariants), which the author combined under the general concept "sampling topology" [1-12].

The work objective is to give a brief analytical review of the development and improvement of the author's methods and algorithms for new topological, including fractal textural detectors of low-contrast radar targets against the background of high-intense ground and sea clutters, as well as meteorological precipitation ones.

1. Fractal-scaling or scale-invariant radiolocation and fractal MIMO-radars as a new kind of radiosystem

For further instantiation of the problems of detection of weak radar signals, we believe initial information to come from a variety of radio systems in the form of a one-dimensional signal and / or a radar image (RI) - Fig. 1. The simplified scheme of primary radiosystems and investigation of radar image and one-dimensional signal in millimeter wave band (MWB) were represented by the author much earlier. Currently, fractal radar, a MIMO-radar and a fractal MIMO radar as well as unmanned aerial vehicles (UAVs) are added to the scheme in Fig. 1. The concept of fractal radar is presented in [1-5, 8, 11, 12], the concept of fractal MIMO-radar is considered in [1-3, 5, 11, 12].

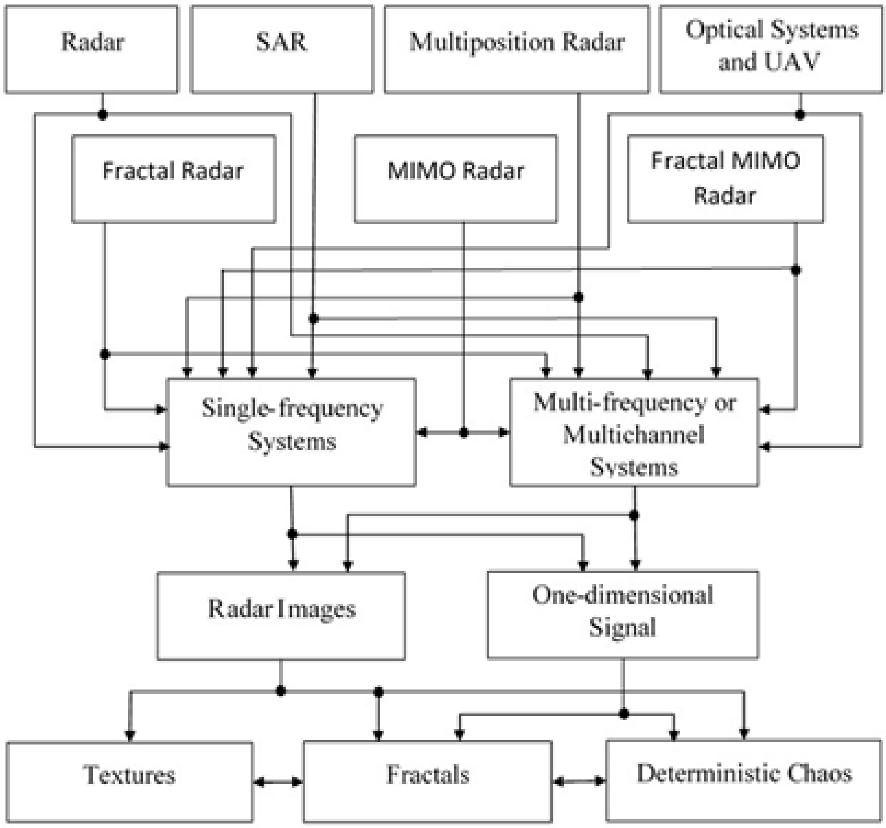

Fig.1. Radio systems of initial information

In general, the technology of MIMO systems implies that each wireless device involved in data exchange, has several spatially distributed receiving and transmitting antennas. The basic idea of fractal MIMO-radars is using fractal antennas and fractal detectors [1-12]. The capability of fractal antennas to work on several frequencies simultaneously or to radiate broadband sounding signal provides a sharp increase in the number of degrees of freedom that defines many of the important advantages of this type of radiolocation and significantly expands adaptation possibilities.

To represent these specifics, in [1-3, 5, 11, 12] a new term «fractal-frequency MIMO systems (FF MIMO)» was introduced, which reflects their physical properties much better. MIMO technologies related to the spatial multi-channel systems provide great opportunities for the application of the author’s global fractal-scaling method for signal processing, various algorithms and technologies of fractal detectors [1-12] at all stages of the synthesis of information MIMO systems. The idea of a fractal radar station (Fig. 1 and 2) is based on the concept of fractal radio systems developed by the author - Fig. 3 [4, 8, 9].

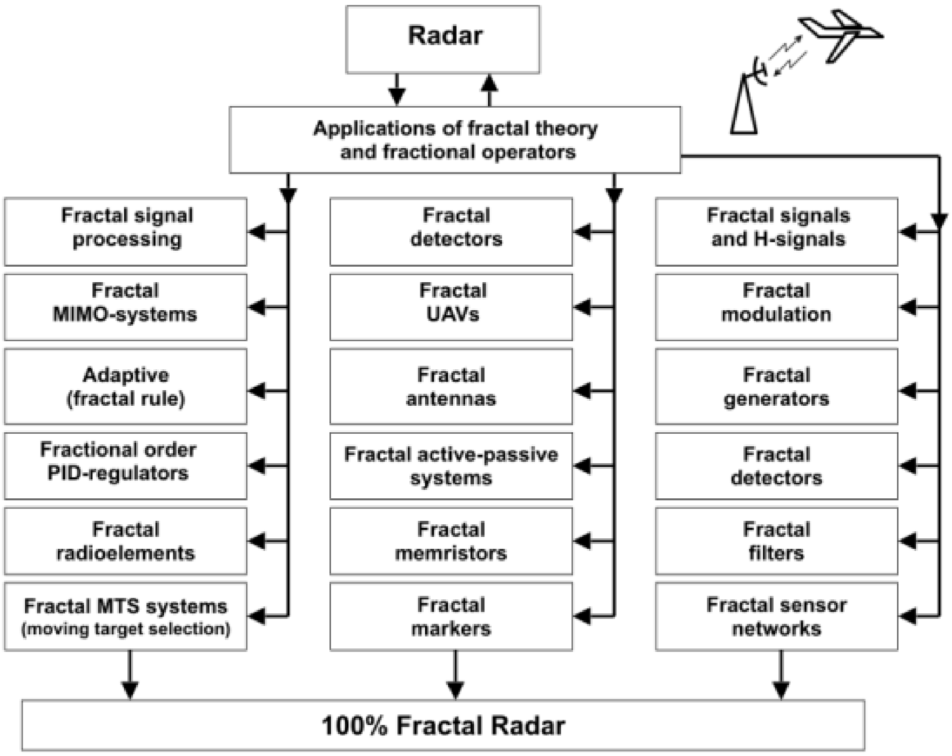

Fig.2. A fractal radar

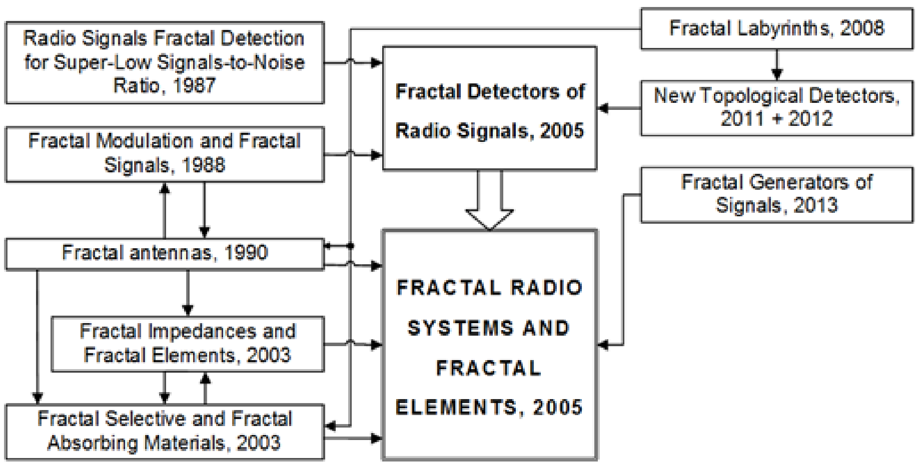

Fig.3. Fractal radio systems

2. New features and topological methods for the detection of low-contrast targets against the background of high-intensity noise

All currently existing and used by the author methods and topological features of low observable objects detection against the background of the high-intensity sea, ground and meteorological phenomena clutters are compactly represented in Fig. 4. The relationship between a variety of features and methods are also marked there. The work on the classification of such methods, algorithms and features started in May 2015 in China during the defense of the project «Leading Talents of Guangdong Province» and finished at the beginning of 2016 in China. That was also when the author essentially completed the work on the book [2], where some of presented here results were introduced for the first time ever.

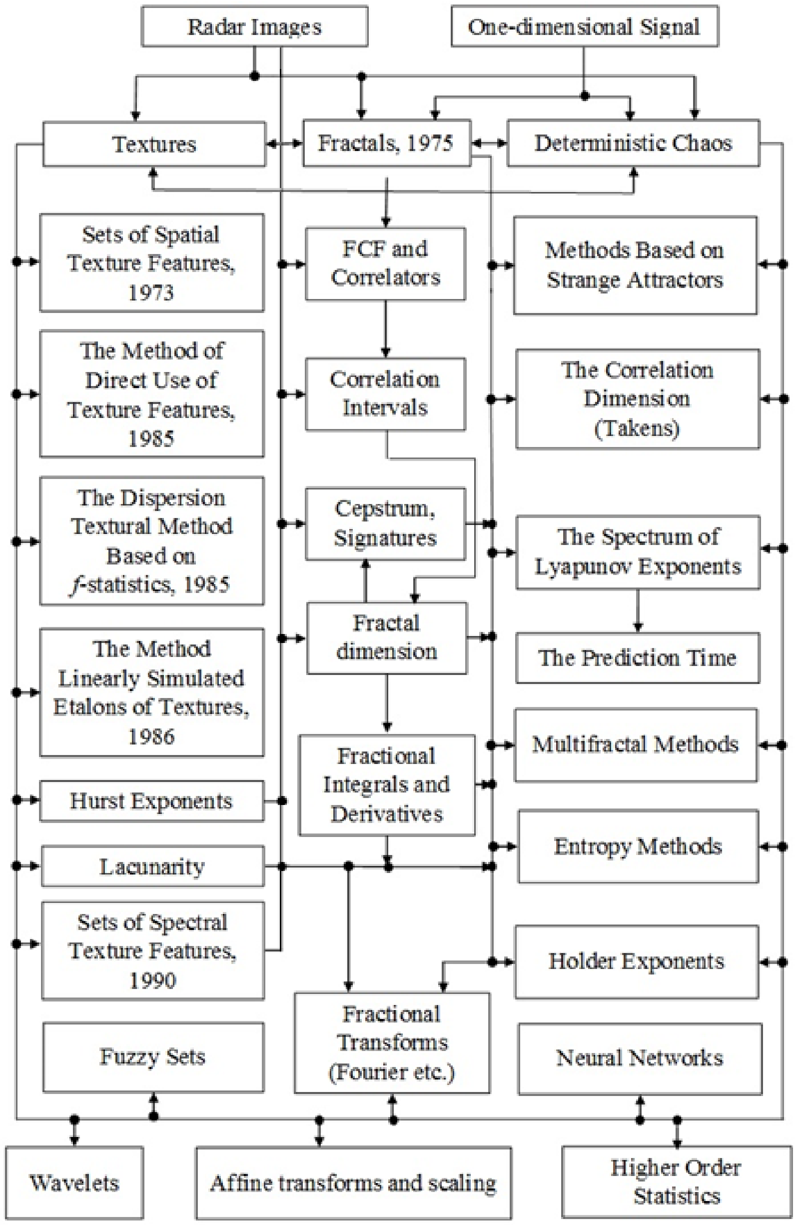

Fig. 4. Topological features and methods for detection of low-contrast targets against the background of high-intense noise.

Introduction of the concept of textural features ensemble to the US in 1973, [13], in the 1980-ies made it possible for the author to be the first to calculate complete ensembles of 28 textural features and to conduct their detailed synchronic analysis for real (optical aerial photography (OAP) and radar images within MMW range at a wavelength of 8.6 mm), as well as for synthesized textures based on autoregressive models, depending on the season [1, 2] 4].

Long-term field experiments were carried out by the author in cooperation with "Almaz" CCB and other leading industrial organizations of the USSR. All investigations were performed at wavelengths λ=2.2 and 8.6 mm (active radiation) and λ=3.5 mm (passive radiation). When extracting a MMW signal scattered by a variety of land covers, back in1985 the author conducted first experiments on sorting areas of frequency and time scaling, the presence of which imply certain fractal properties of the accepted sampling. At the same time, the problem of calculating textural features with account for the drift of their signatures under alternation of seasons was posed and solved. The assessments of the impact of window sizes on the accuracy of determining textural features for images of different land cover types were optimized.

For a long time the works on the study of radar images of the land cover at MMW using textural information have actually been carried out only in Russia and are of interest so far (especially now) [1, 2, 4]. After calculating ensembles of textural features based on optical and radar images, in 1985-1986 the author proposed methods and algorithms for the detection of low-contrast targets against the background of high-intense noise. Those included the method of direct use of textural features (1985), the dispersion method based on *f*-statistics (1985) and a detection method using linearly simulated patterns, i.e. textures (1986) [1-4, 8, 11]. The created methods of detection are quite valid at low signal to noise ratio of the order of or less than one (times). To the author’s knowledge, no textural method for detecting low-contrast target has been proposed abroad. Moreover, an important advantage of the textural methods of processing is the possibility to neutralize speckles at coherent images of the Earth’s surface, obtained by SAR.

The methods of deterministic chaos are widespread; they are shown in the right column of Fig. 4. It should be only noted that the algorithms of radar detection of low-contrast targets against the background of woodlands tor the radar at a wavelength of 2.2 mm were tested by the experimenters in 2001. It was the first time when a strange attractor was reconstructed. It controlled the radar scattering of millimeter radio waves. Its dynamic and geometric characteristics were measured; D fractal dimensions, depending on the value of m embedding dimension were calculated as well. The most accurate estimate of D can be obtained at the breakpoint of $D(m)$ convex curve, at that paying no attention to reduction in scale ratio above and below.

Based on the found maximum Lyapunov exponent λ_1>0.6 bit/s it has been shown that, when measuring the current conditions with an accuracy of up to 1 bit, we lose all predictive power over time during 1.7 seconds. Therefore, *the prediction interval* of echoed signal intensity is by about 8 times greater than classical correlation time τ ($\tau \approx 210$ ms at a wind speed of 3 m/sec). The prediction interval provides an opportunity to estimate roughly the amplitude of further samples in the sample collection and, as noted by the author, it can be used in radar practice. Calculations of Hurst exponent H showed that in two out of three cases, the scattering process of millimeter waves by woodlands corresponds to the persistent process with H>0,5, i.e. to the process with maximal rank.

3. Fractal topological detectors of low-contrast targets in high-intensity noise

Currently, great interest is evinced in various fractal and scaling methods (Fig. 4). Those fractal investigations started almost simultaneously in Russia, the USA and China in the 1980s. [1-12]. And the global problem to detect a fractal object against the intensive fractal background with additive Gaussian and nongaussian noise and interference was once posed [1-12]. Distinguishing features and methodology of the author's approach differed so greatly and were unusual for that time, that it was followed by a number of foreign articles with references to his early works on fractal processing of signals and radar images (see, e.g., [14-16]), in which it was taken further.

At the same time, the fractal dimension D or its signature $D(t, f, \vec{r})$ in different parts of the surface image is also a corresponding texture measure, i.e. the spatial correlation properties of scattering of radio waves from the respective surface areas. Moreover, the texture also determines *lacunarity* (Fig. 4), which uses second-order statistics for fractal images [1-12, 17-26]. Lacunarity is small for large dense texture and it is great when the texture is coarse-grained.

Lacunarity Λ (sensu Mandelbrodt) is defined by the formula

$$\Lambda = \left\langle \left((M / < M >) - 1 \right)^2 \right\rangle .$$

Here, M is a "mass" of a fractal formation, $<M>$ is an anticipated "mass", the brackets <...> stand for data ensemble averaging.

Lacunarity as a feature of objects detection was considered by the author in 1997. The introduction of fractional measures and scaling invariant makes it necessary to work with power-series probability distributions. The basic principles of a fractal detector were discovered and offered as early as in the 1980s; and for the first time ever (Fig. 2 and 3) the operation of the working model of fractal nonparametric detector of radar signals (FNDRS) was performed in 2003-2005. [1-12, 16-25]. In 2005 in the US it was exhibited as part of ISTC project with CCB "Diamond" and IRE RAS and earned a very high opinion of experts [1, 2]. The authors proposed unconventional algorithms of fractal-scaling detection, which offered high resistance. Some original versions of generalized structures of radar fractal detectors are presented in Fig. 5. The schematic view of the conjectured detector is shown in Fig. 5a. Based on a received radio signal or an image, a set of textural and fractal features ξ is determined. Then, in the threshold device at the threshold value of T and a certain level of false alarm probability F, a decision on obtained signal H_1 or its lack H_0 is issued. As ξ features, the value of the fractal dimension D, Hurst exponents $0 \le H \le 1$ for multiscale surfaces, p exponents, lacunarity values, etc. can be used. Hurst exponent is H=3-D for RI and H=2-D for a one-dimensional signal.

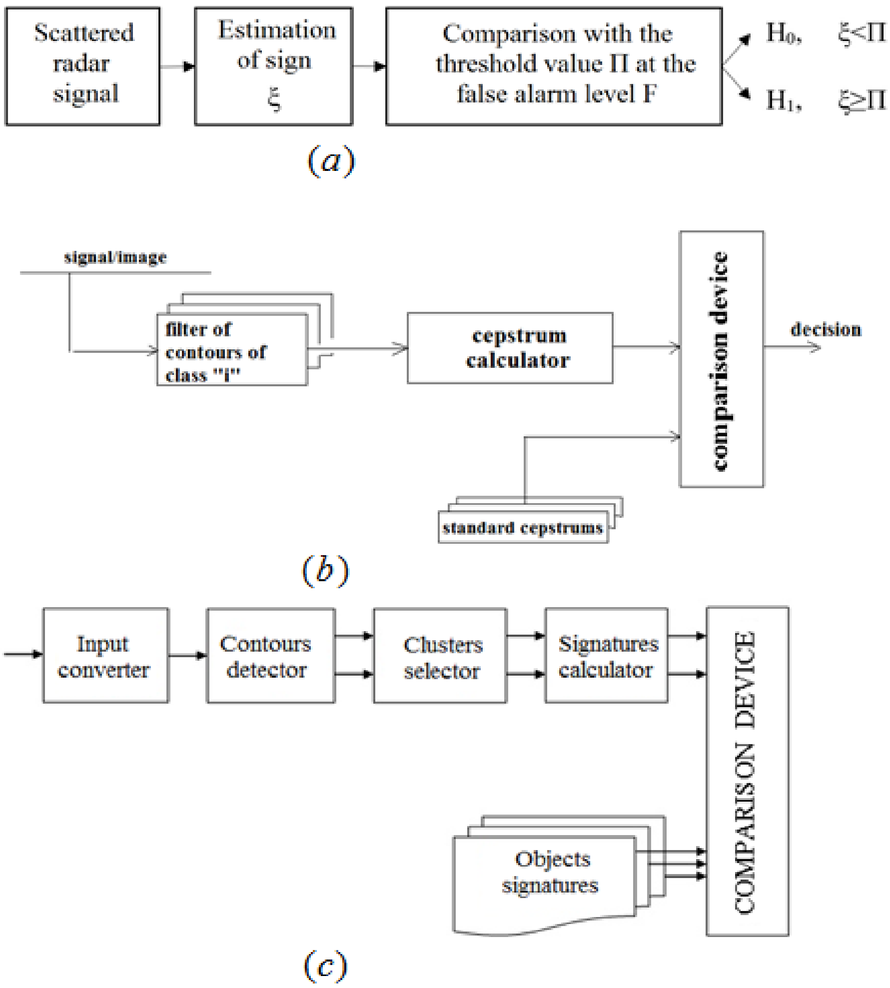

Fig.5. The initial (a) and detailed (b, c) structures of the first fractal detectors.

The integrated structural scheme of the fractal detector of radar signals is shown in Fig. 5 *b*. It consists of a circuit filter and a *fractal spectrum* computer. Further specification of the structural scheme of FNDRS is shown in Fig. 5*c*. An incoming signal (RI, a one-dimensional sample collection) arrives at the input converter.

It is intended to prearrange the analyzed sample collection. This preparation could include either an *induced noise contamination* (in the case of low resolving power of an analog-to-digital radar converter) or, for example, *contrast compression* in the case of sampling with a high dynamic range. Crucially, using the schemes in Fig. 5 it is definitely possible to synthesize absolutely all kinds of other fractal detectors in the future. (The author wishes to emphasize that "new" schemes of fractal detectors have been recently put forward by the authors who do not understand the fractal radiophysics and radiolocation at all and, not just knowing the basics of fractal analysis and dynamic chaos, they lay claim to some originality).

For a long time (over 35 years) the priority in this area in Russia and over the world strictly belongs to V.A. Kotelnikov IRE of RAS and to the author in particular. The author's concept (Fig. 3) of fractal radio systems and fractal devices makes the synthesis of other types of fractal detectors possible (Fig. 6 and 7). The detector based on the Hurst exponent works by using one or more search frequencies of radar (Fig. 6).

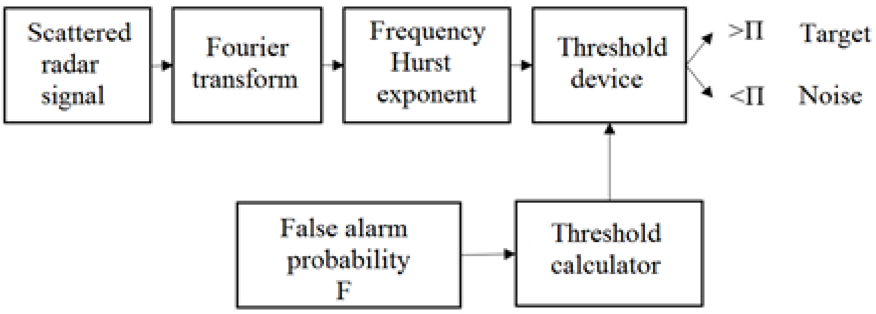

Fig.6. A fractal detector on the basis of the Hurst exponent.

Hurst exponent *H* reflects the irregularity of a fractal object. The smaller *H* exponent, the more irregular the fractal object is. So when an object occurs, the Hurst exponent grows. Fig. 7 is a scheme of a fractional detector with an autoregressive estimate of a power spectrum of the ground clutter. The autoregressive model is a linear prediction model that estimates the power spectrum of the clutter and forms its autocorrelation matrix.

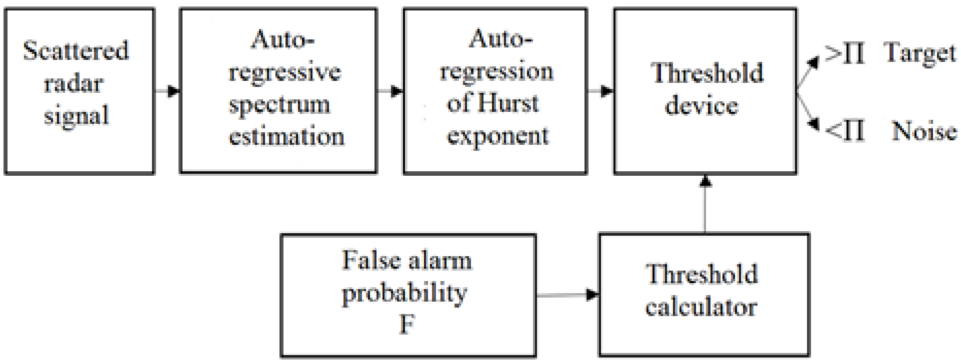

Fig.7. A fractal detector with an autoregression estimate of interference spectrum and the Hurst exponent.

An autoregression equation governs the relationship between the current and previous samples of a sampled stochastic process. Earlier in the 1980-ies the problem of autoregression on the basis of canonical system of Yule-Walker equations with transformation of luminance histogram was solved by the investigators. Thus, the detector in Fig. 7 uses real fractal properties of the power spectrum based on the autoregressive spectral estimation, used for the detection of low-contrast targets. Note that schemes like in Fig. 6 and 7 are often studied in China at present [2]. Similar detectors were used by the author in the texture processing of APS and radar images as early as in the 80-ies of the XX century. The author emphasizes that the correlation dimension (Fig. 4) that requires a large sample collection size, which is unrealistic in radiolocation cannot be considered as detection statistics.

4. Innovative fractal-scaling technologies: creation, development and application of fractal methods for radiolocation tasks and developing the foundations of fractal element base

During 35 years of research, the developed global fractal-scaling method completely lived up to expectations having found numerous applications (Fig. 8). This is a challenge of time. The facts themselves are in the author's favour!

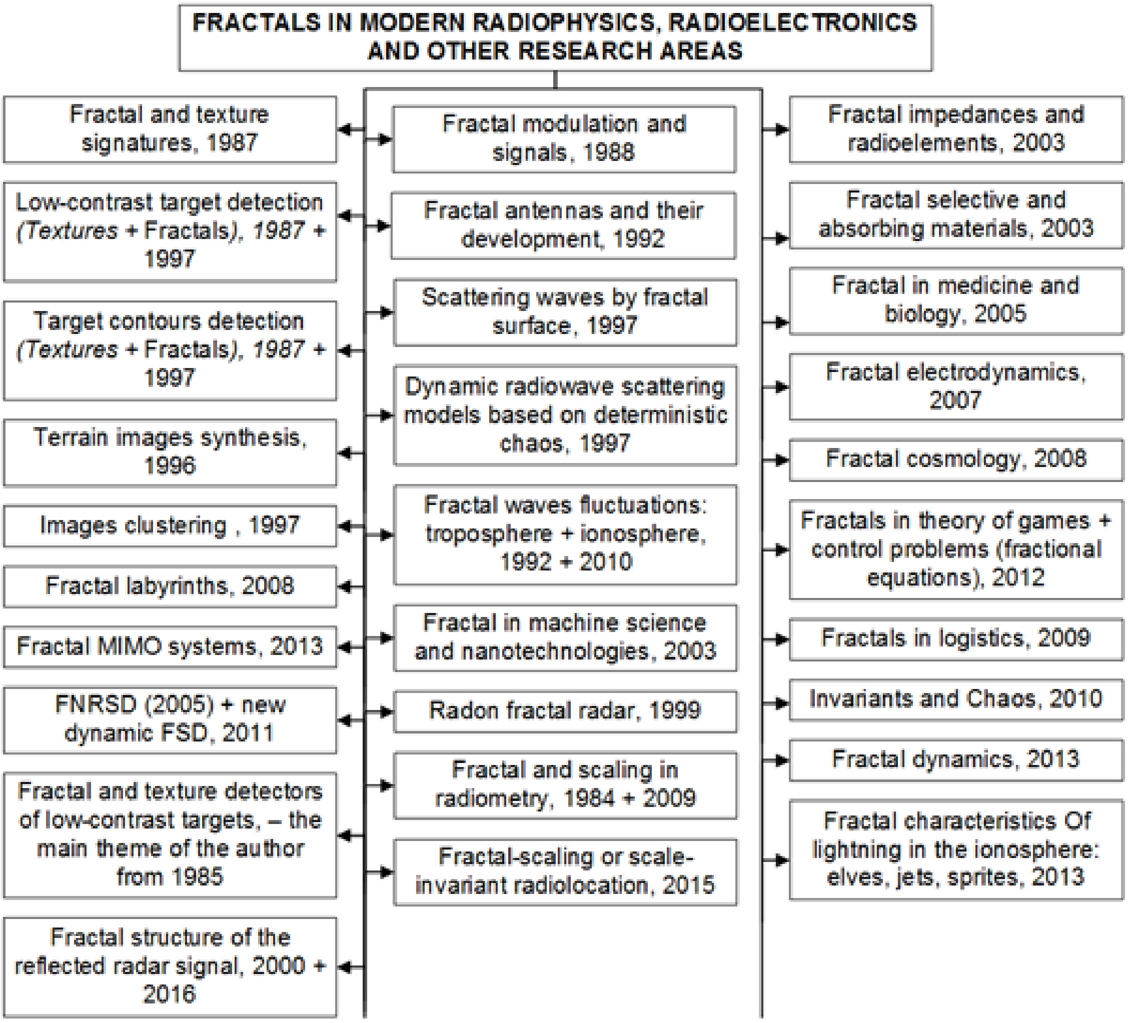

Fig.8. The layout of the author's development of new information technologies based on fractals, fractional operators and scaling effects for nonlinear physics and electronics.

The fundamental principle of "maximum topology with a minimum of energy" for the received signal that makes for more efficient use of the advantages of fractal-scaling processing of information has been developed and introduced; and this principle is consistently being put into practice [1-12, 17-26].

5. Postulates of Fractal Radar

Fractal radar defined in [1-12, 17-26] is based on four main postulates:

1) Intelligent signal processing based on the theory of fractional measure, scaling effects and fractional operator’s theory;

2) Hausdorff dimension or fractal dimension *D* of a signal or a radar image is directly connected with the topological dimension;

3) robust non-Gaussian probability distributions of the fractal dimension of the processed signal;

4) “Maximum topology with a minimum of energy” for the received signal. It allows take advantages of fractal scaling information processing more effectively.

The key point of fractal approach is to focus on describing and processing of radar signal (fields) exclusively in the space of fractional measure with the use of the scaling hypothesis and distributions with heavy-tailed or stable distributions (non-Gaussian). Fractal-scaling processing methods of signals, wave fields and images are in a broad sense based on the pieces of information, which isn’t usually taken into account and irretrievably lost if classical methods of processing are applied.

This work is concerned with the main radio physical area – radiolocation and it aims to ascertain what's done and things to do in this field on the basis of the fractal theory. Investigations carried out showed the correctness of the path chosen by the author (since 1980) to improve the radiolocation technique.

Is necessary to think about the processing of the input signals with a low threshold at high levels of false alarm and then a transition to a low level of false alarms. Moreover, the false alarm probability is never measured in real time. In principle, we need a new metric, and the new parameters of radar detection.

6. A New Direction in the Theory of Statistical Solutions

Fast development of the fractal theory in radar and radio physics led to establishing of the new theoretical direction in modern radar. It can be described as «*Statistical theory of fractal radar*». This direction includes (at least at the initial stage) the following fundamental questions:

1). The theory of the integer and fractional measure.
2). Caratheodory construction in the measure theory.
3). Hausdorff measure and Hausdorff-Besicovitch dimension.
4). The theory of topological spaces.
5). The dimension theory.
6). The line from the point of view of mathematician.
7). Non-differentiable functions and sets.
8). Fundamentals of the theory of probability.
9). Stable probability distributions.
10). The theory of fractional calculus.
11). The classical Brownian motion.
12). Generalized Brownian motion.
13). Fractal sets.
14). Anomalous diffusion.
15). The main criteria for statistical decision theory in radar.

16). Wave propagation in fractal random media.
17). Wave scattering generalized Brownian surface.
18). Wave scattering surface on the basis of non-differentiable functions.
19). Difractals.
20). Cluster analysis.
21). Theory and circuitry of fractal detectors.
22). Fractal-scaling or scale-invariant radar.
23). The multi-radar.
24). MIMO radar.
25). Cognitive radar.

This list of studied questions, of course, is supposed to be expanded and refined in the future. The author has been dealing with it for nearly 40 years of his scientific career.

Conclusion

The author created, developed and applied fractal-scaling methods for radiolocation problems and forming the foundations of fractal element base [1-12, 17-26]. For the first time ever approaches to development of a fractal radar and a fractal MIMO- radar were considered. The author emphasizes that the synthesis of topological (fractal, textural, chaotic, etc.) detectors makes for a fresh look at the problem of detecting super weak actual signals. As a result of that, the author's discovery in the away-back 1980-ies takes the meaning of *generalized detection*. Thus, pure energy and pure topological detectors are not contrary to each other and they do not duplicate, but complement one another.

Due to topological detectors it is possible to see the process of energy detection in a new light and to find some essential faults in it. Consequently, topological detection becomes not less, if not more, valuable for theory and practice than energy detection. The theory of topological detection is formulated in [1-12, 16-25]. It is especially necessary for the purpose of reexamining the former theory and in that way producing new results that are not available to traditional concepts of radiolocation.

Thus, topological detection opens the door to a radically new field of statistical decision theory and provides an opportunity to correct ideas in this field, and even to create new ones, which is of great theoretical and practical importance. The sufficiently detailed reasoning reported here should contribute to a better understanding of proposed by the author fundamentally new interpretation of the problem of radar (and other kinds of) detection. The proposed theory has much in common with cognitive radar.

Thus, during more than 35 years, almost from scratch, fundamental bases of the theory that will be applied in the following decades were formed. Not results, not specific solutions are the most valuable, bur namely the solution method, the approach to it. The created method is presented in [1-12, 17-26].

The author raised the foregoing problems as early as in 1980 and for more than 35 years he has been successfully working on their solution and development. Careful bibliographic studies show complete and absolute world priority of the author in all "fractal" fields of radiolocation and radio-physics (the list of the author's works in cooperation with students has about 800 publications, including 23 monographs).

Acknowledgements

The author prepared this article during working on the project "Leading Talents of Guangdong Province", № 00201502 (2016-2020) in the Jinan University (China, Guangzhou).

REFERENCES

1 Potapov A.A. *Chaos Theory, Fractals and Scaling in the Radar: A Look from 2015. Chapter 12 in: The Foundations of Chaos Revisited: From Poincaré to Recent Advancements*. Ed. C. Skiadas. Switzerland, Basel: Springer Int. Publ., 2016, pp. 195 – 218.

2 Potapov A.A., Wu Hao, Foukzon J., Podosenov S.A., Men'kova E.R. *Fractals in Radar, Fields, Control and Low-Contrast Target Detection*. Ed. A.A. Potapov. China, 2016 [appear.]

3 3. Potapov A.A. The Fractal - Scaling Radiolocation: Formation History 1980 – 2015. *Chaotic Modeling and Simulation (CMSIM),* 2016, No. 3, pp. 317 – 331.

4 Potapov A.A. The Textures, Fractal, Scaling Effects and Fractional Operators as a Basis of New Methods of Information Processing and Fractal Radio Systems Designing. *SPIE.* 2009, Vol. 7374, pp.73740E-1–73740E-14.

5 Potapov A.A. New Conception of Fractal Radio Device with Fractal Antennas and Fractal Detectors in the MIMO Systems. *Abstracts of the 9th Int. Conf. on Chaotic Modeling, Simulation and Applications (CHAOS'2016)*, University of London, London, U.K., 2016, pp. 85.

6 Potapov A.A., German V.A. Detection of Artificial Objects with Fractal Signatures. *Pattern Recognition and Image Analysis*, 1998, Vol. 8, No. 2, pp. 226 – 229.

7 Potapov A.A., German V.A. Fractals, Fractal Target Selection and Fractal Antennas. *Proc. Of the 1st Int. Workshop on Mathematical Modeling of Physical Processes in Inhomogeneous Media.* Mexico, Guanajuato, 2001, pp. 44 – 46.

8 Potapov A.A. New Information Radiophysical Technologies Fractal in Radiolocation: Fractal and Synergetic. *Proc. of the 28th ESA Antenna Workshop on pace Antenna Systems and Technologies.* Noordwijk: ESTEC, Netherlands, 2005, Part. 2, pp. 1047 – 1050.

9 Potapov A.A. Can We Build an Adaptive Fractal Radio System? *Proc. of the PIERS 2009 in Moscow «Progress in Electromagnetics Research Symp.»* Cambridge, MA: Electromagnetics Academy. 2009, pp.1798 – 1802.

10 Potapov A.A. The Global Fractal Method, Fractal Paradigm and the Fractional Derivatives Method in Fundamental Radar Problems and Designing of Revolutionary Radio Signals Detectors . *Zbornik radova Konf. MIT − Matematicke i informacione tehnologije. Kosovska Mitrovica, Serbia,* 2014, pp. 539 – 552.

11 Potapov A.A. Fractals, Scaling and Fractional Operators in Modern Physics and Radio Engineering. *Abstracts of the Int. Conf. XIV Khariton's Topical Scientific Reading «High - Power Pulsed Electrophysics».* Sarov: RFNC-VNIIEF, 2014, pp. 81 – 82.

12 Potapov A.A. Fractal Radar: Towards 1980 – 2015. *Proc. of the Int. Conf. "CHAOS 2015",* France, Paris, Henri Poincaré Institute, 2015, pp. 559 – 573.

13 Haralick R.M., Shanmugan K., Dinstein I. Textural Features for Image Classification. *IEEE Trans*. 1973, Vol. SMC-3, No. 6, pp. 610 – 621.

14 Du G. Detection of sea-surface radar targets based on fractal model. *Electronics Letters*. 2004, Vol.40, No. 14, pp. 906 – 907.

15 Soumeya Cherouat, Faouzi Soltani, Françoise Schmitt, Franck Daout. Using fractal dimension to target detection in bistatic SAR data. *Signal, Image and Video Processing*. 2015, Vol.9, No. 2, pp. 365 – 371.

16 Coopmans C., Malek H., Spencer E. Radiation and Impedance Characteristics of a Circular Loop Antenna Driven by Fractional Order Electronics. *Proc. of the Int. Design Engineering Technical Conf. ASME 2013 & Computers and Information in Engineering Conf. IDETC/CIE*. Portland, American Society of Mechanical Engineers, 2013, pp. V004T08A028 - V004T08A028.

17 Potapov A.A. At the origins o fractal scaling or scale-invariant radiolocation (1980-2015). Radio engineering. 2015, No.8, pp. 95-108. [in Russian]

18 Potapov A.A. Fractal-scaling or scale-invariant radiolocation principles and their application in synthetic aperture radars. Coll. of scientific papers of III All-Russian STC "Prospects of development of early warning RS, integrated systems and information support complexes of ASD and information management and processing systems:" RTI Systems of ASD-2015", Moscow, N.E. Bauman MSTU Publishing House, 2015, pp. 573-590. [in Russian]

19 Synthesis of new kinds of dynamic textural-fractal detectors of low-contrast targets with contour extraction and the coordinate location against the background of high-intense ground, sea and rainfall clutters. Proceedings of the 26th Intern. Crimean Conf. "Microwave engineering and telecommunication

technologies". KryMiKo'2016. Moscow; Minsk; Sevastopol: A.S. Popov CSTC, 2016, Vol. 12, pp. 2625-2636. [in Russian]

20 Potapov A.A. On the strategic directions in the synthesis of new kinds of textural fractal radar detectors of low-contrast targets with contour extraction and the coordinate location against the background of high-intense ground, sea and rainfall clutters. Proc. of the IV All-Russian STC "Prospects of development of early warning radar systems, integrated systems and information support complexes of aerospace defense and information management and processing systems "RTI Systems of ASD-2016 ". Moscow, OJSC «Academician A.L. Mintz RTI », 2016, pp.12. [in Russian]

21 Potapov A.A. Strategic Directions in the synthesis of new topological radar detectors of low contrast targets against the background of intense ground, sea and rainfall clutters. The non-linear world, 2016, Vol. 14, No. 3, pp. 6-22. [in Russian]

22 Potapov A.A. Processing of blurred images obtained by UAVs flying over nonuniform terrain using fractal-scaling and integrated methods. Radio Engineering, 2016, No. 7, pp. 119-124. [in Russian]

23 Potapov A.A. *Fractals in radio physics and radio location: Sampling topology*. The 2-nd revised and enlarged edition. Moscow, Universitetskaya kniga, 2005, 848 p.

24 Potapov A.A., German V.A. A Local-Dispersion Method of Measuring a Fractal Dimension and Fractal Signatures. *Abstracts and Final Program of the 2016 CIE Int. Conf. on Radar.* Guangzhou, Beijing, Chinese Institute of Electronics (CIE), 2016, p. 92.

25 Potapov A.A., German V.A., Pahomov A.A. Processing of Images Obtained from Unmanned Aerial Vehicles in the Regime of Flight over Inhomogeneous Terrain with Fractal-Scaling and Integral Method. *Abstracts and Final Program of the 2016 CIE Int. Conf. on Radar.* Guangzhou, Beijing, Chinese Institute of Electronics (CIE), 2016. pp. 114.

26 Potapov A.A. Strategic Directions in Synthesis of New Topological Radar Detectors of Low-Contrast Targets against the Background of High-Intensity Noise from the Ground, Sea and Precipitations // *Abstracts and Final Program of the 2016 CIE Int. Conf. on Radar.* Guangzhou, Beijing: Chinese Institute of Electronics (CIE). 2016, pp. 122.

Article accepted for publication 11.11. 2016

UDC 622.86:622.33:338.28

THE ANALYSIS OF ROOF FALL RISK ASSESSMENT METHODS IN UNDERGROUND WORKINGS

Domrachev A.N., Govorukhin Yu.M., Krivolapov V.G., Paleev D.Yu.

National Mine Rescue Centre, Aviatorov av., 54, Novokuznetsk, Kemerovo region, Russia,
nio.ngc2016@gmail.com

This article proves the relevance of the roof fall risk assessment. It bases both in terms of predicting the possibility of their reuse and keeping the coal pillars stability, and the risk of the origin of closed unventilated areas, which unavoidably accumulate explosive gas-air mixtures. The most widespread foreign methods of roof fall risk assessment in mine workings have been considered. They include an algorithm for calculating the index of the level of roof fall risk (RFRI) and the method of assessing the stability of the pillars of the New South Wales University (UNSW). The possibility of using of the roof fall risk assessment methods to improve the efficiency and safety of mining operations in South Kuzbass mines has been tested on a specific example.

Keywords: a probability of risk fall, factor of probability, weight factor, roof support, expert estimation, category of risk

Introduction

The probability of the roof fall in mine workings, both in mining operations and in case of accidents in coal mines depends on many factors: the geological parameters of the mined seams; the schema and the method of seams opening and preparation, mining technology, and others., and its determination is quite a challenge, often not having a unique solution. However, the authors think, that the roof fall risk assessment, and as a consequence, the prospects for their re-use in partial or complete preservation, as well as the risk of an origin of unventilated closed areas, in which the accumulation of explosive mixtures is inevitable, is very important.

During the analysis of reference sources [2-8], it was found out that the most frequent use have expert, probabilistic (statistical) and mixed methods of roof fall risk assessment. The development of the probabilistic method is in the simulation of the risk of roof fall using the Monte-Carlo method, but this approach cannot be recommended as a basis for the implementation of a common procedure.

1. Theoretical part

To perform expert evaluation, we use the index value of the level of roof fall risk (RFRI) [1, 2] by the categories of roof defects for various parameters (Table 1) on the factors given in the table. RFRI is calculated in accordance with the algorithm shown in table 2. When the value of RFRI is 7-32 the risk of the fall is considered to be low, 33-66 – average, 67-138 – high. The numerical value of the roof fall probability can be estimated by the formula (1) as:

$$RFRI_p = \frac{\sum (AV_i \cdot W_i)}{\sum (MAV_i \cdot W_i)}, \qquad (1)$$

where AV_i – estimate for a given category;
W_i – a weighting factor of this category;
MAV_i – the maximum estimate on the i-th category (or =6).

Table 1 – The categories of roof defects for the assessment of RFRI value

Category	Factor	AV_i value interval	Weigh-ting factor W_i
1	2	3	4
Geological	Large angular discontinues, join frequency, layer thickness	1-5	1
Technological	Shear rupture surface, joint separation, strata shifting, strata separation	1-5	2
Roof profile	Roof rock debris on floor, roof shape	1-5	1
Moisture	Moisture/groundwater	1-5	1

Table 2 – Algorithm of RFRI index calculation

Vertical sum on all categories	$\sum AV_i W_i$
Multiply by 1,1	$1{,}1\sum AV_i W_i \prod$
Matching micro seismic activity No micro seismic activity – subtract 5; Presence of micro seismic activity – add 25.	$1{,}1\sum AV_i W_i$ -5 $1{,}1\sum AV_i W_i$ +25
Matching roof deformation intensity No roof deformation; Constant roof deformation; Accelerating roof deformation.	$1{,}1\sum AV_i W_i - 5$ $1{,}1\sum AV_i W_i + 15$ $1{,}1\sum AV_i W_i + 30$
Index of roof fall.	RFRI

Quantitative expert and probabilistic fall risk assessment is based on the classification by coal mine roof rating (CMRR), which is a number in the range 0 (weak roof) - 100 (maximum strong roof) [3]. The calculation algorithm [4] is a combination of statistical and expert methods and includes sequential selection of the parameters, depending on the geological and mining characteristics with the subsequent calculation of probability based on regressional dependences. For each *j*-th module (rock layer) of the roof individual discontinuity rating is determined - (IDR_j). If the module includes only one lithology layer, the *IDR* is defined once for the whole series.

$$IDR_j=CR_j+SP_j, \tag{2}$$

where CR_j is the value of cohesion-roughness parameter;
SP_j is the value of spacing-persistence parameter.

Then on the basis of the above data the module rating is determined (unit rating, UR_i)

$$UR_i=min(IDR_j)+MDA_i+US_i+UMS_i, , \tag{3}$$

where IDR_j - is individual discontinuity rating for *j*-th layer;
MDA_i is parameter of multiple discontinuity adjustment;
US_i is factor of the unit strength;

UMS_i is factor of responsiveness to water content (unit moisture sensitivity).

On the basis of *USi* values calculated for each *i*-th layer (unit), a bed strength parameter SB (strong bed) is calculated, $SB=max(UR_i)$. Further, in view of US_i values and bolted interval *BI* the weighted average of the unit ratings RR_w is calculated.

$$RR_w = \frac{\sum_{i=1}^{N} UR_i m_i}{BI}, \tag{4}$$

where UR_i – unit rating value (rock formation) for *i*-th unit;
m_i – rock thickness of the *i*-th unit;
BI – bolted interval (bolts length), m.

For certain values of *SB* и RR_w the adjusted strong bed difference (*SBD*) of the ground (roof) rock is determined

$$SBD=SB-RR_w, \tag{5}$$

where SB – individual discontinuity rating;
RR_w – individual unit rating (massive structure discontinuity parameter).

Strong bed adjustment, *SBAJ* can be determined as

$$SBAJ=[(0,72SBD\times HSB)-2,5]\times[1-0,33(HSB-0,5)], \tag{6}$$

where HSB – thickness of the strong roof layer, m;
SBD – strong bed difference (adjusted roof rock strength).

The factor *CMRR* (Coal Mine Roof Rating) is determined as

$$CMRR=SBD+SBAJ+UCA+GA+SA, \tag{7}$$

where SBD – strong bed difference (formula 5);
SBA – strong bed adjustment (ground (roof) strength factor);
UCA – unit contact adjustment (contact strength factor);
GA – ground water adjustment (water content effect factor);
SA – surcharge adjustment (roof strengthening effect factor).

To determine the probability of roof fall we use two parameters – the probability factor (probability factor (PF)) and the weight (value) of each parameter. Examples of the probability factor and its values for the combination of factors are shown in Table 3.

The probability of a roof fall (retreat mining) during panel (pillar) mining *P*, % is determined as

$$P = 100\left[\frac{\sum_{i=1}^{n} PF_i W_i}{\sum_{i=1}^{n} MPF_i W_i}\right] = 0,33\left(\sum_{i=1}^{n} PF_i W_i\right), \tag{8}$$

where PF_i – the value of *i*-th factor of the fall probability;
W_i – the weight of *i*-th factor of the fall probability.

Table 3 – Parameters affecting the risk of the workings fall

№	Parameters	Value interval	Probability Factor	Weight Factor
1	2	2	3	4
1	Depth of cover H, m	40-600	1 – 4	9
2	CMRR	45 - 85	0 – 4	10
3	Floor rock quality	week-strong	1 – 3	4
4	Overlying massive strata, m	0 – 20	0 – 3	5
5	Multiple-seam interaction/ Interburden thickness	0 – 60h	0 – 4	7
6	Panel width	Sub-, super critical	1 – 3	3
7	Panel uniformity	Uniform –non uniform	1 – 3	1
8	Entry width, m	5 - 7	1 – 3	8
9	Pillar design	Suitable-unsuitable	1 – 4	6
10	Roof bolting (density)	1 – 1.5	1 – 3	7
11	Panel age (years)	1 – 2	1 – 3	2
12	Supplemental support	MRS, timber post	1,4	7
13	Cut sequence	Outside lift, left-right, other	1 ,2, 3	6
14	Final stump	Proper, unproper	1,4	8

Currently, the most common probabilistic method of determining the parameters of new workings protected by pillars and assessing the stability of the existing ones is the University of New South Wales (UNSW) Pillar Design Method [7] acceptable for rectangular and rhomb-shaped pillars. According to this method, the strength (resistance) R for $R \leq 5$

$$R = 8{,}6\frac{(w\Theta)^{0{,}51}}{h^{0{,}84}}, \tag{9}$$

where w – "adjusted" pillar width, $w = w_1 \sin\theta$, m;
w_1 – pillar minimum width, m;
θ – angle between adjacent sides (pillar), typically=0;
Θ – dimentionless factor (ratio value of width / height of the pillar);
h – pillar height, m.

For ratio w/h<3 Θ=1; on condition $3 \leq w/h \leq 6$ the parameter Θ makes

$$\Theta = \left[\frac{2w_2}{(w_1 + w_2)}\right]^{\frac{R-3}{3}}, \tag{10}$$

where w_1 – pillar minimum width, m;
w_2 – pillar maximum width (or pillar length), m.

When the ratio w/h>6 the parameter Θ makes

$$\Theta = \frac{2w_2}{(w_1 + w_2)} \,. \tag{11}$$

The current load on the coal pillar is determined by the indirect method

$$S = \rho H \frac{(w_1 \sin\theta + b_1)\left(w_2 + \dfrac{b_2}{\sin\theta}\right)}{w_1 w_2 \sin\theta} \,, \tag{12}$$

where b_1 – roadway width (with respect to pillar width), m;
b_2 – roadway length (with respect to pillar length), m;
H – depth of overburden, m;
ρ – density of overburden, MH/m^3.

R and *S* parameters are defined in the stress units (MPa). The Factor of safety *FoS* is defined as

$$FoS = \frac{R}{S} \,. \tag{13}$$

The probability of pillar failure (p_{of}) (and workings fall) can be determined as

$$p_{of} = 1 - \Phi\left(\frac{\ln FoS}{\sigma}\right), \tag{14}$$

where σ – mean-square deviation;
$\Phi()$ – standard function of normal distribution.

The standard mean-square deviation is based on the power model of pillar strength using the University of New South Wales (UNSW) Australian database, thus σ=0.157.

2. Discussion of results

To assess the possibility of this methodology when evaluating the risk of roof fall in the workings of Kuzbass conditions we have calculated the drift of Sychevsky-IV seam of “Gramoteinskaya” mine.

In case of the width of the sill pillar up to 30 m, the width of workings 4.5 m, and the bolting height of 2.5 m, the probability of the fall using CMRR was 0.168, while the calculation according to the UNSW Pillar Design Method resulted in 0.147, that is an acceptable indicator for predicting the stability of the stope for the period of its operation. A technological reason of a sufficiently high probability of the working fall can be a decision to leave in the roof a coal bench up to 0.75 m thick.

Conclusion

The presented analyzes allowed not only to evaluate the methods for determining the probability of roof fall in mine workings, but also to identify possible areas of the use of the gained results. The authors presume that the obtained results would have the most importance at working out the annual and quarterly plans for the development of mining operations, particularly at the evaluation of the possibility of secondary use of the preserved mine workings, monitoring of the calculated and actual parameters of interchamber and goaf pillars at short wall mining, as well as when forecasting possible unventilated mine workings during rescue operations in coal mines.

REFERENCES

1 Domrachev A.N., Krivolapov V.G., Govorukhin Yu.M., Maslenkov A.V. *The methodology of analysis and risk assessment during rescue operations in mines*. Kemerovo, 2013, 204 p.

2 Iannacchione A.T., Prosser L.J. Jr., Esterhuizen G.S., Bajpayee T.S. *Assessing roof fall hazards for underground stone mines: a proposed methodology*. – [electronic source]. Available at: www.cdc.gov/niosh/mining/UserFiles/works/pdfs/arfhf.pdf

3 Devidas S.N., Shiva S. Development of software to evaluate roof fall risk in bord and pillar method – depillaring phase. *GeoScience Engineering*, 2015, Vol. LXI, No. 2, pp. 14-22.

4 Molinda G.M., Mark C., Debasis D. Using the coal mine roof rating (CMRR) to assess roof stability in U.S. coal mines. [electronic source]. Available at: www.cdc.gov/niosh/mining/ userfiles/works/pdfs/utcmr.pdf

5 Ghasemi E., Ataei M., Shahriar K., Sereshki F., Esmaeil S.J., Ramazanzadeh A. Assessment of roof fall risk during retreat mining in room and pillar coal mines. *International Journal of Rock Mechanics and Mining Sciences*, 2012, Vol. 54, pp. 2-9.

6 Mark C., Papas D.M., Chase F.E. Reducing the risk of ground falls during pillar recovery. *Society Mining Metallurgy and Exploration*, 2003, Vol. 314, pp. 153-160.

7 Mark G. Stewart A. Probabilistic risk assessment of mine subsidence. *Australian Geomechanics*, 2008, Vol. 43, No. 3 pp. 1-12.

8 Shahriar K., Oraee K., Bakhtavar E. *Roof falls: An inherent risk in underground coal mining*, 2009 – [electronic source]. Available at: http://icgcm.conferenceacademy.com/CMS/ publicationsdtl.aspx. http://hdl.handle.net/1893/2329;

Article accepted for publication 25.11.2016

UDC 537.6; 537.311.33

RESONANT DISSIPATIVE MODEL OF THE FARADAY EFFECT IN A DIELECTRIC MULTILAYER NANO – STRUCTURES

Zhumaev M.R., Sharipov M.Z.

Bukhara Engineering - Technologies Institute, 200100, Bukhara, Uzbekistan
e-mail: m.z.sharipov@rambler.ru

The theory of the rotation angle of the plane of polarization in dielectric media has been considered. In paper the dissipative model resonance Faraday effect in dielectric multilayer nanostructures is proposed. Found amplification condition of the Faraday effect in multilayer nano-structures. It is shown the possibility of resonance amplification of the Faraday rotation angle under the influence of an external magnetic field. The frequency dependence of the refractive indices for right and left polarized light was analyzed.

Keywords: Faraday effect, resonant amplification, refractive index, light field polarization

Introduction

The main problem of designing nano-dimensional structures for various applications is to increase the value of the angle of rotation of the plane of polarization and intensity of the light propagating through the multi-layer crystals. This is due to the fact that they play an important role for the development of magnetic devices of nanoelectronics. They are also important for the design of radically new magnetic memory elements.

In this paper we investigate the above mentioned problems for nano sized nonmagnetic multilayer dielectric crystals. This choice is due to the fact that only in a purely dielectric materials can be excited waveguide modes. At the same time, the metal - dielectric structures are coupled oscillations of the electrons and the localized electromagnetic field.

Given the presence of absorption in the non-magnetic insulators, we have shown that perhaps the resonance enhancement of the Faraday effect under the influence of an external magnetic field. To determine the transmission and reflection coefficients of multilayer systems, we used a method based on the summation of the Fresnel formulas.

1. Rotation of the plane of polarization in dielectric media

It is known that the permittivity of isotropic and homogeneous media, according to Maxwell's theory is given by [1]

$$\varepsilon = 1 + \alpha . \tag{1}$$

It characterizes the polarizability of the medium and determines the resulting electric dipole moment of electrons per unit volume

$$\vec{p} = Nq\vec{r}_0 = \varepsilon_0 \alpha \vec{E}_0 . \tag{2}$$

Where: N - the concentration of the electron, $q = -e$ - electron charge, $\vec{E}_0$ - the amplitude of the electric field of light, ε_0 - electrical constant (permittivity of free space), $\vec{r}_0$ - the amplitude of the displacement of the electron relative to its equilibrium position.

Consequently, for a finding of polarizability α dielectric permittivity ε and the amplitude of the electron oscillations $\vec{r}_0$ should be expressed in terms of the field amplitude $\vec{E}_0$. Strictly speaking, in this case one must consider itinerant electron oscillations, so-called polarization wave, along with the electromagnetic field [2]. But we shall confine ourselves to the case where the problem can be solved in the linear approximation.

In this case, the electric field of the light can be considered uniform, and assume that the quasi elastic restoring force and the drag force acting on the electron, too linear, i.e., proportional to the displacement $\vec{r}$ and velocity $\vec{\vartheta}$. Thus, a linear approximation equation of motion of the electrons can be written as follows

$$m\frac{d\vec{\vartheta}}{dt} = -a\vec{r} + b\vec{\vartheta} + q(\vec{E} + \text{[redacted]}, \vec{B}]). \qquad (3)$$

Where: a - the effective coefficient of elasticity, b - effective coefficient of resistance, $\vec{E} = (E_x, E_y, 0)$ - the electric field strength of the electromagnetic wave, $\vec{B} = (0,0,B)$ - an induction of an applied magnetic field.

Further recording vector equation of motion (3) in the scalar form we obtain the following system of equations coupled oscillations

$$\left.\begin{aligned} m\frac{d\vartheta_x}{dt} &= -ax - b\vartheta_x + qE_x + qB\vartheta_y \\ m\frac{d\vartheta_y}{dt} &= -ay - b\vartheta_y + qE_y - qB\vartheta_x \end{aligned}\right\} \qquad (4)$$

The last set of equations of motion can be solved by taking advantage of its line, believing

$$\vec{E} = \vec{E}_0 e^{i\omega t}, \qquad (5)$$

and reducing it to a system of linear equations for the components $\vec{r}_0 = x_0\vec{i} + \vec{y}_0\vec{j}$. However, the use of conversion

$$\left.\begin{aligned} x &= \frac{1}{2}(r^+ + r^-), y = -\frac{i}{2}(r^+ - r^-) \\ E_x &= \frac{1}{2}(E^+ + E^-), E_y = -\frac{i}{2}(E^+ - E^-) \end{aligned}\right\}, \qquad (6)$$

It allows us to reduce the system of equations related to the vibrations of mind:

$$\left.\begin{aligned} m\ddot{r}^+ &= -ar^+ - b\dot{r}^+ + qE^+ - iqB\dot{r}^+, \\ m\ddot{r}^- &= -ar^- - b\dot{r}^- + qE^- + iqB\dot{r}^-. \end{aligned}\right\} \qquad (7)$$

i.e. to a system of independent variables r^+ and r^-.

Now, as usual, considering that

$$E^{\pm} = E_0^{\ \pm} e^{i\omega t}, \quad r^{\pm} = r_0^{\ \pm} e^{i\omega t}, \tag{8}$$

from (6) we find:

$$r_0^{\ \pm} = \frac{qE_0^{\ \pm}}{(a - m\omega^2 \mp qB\omega) + ib\omega}. \tag{9}$$

Finally, with the help of (2) of the expression (9) determine the polarizability of the dielectric medium:

$$\alpha^{\pm} = \frac{Ne^2}{\varepsilon_0 \left[(a \pm eB\omega - m\omega^2) + ib\omega\right]}. \tag{10}$$

Thus, due to the action of an external magnetic field with induction perpendicular to the dielectric medium appears toopolarizabiliti media, namely the difference polarizabilities right (α^{+}) and left (α^{-}) polarized light components. ($e = 1.6 \cdot 10^{-19} C$) - the value of the elementary charge, m - mass of the electron).

Concluding the section is the expression components of the electric field of an electromagnetic wave believing $E_0^{+} = E_0^{-} = E_0$ that $\vec{k} = (0,0,k)$. Then

$$E^{\pm} = E_0 e^{i\omega t} e^{-ikn^{\pm} z}, \; n^{\pm} = \sqrt{\varepsilon^{\pm}} \tag{11}$$

where $n^{\pm}$ - the refractive indices of the right and left polarized light component, to k - the wave vector of the light field.

Further, taking into account (11) and lower expression of the transformation (6) define E_x and E_y

$$\begin{Bmatrix} E_x \\ E_y \end{Bmatrix} = E_0 e^{i\omega t} e^{-\frac{i}{2}(k^{+}+k^{-})z} \cdot \begin{Bmatrix} \cos(\frac{k^{-} - k^{+}}{2} z), \\ \sin(\frac{k^{-} - k^{+}}{2} z). \end{Bmatrix} \tag{12}$$

It follows that rotates the plane of polarization of the electromagnetic wave- Faraday effect and the angle of rotation is determined by the difference between the refractive indices of the right (n^{+}) and left (n^{-}) polarized light components

$$\varphi(z) = \frac{\omega}{2c}(n^{-} - n^{+})z, \tag{13}$$

where: ω - the cyclic frequency of the light field, c - the speed of light in vacuum.

2. The increase in the Faraday rotation angle under the influence of an external magnetic field

Now we examine the angle of rotation of the plane of polarization in the dielectric layer thickness d :

$$\varphi = \frac{\omega}{2c}(n^- - n^+)d\,. \tag{14}$$

The expressions for the refractive index difference and the right (n^+) polarized waves (n^-) manage to simplify the fact that for dielectric media polarizability much smaller one, i.e. $\alpha^{\pm} << 1$. Then according to the expression (1) and (11) we obtain

$$n^- - n^+ \approx \frac{1}{2}(\alpha^- - \alpha^+)\,. \tag{15}$$

Further, by introducing features

$$A^{\pm} = a \pm eB\omega - m\omega^2 + ib\omega\,, \tag{16}$$

refractive index difference we give to the following form

$$n^- - n^+ \approx \frac{Ne^2}{2\varepsilon_0} \cdot \frac{A_1 - iA_2}{A_1^{\ 2} + A_2^{\ 2}} \cdot 2eB\omega\,. \tag{17}$$

Here A_1 and A_2 are the real and imaginary parts of the functions A^+ and A^- are determined according to (16), (17) the following expressions

$$\left.\begin{aligned} A_1 &= m^2\omega^4 - \omega^2(2am + e^2B^2 + b^2) + a^2, \\ A_2 &= 2b\omega(a - m\omega^2). \end{aligned}\right\} \quad \begin{aligned} &(18.1) \\ &(18.2) \end{aligned}$$

As seen from (17) and (18), the difference in refractive indices $n^- - n^+$ is a complex function of the cyclic frequency of a light wave ω. Therefore, further restrict the analysis $A_2 = 0$. Then case of (18.2) it follows that

$$\omega_1 = 0\,,\ \omega_2 = \sqrt{\frac{a}{m}} \equiv \omega_c\,, \tag{19}$$

where ω_c - cyclic frequency of oscillations of electrons.

Consequently, in $\omega_1 = 0$ that under the influence of a constant electric field polarizabilities difference right (α^+) and left (α^-) polarized light waves disappear and the Faraday effect will not occur. However, the frequency of the light field is equal to the frequency of oscillations of electrons (17) that:

1) first, the difference in the imaginary parts of the complex refractive index of the right (n^+) and left (n^-) polarized light component is equal to zero;

2) in the second module of the Faraday rotation angle is determined by the difference of the real parts (n^+) and (n^-) will be expressed as follows:

$$|\varphi(d)| = \frac{Ne^2 d}{2\varepsilon_0 c} \cdot \frac{eB}{b^2 + e^2 B^2} \ . \tag{20}$$

From the last expression it follows that the modulus of the Faraday rotation angle is at the maximum value of the induction of the external magnetic field (called critical) (see. Fig. 1):

$$B_{кр} = \frac{b}{e} \ . \tag{21}$$

The maximum value of the modulus of the Faraday rotation angle in this case will be:

$$|\varphi_{макс}| = \frac{Ne^2 d}{4\varepsilon_0 bc} \ . \tag{22}$$

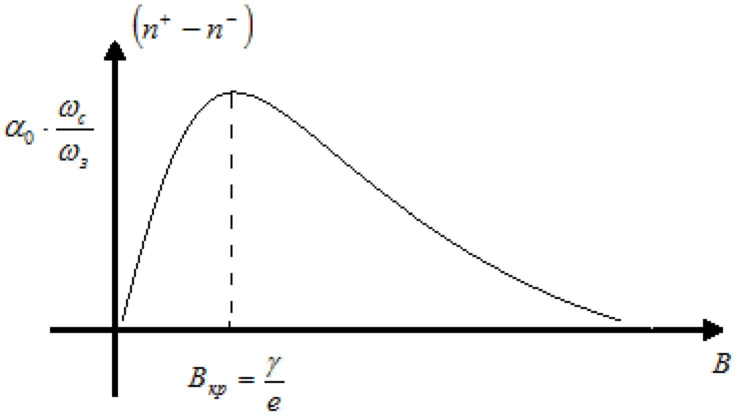

Fig.1. The dependence of the refractive index difference right - and left-polarized electromagnetic waves from the magnetic field

Further, given that the static polarizability of the dielectric medium is given by ($\alpha^{\pm}$ when $\omega \equiv 0$)

$$\alpha_0 = \frac{Ne^2}{\varepsilon_0 \alpha} \ , \tag{23}$$

the preceding relation can be written as

$$|\varphi_{\max}(d)| \equiv \frac{\alpha_0 ad}{4bc} . \tag{24}$$

Since usually the cyclic frequency of natural oscillations of the electrons ($\omega_c = \sqrt{\frac{a}{m}}$) substantially predominates over the cyclic frequency attenuation of light ($\omega_з = \frac{b}{m}$), the maximum difference between the right (α^+) and left (α^-) polarizations polarized components of the light field will be equal to

$$\max(\alpha^{-} - \alpha^{+}) = \alpha_0 \cdot \frac{\omega_c}{\omega_з}. \qquad (25)$$

Thus, if the frequency of the light wave is equal to the frequency of the electron and the magnetic induction of the external field is equal B_{cr} (21), the maximum polarizability difference of left (α^-) and right (α^+) of polarized light components can be increased by two - three orders, as

$$\frac{\omega_з}{\omega_c} \approx 10^{-3} - 10^{-2} \text{ [3-4]}.$$

Concluding the section, we present an expression of the maximum modulus of the Faraday rotation (22) to the following form

$$|\varphi_{\max}| = \frac{\alpha_0}{4c} \cdot \omega_c \cdot \frac{\omega_c}{\omega_з} d \equiv \frac{1}{4} \cdot \frac{2\pi d}{\lambda_0} \cdot \alpha_0 \frac{\omega_c}{\omega_з}, \qquad (26)$$

convenient for applications. Here, λ_0 - wavelength of light in vacuum.

3. Amplification magneto-optical effects in multi-layer nano – structures

As shown in the previous section, the difference in the refractive indices, as well as the magnitude of the Faraday rotation angle can be substantially increased when $\omega = \omega_c$ action of a small external magnetic field $\sim 1.7 \cdot 10^{11} Cl/kg$. This is due to the fact that the specific charge of an electron is very large. At the same time the difference between the imaginary parts of the complex refractive index of the right (α^+) and left (α^-) polarized components of the light is zero. Otherwise, i.e. if it is $\mathrm{Im}(n^- - n^+) \neq 0$, it is well known, the amplitude of the light field is reduced during the passage through the medium in an exponential fashion. Thus, even when there is absorption in dielectric media magnetooptical effects can be enhanced by the above method. But there are also other ways of strengthening them, including on the basis of multi-layer nano-structures. In the latter case it used multiple transmission and reflection of light through the media periodically or multilayer crystals.

Next to consider the specificity of light propagation through the dielectric layer with permittivity ε_2, and bounded by the planes $z = 0$ that $z = d$ separates the dielectric constants ε_1 and ε_3 the environment. Let this layer normally falls to the surface of the $z < 0$ electromagnetic wave field. We want to determine when executed, any conditions reflectance dielectric layer is minimal. It is clear that only in this case, the transmittance is maximized, and may increase the magneto-optical effects in multilayer structures.

Note that the reflectance of the dielectric layer can be found in two ways:

1) By using the continuity conditions for the electric field and its derivative at the boundaries of adjacent layers, i.e. $z = 0$ and $z = d$ when. In this case, it is necessary to solve the system of algebraic equations, which determines the amplitude of the reflected field in the first medium, the amplitude of the field in the intermediate layer - traveling in opposite directions and the amplitude of the field in the third medium. When a similar problem is solved for multilayer structures with finite - dimensional layers (for example, four or five layer structure), this system is much more complicated, and therefore applied a numerical method for solving the so-called matrix method propagation [3-5].

2) There is a second method, which is based on the use of the Fresnel formulas for finding and reflection coefficients of transmission and reflection of the adjacent layers.

In this case, the resulting reflectance is found as the sum of the amplitudes of multiple reflections:

$$R = \alpha_{12} + \beta_{12}\alpha_{23}\beta_{21}\sum_{S=1}^{\infty} \left(\alpha_{21}\alpha_{23}\exp\left(-2ik_2 d_2\right)\right)^{S-1} . \tag{27}$$

Here

$$\alpha_{ik} = \frac{n_i - n_k}{n_i + n_k},\ \beta_{ik} = \frac{2n_i}{n_i + n_k},\ k_2 = \frac{\omega}{c} n_2 , \tag{28}$$

describe the partial reflection and transmission coefficients of adjacent layers, k_2 - the wave vector of light in the second, ie, in the intermediate layer.

Next, using the formula for an infinitely decreasing geometric progression (since $|\alpha_{12}|, |\alpha_{23}| < 1$), and using (27) - (28), we obtain for the reflection coefficient of the three-layer structure similar to the following expression [6-7]

$$R = \frac{\alpha_{12} + \alpha_{23} e^{-2ik_2 d_2}}{1 + \alpha_{12}\alpha_{23} e^{-2ik_2 d_2}} . \tag{29}$$

Now using (29) we can find the reflectance of the multilayer structure of the reflection coefficients multiplying successively the following layers:

$$R = \prod_{l=0}^{S} \frac{\alpha_{l,l+1} + \alpha_{l+1,l+2} e^{-2ik_{l+1} d_{l+1}}}{1 + \alpha_{l+1,l+2} e^{-2ik_{l+1} d_{l+1}}} . \tag{30}$$

Where: S - number of the layer from which light is incident on the subsequent layers. Typically, the dielectric multilayers is located vacuum, or air.

Consequently, the reflection coefficient of a three-layer structure will be zero if the following two conditions:

$$|\alpha_{l,l+1}| = |\alpha_{l+1,l+2}|, \tag{31.1}$$

$$\varphi_{l+1,l+2} - \varphi_{l,l+1} - 2k_{l+1} d_{l+1} = \pi \cdot (j+1). \tag{31.2}$$

Where: j - an arbitrary integer, $\varphi_{l,l+1}$ - the argument is a complex partial reflectance. It is easy to see that the conditions (31.1 - 31.2) lead with $l = 1$ to the following relations:

$$\left.\begin{aligned} n_2^{\,2} &= n_1 n_3 + \frac{n_3 \chi_1^{\,2} - n_1 \chi_3^{\,2}}{n_1 - n_3}, \\ tg(2k_2 d) &= \frac{n_2 (n_1 - n_3)}{n_1 \chi_3 + n_3 \chi_1}. \end{aligned}\right\} \tag{32}$$

Where: n_1, n_2 and n_3 - the refractive indices of the dielectric medium, χ_1 and χ_3 - uptakes outer layers, the intermediate layer is considered transparent, i.e. $\chi_2 = 0$. Obviously, the latter made only to simplify the final formulas of the system (32).

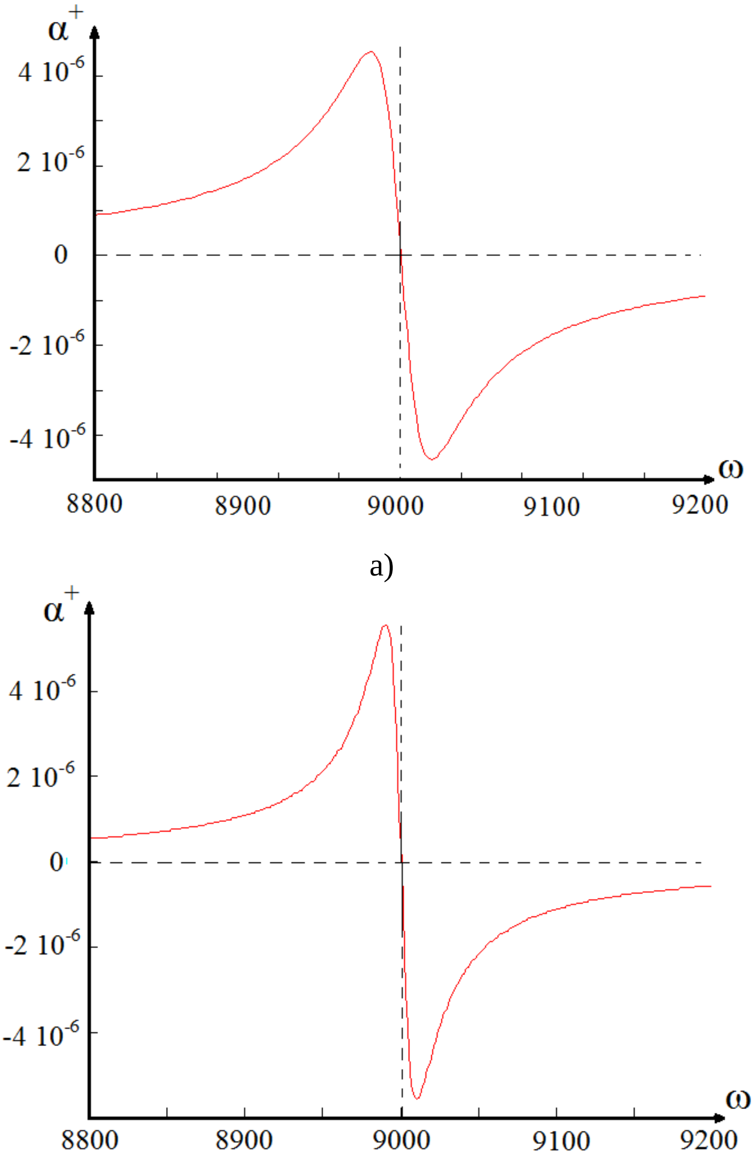

Fig.2. Dispersion curves: a) right polarized (+) and b) left-polarized (-) light waves.

Thus, if the partial reflection coefficients of adjacent layers at an arbitrary *l* satisfies (31.1) and (31.2) in the light passes without being reflected multistructures, i.e. completely. Naturally, the last conclusion holds for the right and left polarized components of the light field.

Concluding the section, we give expression the refractive index of the right (+) or left (-) polarized light component in the frequency range near the resonance frequency, i.e., if

$$\omega \mp \frac{eB}{2m} - \omega_c \to 0$$

that follows from (17) in this approximation:

$$n^{\pm} \equiv 1 + \frac{\omega_{эл}{}^{2}}{4\cdot(\omega_c \pm \frac{eB}{2m})} \cdot \frac{\omega_c \pm \frac{eB}{2m} - \omega}{(\omega_c \pm \frac{eB}{2m} - \omega)^2 + (\frac{b}{2m})^2}. \quad (33)$$

Here: $\omega_{el} = \sqrt{\frac{Ne^2}{m\varepsilon_0}}$ - electron plasma frequency.

Thus, in the frequency range near resonance can enhance the magneto-optical effects, including increasing the Faraday rotation angle, selecting a cyclic frequency ω of the light so that the refractive index difference right (n^{+}) and left (n^{-}) polarized light waves was greatest (Fig. 2).

Conclusion

In paper studied the Faraday effect in the multilayer dielectric nanostructures and obtained the following results:

1. In the purely dielectric media, magneto-optical effects may occur under the influence of external magnetic field.
2. In the light frequency equal to the frequency of oscillations of electrons can maximize the Faraday rotation angle at the critical magnetic field.
3. The conditions for amplification of these phenomena in multilayer nano-structures near the resonant frequencies of the refractive indices of the right and left polarized components of the light field.
4. These results can be used to develop new systems of magnetic nanostructures.

Acknowledgments

This work was supported in part by a grant ЁФ2-1, Uzbekistan

REFERENCES

1 Akhmanov S.A., Nikitin S.Y. *Physical Optics*. M., MGU, 1998, 656 pp, [in Russian].

2 Zvezdin A.K., Pyatakov A.P. Phase transitions and the giant magnetoelectric effect in multiferroics. UFN. 2004, Vol. 4, pp. 465 – 470 [in Russian].

3 Belotelov V.I., Akimov I.A., Pohl M., Kotov V.A., Kasture S., Vengurlekar A.S., Gopal A.V., Yakovlev D., Zvezdin A.K., Bayer M. Enhanced magneto-optical effects in magnetoplasmonic crystals. *Nature Nanotechnology*, 2011, Vol. 6, pp. 370 – 376.

4 Mikhailova T.V. *Magnetophotonic dimensional crystals with a modified magnetically active layer*. Thessis of cand. diss. Simferopol, 2014, [in Russian].

5 Grunin A.A., Zhdanov A.G., Tsema B.B., Ezhov A.A., Dolgova T.V., Ganshina E.A., Hong M.H., Fedyanin A.A. Magneto-optical response enhancement in 1d and 2d magnetoplasmonic crystals. *Proc. of the SPIE 7353, Metamaterials IV*, 73530F, 2009, pp. 73530F-1-73530F-10.

6 Sharipov M.Z. *Investigation linear magneto-optical effects in multilayer magnetic structures*. Master's diss. Bukhara, 2004, [in Russian].

7 Sharipov M.Z., Zhumaev M.R., Hayitov D.E., Urunov R.Zh., Hallokov F.K. Conditions of amplification strengthen the magneto-optical Kerr effect in a three-layer structure. Approbation - Makhachkala, Russia, 2014, No. 2 (17), pp. 7 – 10, [in Russian].

Article accepted for publication 25.11.2016

UDC 621.438.001.8

TO THE METHODOLOGY OF THE RESEARCH OF THE GTE TURBINE BLADES PLATFORMSWEAR

Ivshchenko L.I., Pribora T.I., Komochkin N.S., Sakhnyuk N.V.

Zaporizhzhya National Technical University, Ukraine, nkomochk@zntu.edu.ua

The problem of the gas turbine engine turbine blades platforms wear is discussed. The methodology to solve this problem by defining the processes that occur in platforms is suggested. The object model test and research methods are described. Describes the object modeling techniques and explore patterns of oscillations of the system of coupled oscillations of parts of an aircraft engine turbine. An original setting for the study of the wear of rotor blades was used.

Keywords: wear, platforms, blades, turbines, gas turbine plant.

Introduction

Many compounds of machinery parts in use are under complex loading. This is due to the mutual movements of the functional surfaces in various directions, vibrations, presence or combinations thereof. The consequence of this process is the inevitable wear of the working surfaces of joints. Largely dimensional stability and consistent quality surface determine the resource of individual parts and machinery in general. Question increase wear of contact surfaces of the parts are not lost its relevance today. In various branches of engineering it is solved by the use of more high-quality and expensive structural materials, wear-resistant coatings, and appropriate heat treatment to achieve a certain surface quality in their manufacture. In recent years, scientists are placing more emphasis on the relationship surface engineering and operating conditions of parts. The object of our study are tribomating who work in a complex dynamic loading in combination with a wide range of operating temperatures and speeds. The study of such a system requires a comprehensive approach.

1. Formulation of the problem

Design, technological and strength features of the turbine working blades of the gas turbine engines (GTE) influence largely their gas dynamic characteristics. The turbine blades are the most loaded, essential parts of the massively produced gas turbine plants. In terms of construction, the blades consist of a working part (blade airfoil), root designed for mounting a blade on the wheel, and platforms (Fig.1) responsible for the oscillation stabilization of the blade row and the whole turbine. To improve the gas-dynamic characteristics of the GTE, the stringent requirements on elements wear-resistance, cyclic fracture, corrosion resistance at high temperatures, static resistance, etc. are imposed on the working turbine blades.

In modern aircraft GTE, platform connections of various designs whereby the working turbine blades are combined into a closed circular system are widely used to improve the reliability and durability of the blades. It reduces the rotor sensitivity to vibrations, provides the necessary damping level of vibratory load son the airfoil blade; moreover it reduces the losses of the working gas through the radial gaps between the rotor and the stator, consequently increasing the turbine efficiency. The platforms contact surface work under cyclically varying high temperatures, aggressive gas medium and dynamic loadings. According to the work [1], the platforms are under contact pressure of forces P, (which is perceived from adjacent platforms), torque M from these forces, and the frictional force T (see Fig. 2a).

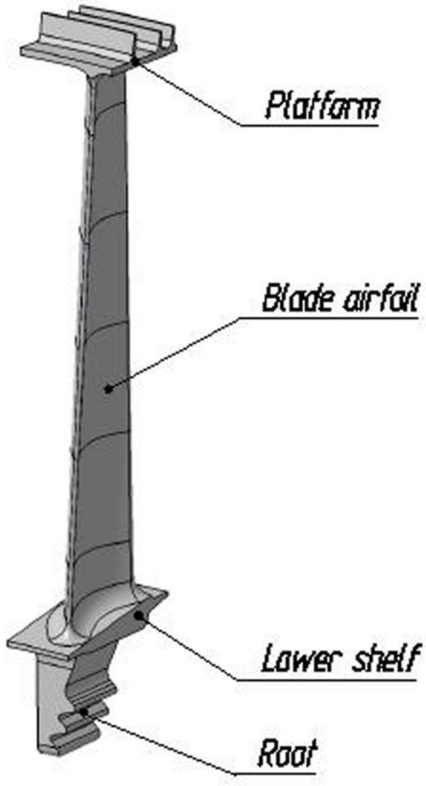

Fig.1. The working blade of the GTE turbine rotor

However, one cannot claim that the platforms surfaces contact will be kept throughout the entire operating time. The increase in the operating temperature, blades growth stretching caused by centrifugal force, the change in the position of platforms contact surfaces with vibrations of various forms will inevitably lead to the gaps emergence S, collision with power P and the following sliding (F – force of sliding friction) (see Fig. 2b).

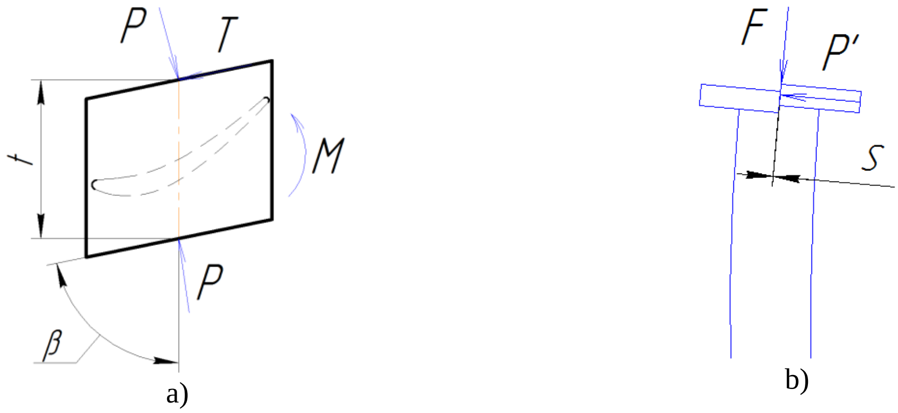

Fig. 2. Forces acting on the platform during operation

Despite significant preload, compressing platforms of adjacent blades, the latter do not remain stationary relative to each other at work. The platform displacement, caused by oscillation of the “shaft-disc-blades” system, leads to a significant wear of their working surfaces.

The analysis results of platforms wear measurement results (the platforms of shrouded pairs of the working blades after 2998 test hours (Fig. 3)), shows that the shrouded platforms wear of the left and right blades is rather uneven. It ranges from 0.005 to 0.130 mm.

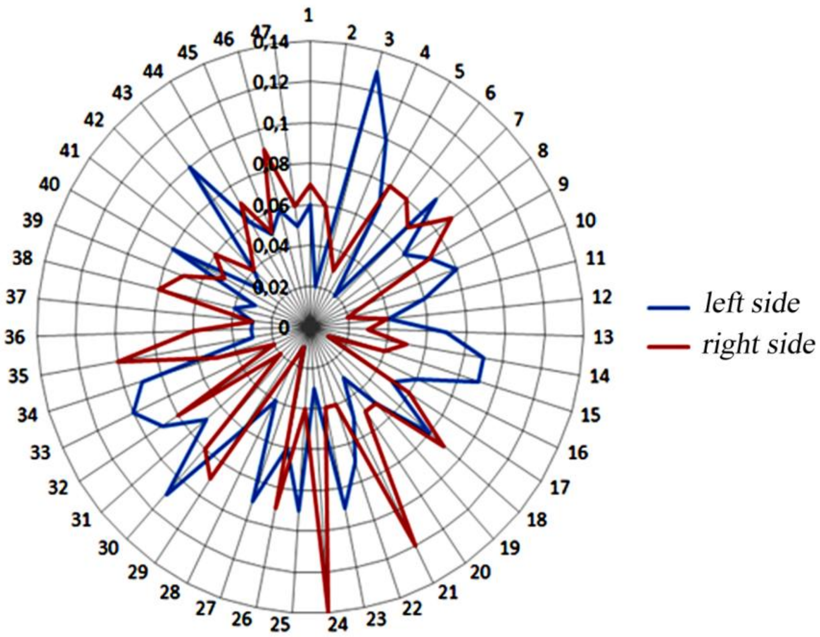

Fig.3. Actual wear of the contact surfaces of the turbine working blades platforms

Such unevenness is caused by the action of the loads in the system of the mutually superimposed oscillations of the parts, forming the turbine rotor (turbine shaft, disk and blades vibration). At the moment of the parts resonant oscillation, the amplitude of the blades oscillation as the final link, taking the vibrations of the entire system, increases by many times. This will lead to the amplitude of the platforms displacement and the contact loads, hence the platforms wear will be maximized.

To date, the decision on reducing the degree of platforms wear is possible due to the usage of wear resistant coating of the platforms contact surface, as well as to reducing the oscillation amplitude and reduction of pressure in the contact using constructive-technological methods. However, the most promising, in our view, could be a resonance oscillation elimination method in the “shaft-disc-blade” system, due to the natural frequency detuning of the system parts oscillations.

The aim of this work is to simulate the loading condition of the platforms based on the laws of “shaft-disc-blade” system oscillation and the development of a physical model for the study of the tribological processes in the contact zone.

2. Object model test and research methods

The modern methods of coupled oscillation calculation are used to determine the patterns of oscillation of the “shaft-disc-blade” system by means of the three-dimensional model of the GTE turbine rotor (Fig. 4). Modern GTE turbine rotor is a complex contraction consisting of structural elements of different stiffness, made from different materials. The considered system includes a rotor shaft and a blade wheel, equipped with twin moving blades, closed into a ring by means of platforms. To investigate the vibration stress state of the system under the influence of the forces applied, with the consideration of the impact of physical and geometrical design parameters, material properties, rotor speed and operating temperature, the numerical computational methods such as finite element method (FEM) are used.

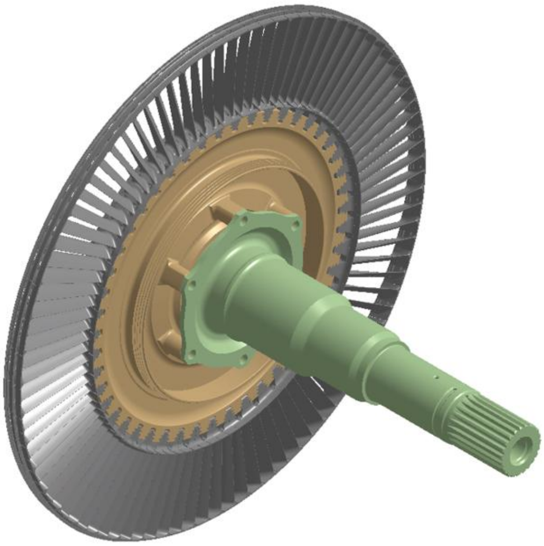

Fig.4. The three-dimensional model of the GTE turbine rotor

The three-dimensional models use allows obtaining accurate displacement amplitudes values of the nodal points of the moving blades platforms contact surfaces with the consideration of the main construction loading factors. The construction of the GTE turbine rotor design model, setting of the loading factors, as well as providing the ability to investigate the design elements concurrent working in the multiply-connected finite element model and using the contact elements allows bringing the estimated vibration stress state of the node to the real one.

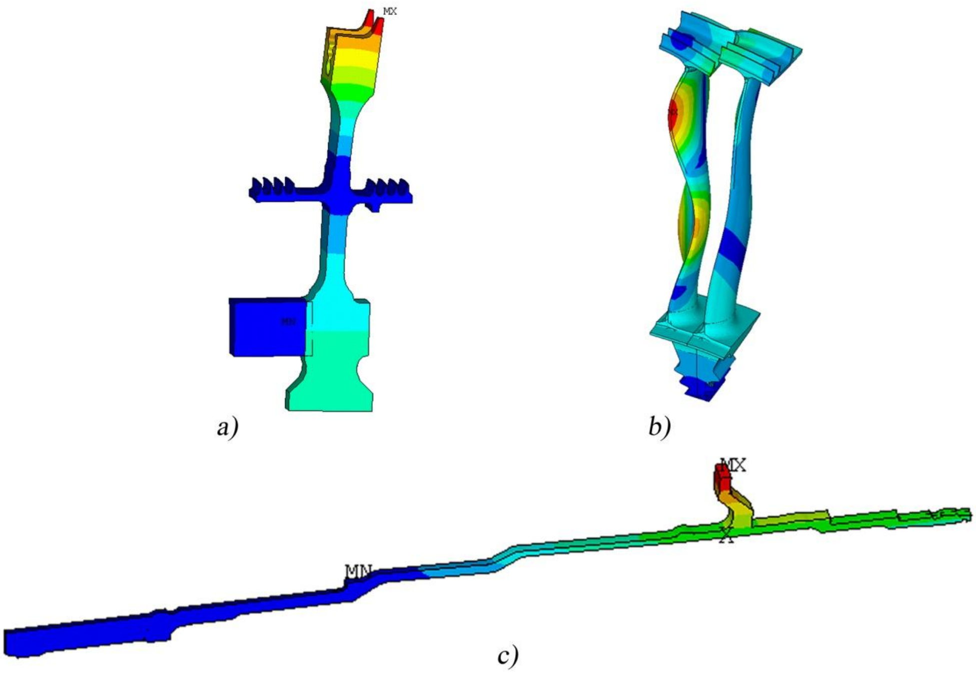

Fig.5. The analysis of the finite element models of the III step disc, left and right blades, and the LPT shaft: a) Disc; b) Blades; c) Shaft

We have created the three-dimensional models of the left and right blades, the III step disc and the low pressure turbine (LPT) shaft. The finite element models of these parts (Fig. 5) were generated by ANSYS software environment. The static and modal analysis of the unit assembly and the parts were held incoming. Independently the displacement amplitude of the platform blades nodal points was calculated. On analyzing the data, we get a picture of the nodal points' displacement in the three directions depending on the value of natural oscillation frequency of the parts (Fig. 6).

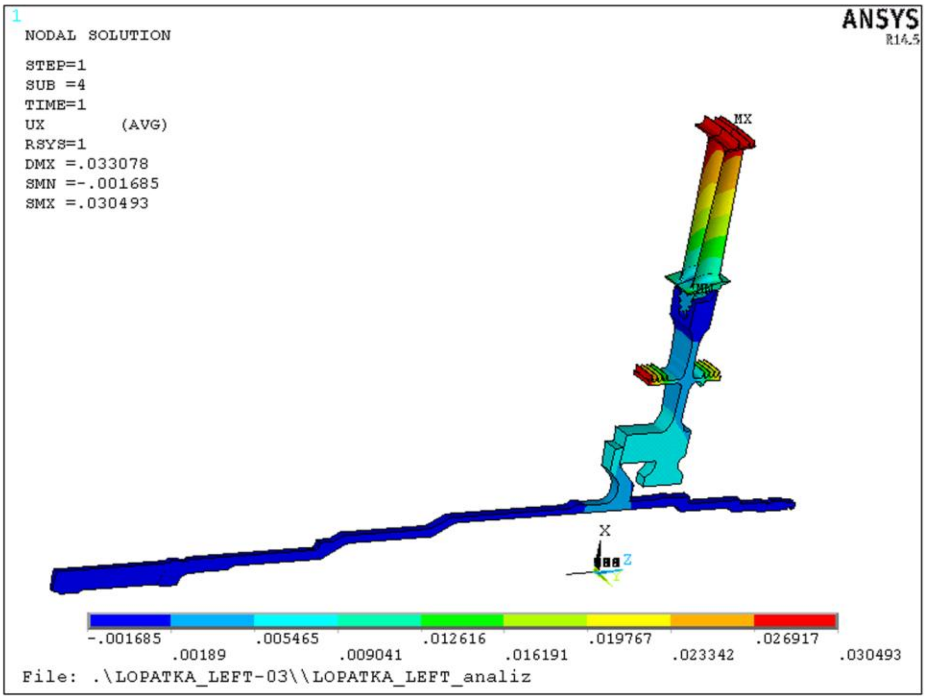

Fig.6. The analysis of the finite element models of the assembled turbine

The displacements amplitudes values of characteristic points of the blades platforms contact surfaces are used to determine the contact pressure in the contact areas, which are the initial load parameters in the wear analog modeling (Fig.7). The slip in the two orthogonally related directions is provided by the spring plate clips twist. At the same time, it imposes a constraint conforming the motion of the samples with different degrees of freedom, so that the ratio rating of these movements remains constant, due to the elastic properties of the spring clips.

The plant consists of the oscillation amplitude setting unit 1, samples attachment lug 2, and the load setting unit 3. The load setting unit 3 contains the lever 4, which is pivotally connected to the thrust rod 5 with the load spring 7 on it, connected to the stepper motor 8 via the thrust washer 6 through feed nut assembly. The samples attachment lug 2 includes cantilever fitted spring plate clips 10. They have a twist and can contain of the cross-section area a variable height and width. There are struts 11 parted by the roller 9 on the clips. Also there are samples 12 which are fixed on the struts. The longitudinal oscillation amplitude setting unit 1 consists of the cam 15 connected by coupling with the electric motor 13. By dint of the feed nut assembly the stepper motor 14 is connected through the roller 16 to the samples attachment lug 2. The plant is also equipped with the electronic unit 18 and the temperature setting unit chamber 19.

The samples are installed in the struts of the samples attachment lug. The constant distance between them in movable and immovable states is provided by the roller which also excludes the deflection effect of the spring plate clips on the completeness of working surfaces contact of the samples.

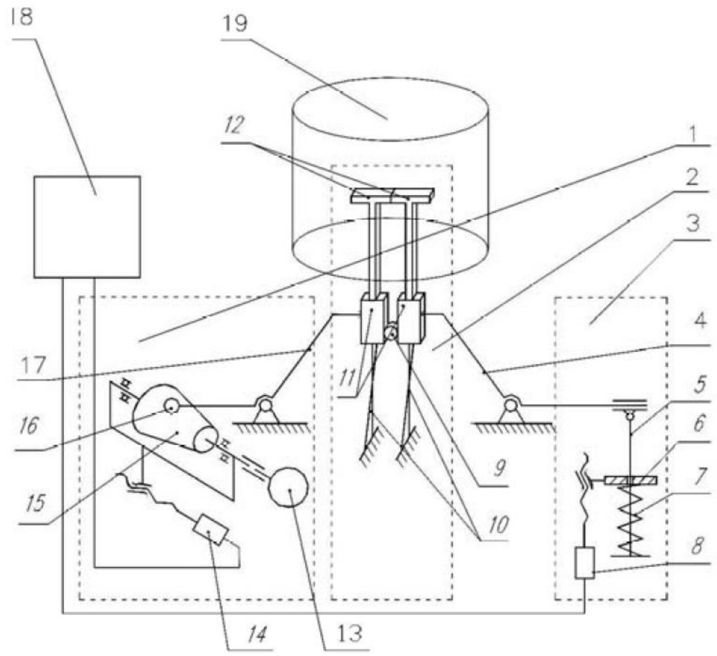

Fig.7. The scheme of the wear analog modeling: 1 –the longitudinal oscillation amplitude setting unit; 2 –samples attachment unit; 3 –load setting unit; 4 –lever; 5 –thrust rod; 6 – thrust washer; 7 – load spring; 8 – stepper motor; 9 – roller; 10 – spring plate clips; 11 – struts; 12 – samples; 13 – electric motor; 14 – stepper motor; 15 – cam; 16 – roller; 17 –tappet arm; 18 – electronic unit; 19 –temperature setting unit chamber.

A movement with the required longitudinal oscillation amplitude is provided by the amplitude setting unit. The rotation of the cam, carried out by the electric motor, results in oscillatory motion with the necessary amplitude by means of the tappet arm of the clips, struts and samples. Herewith there is a collision and sliding of the samples surfaces in the longitudinal direction. The necessary contact pressure is provided by the load transfer to samples through the lever from the load spring. It is controlled by varying the degree of compression of the latter by moving the thrust washer along the thrust rod (load setting unit). To reduce the wear of the cam 15 and pusher-arm rocker contact the roller 16is used. The wear reduction of the cam 15 contact and the beam tappet arm is provided by means of the roller 16.

The change in the load and samples displacement amplitude directly during the test can be provided by the change in the spring compression and the displacement of the cam by using the stepper motors in accordance with a program set by the hardware control unit (electronic unit).To carry out the tests at temperatures different from room temperature, the samples are placed in the chamber with the necessary temperature. The presence of the twist and the spring plate clip areas of different stiffness gives rise to vibrations of the clips and, consequently to the samples slip in the cross-section direction. As a result, the three-dimensional loaded state of samples surfaces is realized: a kick followed by slippage in the two orthogonally related directions.

3. Discussion of results

The determination of fracture patterns upon platforms contact interaction and changing of the physical and mechanical properties of the surface layers of the samples were investigated by tribospektrum method during continuous pressing and scanning by indenter of the “Micron-gamma” device developed by the NAU Ukraine. The scan method is based on continuous registration of resistance to movement of the indenter on the surface depending on the load applied [2]. The determination of statistical relationships between the resistance of local micro volumes of material to the contact deformation allows producing a comprehensive assessment of the state of the surface layer on the scan track and, in particular, allows evaluating the relative average strength on the scan track, assessing the dispersion and heterogeneity of the strength properties, and simulating the elementary acts of friction and wear processes.

The assessment of the surface layer of the materials, largely dependent on their electronic structure, was produced by a change in the electron work function. This method is one of the most informative ones for determining changes in the surface layer energy state of the materials that interact in friction process – the analysis of the value distribution of the electron work function (RWF) on the surface. This parameter is required in the calculation of the surface energy of solids. One of the areas of study of naturally complex physical and chemical processes is based on RWF change. That processes occur in the contact zone of the friction pairs [3].

The research methodology of tribological processes in the platforms also provides methods for determining:

- oscillation frequency of the individual elements and the entire “shaft-disc-blade” system;
- specific pressures in contact, consisting of static and dynamic components;
- platforms oscillation amplitudes;
- temperature loading mode;
- way of friction in oscillatory motions of the platforms, that is the basis of determining their wear rate.

Conclusion

High service life of turbine aircraft engines and power plants is of particular importance for the safety of human activity. At the same time the possibility of increasing the wear resistance of the contact surfaces of the parts due to the use of wear-resistant materials are practically exhausted. To date, no studies that have covered or solved the issue of increasing the wear resistance of components under the influence of the complex vibrations of complex mechanical systems. Note that the finite element method in tribotechnology still unused.

The suggested methodology allows establishing patterns of blades platforms wear at the turbine blade wheel, determining the parameters of contact interaction and their impact on the wear rate, and ultimately, offering constructive-technological methods of increasing the wear resistance of the platforms contact surfaces. Similarly, it can be investigated torbosopryazheniya of parts and components of various branches of mechanics, mechanical engineering, instrumentation, aerospace and transportation.

REFERENCES

1 Merkulov V.M., Ilyushchenko F.D. Development of the shrouded turbine rotor blades by taking into account the requirements of reliability and manufacturability. *Aviatsionno-kosmicheskaya tekhnika I tekhnologiya [Aerospace Engineering and Technology*], 2006, No. 9/35, pp. 86–89. [in Russian]

2 Ignatovich S.R., Zakiev I.M., Borisov D.I. Damage assessment of the surface layer of materials under cyclic loading by nanoindentation and nanosclerometry methods. *Problemy prochnosti [Strength problems*], 2006, No. 4, pp. 132 – 139. [in Russian]

3 Markov A.A. *Izmerenie raboty vykhoda elektrona pri trenii* [*Measurement of frictional electron work function*]. Moscow, Nauka Publ., 1973, pp. 28–34

Article accepted for publication 25.11.2016

UDC 621.762:536.75

PHYSICOCHEMICAL ANALYSIS OF THE PROCESSES OF FORMATION OF NANODIAMOND-BASED POLYCRYSTALLINE MATERIALS

Kheyfetz M.L.[1], Vityaz P.A.[2], Senyut V.T.[3], Kolmakov A.G.[4], Klimenko S.A.[5]

[1] "Center" SSPA of NAS of Belarus, Minsk, Belarus, mlkz@mail.ru

[2]Presidium of the National Academy of Sciences of Belarus, Minsk, Belarus, vityaz@presidium.bas-net.by

[3] Joint Institute of Mechanical Engineering of NAS of Belarus, Minsk, Belarus, vsenyut@tut.by

[4] A.A. Baykov Institute of Metallurgy and Materials Science, RAS, Moscow, Russia, Russia, agk10 @ bk.ru

[5] V.N. Bakul Institute for Superhard Materials. NAS of Ukraine, Kiev, Ukraine, atmu@ism.kiev.ua

Based on the physicochemical analysis of the carbon phase diagram, thermodynamic conditions for diamond formation are studied. The possibility and probability of various mechanisms of synthesis of diamond nanostructured materials under nonequilibrium conditions are considered. It is shown that nanodiamonds possess catalytic properties and can act as activators of the phase transformation of graphite into diamond under high pressures and temperatures. Process parameters for obtaining of diamond polycrystalline materials from detonation nanodiamond powders are defined.

***Keywords*:** polycrystalline materials, nanodiamonds, the phase diagram of carbon, physicochemical system, topological model, synthesis

Introduction

It is possible to investigate structures and phases of materials formed during synthesis and to determine their amounts by making physicochemical analysis of diagrams, which are geometric images of system property-to- structure ratios [1]. The bases for the analysis of physicochemical diagrams are formulated by N.S. Kurnakov two principles, continuity and consistency [2], as well as the third principle, the compatibility proposed by Y.G. Goroshchenko [3].

Due to non-equilibrium of high-speed processes of material synthesis, their phase diagrams are metastable [4]. The phase diagrams analysis is complicated by the fact that the processes run in short periods of time in very limited quantities at high temperature and pressure gradients, in the presence of active impurities, often acting as catalysts [5]. Therefore, it is necessary to extend the basic principles of analysis of physicochemical diagrams to study non-equilibrium processes of structure and phase material formation at macro-, meso-, micro- and nanostructure levels [1]. Phase transitions in carbon in view of their diversity in high-speed non-equilibrium or metastable processes of diamond synthesis are insufficiently studied. To actuate them, ultra-high pressures are usually required; this fact increases the cost and complicates the synthesis of diamond materials.

The work objective is to develop new approaches and process solutions with regard to obtaining nanodiamond-based polycrystalline materials using physicochemical analysis of the carbon phase diagram.

1. The phase diagram of carbon

From the viewpoint of thermodynamics of non-equilibrium open systems based on the principles of self-organization of physicochemical systems [6, 7], we consider the processes of synthesis of superhard materials [8] through the example of carbon phase diagrams. The synthesis of diamond from graphite (Fig. 1 a) at high static pressures (greater than 4.0 GPa) and temperatures (in excess of 1400 K) is carried out in the presence of catalysts, such metals as Ni, Fe, Co, etc. used as carbon-solvents [9]. However, the determination of the mechanism of diamond formation in the

.

presence of transition metals and their alloys at high static pressures was one of the most difficult problems for a long time.

The study of various physicochemical systems Me-C at high pressures has shown [9] that the diamonds originate and grow in a supersaturated solution of carbon in a metal, which in a certain period becomes supersaturated with respect to the diamond concentration, but undersaturated with respect to graphite concentration. In the study of diamond formation mechanism is necessary to consider the process of nucleation. In the synthesis of a diamond, a crystal nucleus should have a certain structure, size and surface properties.

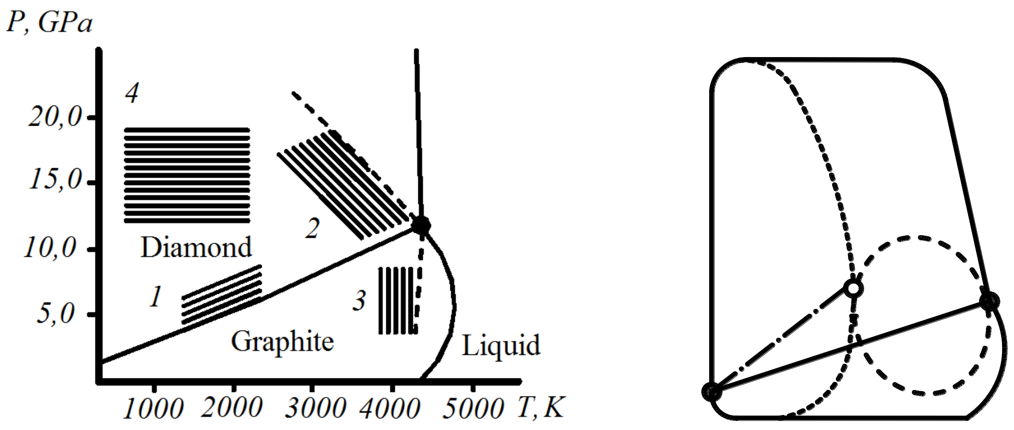

a) b)

Fig.1. The phase diagram of carbon (a) and the topological model corresponding to the physicochemical system (b): 1 – the area of the catalytic synthesis of diamond from graphite; 2 – the area of the direct transformation of graphite into diamond; 3 – the area of the direct transformation of diamond into graphite; 4 – the area of the direct transformation of graphite into lonsdaleite

When the nucleus emerges, a metastable phase is transformed into a more steady stable phase. Experiments proved [9] that the graphite crystallites are sources of diamond crystallization centers. Crystallites are graphite particles with a high degree of order. Being dissolved by the metals, these particles reach a certain size, and become centers of diamond crystallization.

Therefore, the formation of the diamond at static pressures in the system, dissolving carbon, represents the crystal growth from the oversaturated carbon solution in the molten metal; and the crystal growth is carried out by diffusion of carbon atoms through the molten metal. In this case, graphite crystallites are sources of crystallization centres [10].

At a pressure of greater than 12 GPa and a temperature above 4000 K (Fig. 1a) a direct transformation of martensite-type graphite into diamond takes place. This transition takes place when a graphite lattice transforms into a diamond one without a carbon-solvent metal. It would appear reasonable that under pressures and temperatures lower than those corresponding to conditions for the direct transition, in the presence of carbon solvent, crystal growth is possible due to carbon atoms diffusion and graphite microgroups through the molten metal.

2. The topological model of a nonequilibrium system

Based on the experimental data [5, 9], we consider the topology of the carbon phase diagram (Fig. 1b) according to the model proposed in [10], taking into account the introduction of additional components and the formation of new bonds in the physicochemical system when the number of degrees of freedom, stability and equilibrium of system are changed.

The topological model (Fig. 1 b) was developed on a phase diagram (Fig. 1a), based on the analysis of the number of degrees of freedom of the physicochemical system [10] in metastable states, taking into account the stability of non-equilibrium processes in system evolution to a stationary state.

The analysis of bonds formation in a topological model (Fig. 1b) shows that the addition a loop covering metastable states (indicated by a dashed line) to the (dark) singular point, provides a system by three degrees of freedom and the opportunity of transition to a chaotic state, without the possibility of stabilization of nonequilibrium processes. When introducing an additional component, the stabilization of the limit state (indicated by a dash-dotted line) at one of the points (the light one) is not possible as well. Therefore, only considering the new node (the light point) as the formation of a new chemical compound with the addition of lines that separate it from the solution (dashed lines), it is possible to make a provision for stability of the system in its evolution to the stationary state.

Thus, according to the considered topological model, it is confirmed that the synthesis of diamond proceeds in two ways: direct and catalytic ones; besides, the catalytic and the direct ways can be combined (transition from one to another). Consequently, depending on the conditions of formation of diamond, the synthesis of diamond from graphite can be carried out through various mechanisms:

1) under extreme conditions (conditions of direct transition of graphite into diamond without the use of carbon solvents) the transformation of a graphite lattice into a diamond one takes place (martensite-type transition);

2) in the synthesis of diamond monocrystals (at low supersaturation), crystal growth proceeds due to the diffusion of carbon atoms through a molten metal;

3) in the synthesis of polycrystalline diamonds (at high supersaturation), crystal growth can proceed simultaneously due to diffusion of graphite microgroups and carbon atoms through a molten metal [4, 9].

In the case of graphite and diamond crystallites of small sizes, for which the contribution of the surface energy to the thermodynamic potential is significant, the conditions of graphite-diamond phase equilibrium differ essentially from the predicted by the stated carbon phase diagram. There are assumptions confirmed by calculations [11], according to which, for small size of nanoparticles it is diamond rather than graphite that is a thermodynamically stable form of carbon.

In this case, a diamond stability boundary should be circumscribed by a surface in the "pressure-temperature-crystallite size" space [12].

When the crystallite size is reduced by less than 10 nm, the phase equilibrium surface deviates considerably from the plane in the direction of low pressures; and when its size is about 1 nm, diamond is stable as well in the absence of external pressure to temperatures of about 2000 K. The size area in which one would expect diamond-structured crystallites to occur at "zero" pressure, is in the range of 0.3-1.5 nm.

3. Catalytic properties of nanodiamonds

Diamond possesses high surface energy, which for different facets is from 3 to 10 J/m^2 [9, 13]. Estimates show that the value of nanodiamond surface energy is in the range of 1100-3900 kJ/kg. In practice, not individual particles but particle aggregates of nanodiamonds are used, which sizes are larger than 100 nm and can reach 1 micron. The active surface is reduced respectively (for 0.1-0.5 micron particles which are formed during nanodiamonds sintering under high pressures, their surface area is by several times less than that of the initial particles).

Detonation-synthesized nanodiamonds represent one of the most chemically reactive of the known forms of carbon with a highly active surface state with the value of up to 400 m^2/g; they can make for breaking π-bonds on the surface of graphite particles under high-pressure conditions. Each nanodiamond crystallite has a large number of unpaired electrons (3-7)•10^{19} spin/cm^3, and it is a powerful multiradical [13, 14].

.

After chemical removal of impurities and non-diamond carbon forms, on the surface of nanodiamonds there are 1-2 closed graphene layers [14]. The annealing of nanodiamonds in vacuum results in an increase in the number of graphene layers and the formation of onionated carbon globules of fullerene-like structure. Investigation of chemical state of the carbon atoms on the surface of nanodiamonds using Auger spectroscopy showed that in this case a previously unknown chemical state of carbon atoms localized in a graphene monolayer is realized. A similar state in $\sigma_s^1\sigma_p^2\pi^1$ graphite is realized as well, but unlike the graphite in the case of nanodiamonds there is no overlapping of π-states of carbon atoms. The surface state of nanodiamonds determines their catalytic activity and makes for $sp^2 \rightarrow sp^3$ transition in the graphite particles contacting nanodiamond crystallites.

In this context, a promising option of obtaining nanostructured polycrystalline diamond powders is the use of nanodiamonds coated with nanostructured carbon [13]. On the one hand, the nanodiamond particles are ready centers of crystallization in the synthesis of diamond using metal catalysts. On the other hand, nanodiamonds themselves may act as activators making for transformation of graphite particles under high pressures and temperatures.

4. Thermobaric treatment of graphitized surface nanodiamonds

The synthesis scheme when the carbon material is applied directly to the surface of the nanodiamond particles seems the most preferable. In its turn, it makes possible:

- to increase the contact area of nano-dispersed particles of diamond and graphite (graphite-like carbon);
- to create conditions for a coherent intergrowth at the "diamond particle-graphite particle" boundary;
- to provide a direct contact of the surface of the diamond and graphite to increase the probability of diamond nucleation due to autoepitaxy;
- to minimize the amount of impurities in the obtained diamond particles.

Based on the carbon phase diagram, which is established for ideal structures of perfect crystals, conditions of possible mutual transformation of graphite and diamond are defined. Besides thermodynamic conditions of the process probability, the rate of such a transformation is important; and it may be very slow [9-11]. Thus, although at low pressures and temperatures the transformation of diamond into graphite is accompanied by decrease in the free energy, and it is thermodynamically quite possible, this transformation rate is low, and the diamond is remained unchanged for a long time. Direct transformation of macroscopic graphite into diamond proceeds at very high pressures up to 15 GPa. So far as the crystal sizes reduce, the energy of facets, edges and tips makes greater contribution to the total free energy of the system. With fairly small crystallite sizes, the contribution of the surface energy to the total energy becomes very significant.

Thermodynamic calculations show [14, 15] that thin layers of graphite deposited on the surface of diamond crystals are especially easy to transform into diamond due to the decrease in the free energy of the system. Therefore, the use of nanodiamonds coated with thin layers of carbon (graphite) will make for sintering of nanodiamonds accompanied by formation of diamond particles of micron range.

Conditions and regimes of synthesis of diamond polycrystalline materials based on nanodiamond particles modified with non-diamond carbon forms were studied experimentally. Nanodiamonds, the surface of which was coated with a thin layer of non-diamond carbon of about 1 nm thick, were sintered under high pressure and temperature conditions. The coating was formed by annealing purified nanodiamonds in vacuum at 10^{-3} mm of mercury in the temperature range of 900-1100°C. The resulting "nanodiamond-nanographite" composite powder was a metastable system, characterized by excess surface energy. The thermal treatment of the powder under pressure was carried out both in the diamond and graphite stability areas. When processing the obtained "nanodiamond-nanographite" composite powder under high pressures and temperatures, larger particles of diamond of sub-micron and micron size with retained nanostructure were observed to form (Fig. 2).

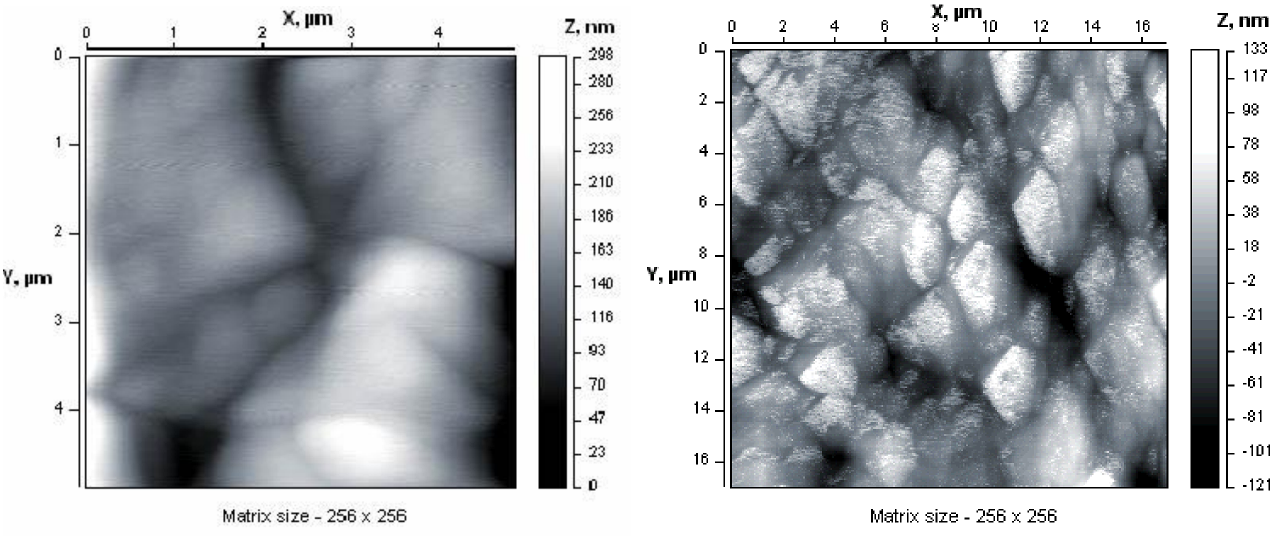

a) b)

Fig.2. The structure of the polycrystalline nanodiamonds obtained from "nanodiamond-nanographite" composite powder: a) at a pressure of 2 GPa; b) at a pressure of 4 GPa

In the material obtained at a pressure of 2 GPa, diamond crystallite sizes increased slightly compared to the original sizes of the nanodiamond particles and were of 20-30 nm; the polycrystalline particle sizes were 1-1.5 microns (Fig 2a). In polycrystalline samples obtained at pressures up to 4 GPa, polycrystalline diamond particles reached the size of 2-3 microns (Fig. 2b). With increasing temperature up to 2300°C at a pressure of 7 GPa, the formation of polycrystalline diamond particles up to 10 microns and diamond crystallites of up to 150-100 nm sizes was observed.

Conclusion

1. According to the considered topological model, it is confirmed that the synthesis of diamond proceeds in two ways: direct and catalytic ones; besides, the catalytic and the direct ways can be combined (transition from one way to another).

2. In the case of graphite and diamond crystals of small sizes, for which the contribution of the surface energy to the thermodynamic potential is significant, the phase equilibrium conditions graphite-diamond differ essentially from the predicted by the stated carbon phase diagram. The size area of carbon particles in which diamond-structure crystallites are expected to occur at "zero" pressure, is in the range of 0.3-1.5 nm.

3. During processing of nanodiamond-based "nanodiamond-nanographite" composite powder under high pressures and temperatures, nanostructured diamond particles of submicron and micron sizes are formed.

Acknowledgements

The research was supported by "Physical material science, new materials and technologies" State Research Program, subprogram "Nanomaterials and Nanotechnologies", task 2.50 and T16R-176 grant of Belarusian Republican Foundation for Fundamental Research.

REFERENCES

1 Anosov V.Ya., Ozerova M.I., Fialkov Yu.Ya. *Fundamentals of physicochemical analysis*. Moscow, Science, 1976, 504 p.

2 Kurnakov N.S. *Introduction to physicochemical analysis*. M.-L.: USSR SA, 1940, 562 p.

3 Goroshchenko Ya.G. *Physicochemical analysis of homogeneous and heterogeneous systems*. Kiev, Naukova Dumka, 1978, 490 p.

4 Kheyfetz M.L. *Combined treatment process design*. Moscow, Mechanical Engineering, 2005, 272 p.

5 Vityaz P.A., Gritsuk V.D., Senyut V.T. *Synthesis and use of superhard materials*. Minsk, Belarusian Science, 2005, 359 p.

6 Vityaz P.A., Ilyushchenko A.F., Kheyfetz M.L., Chizhik S.A., Solntsev K.A., Kolmakov A.G., Alymov M.I., Barinov S.M. *Technologies of nanostructured construction materials and coatings*. Minsk: Belarussian Science, 2011, 283 p.

7 Berge P., Pomeau Y., Vidal Ch. *Order in chaos: On the deterministic approach to turbulence*. Moscow, Mir, 1991, 368 p.

8 Glensdorf P., Prigozhin I. *Thermodynamic theory of structure, stability and fluctuations*. Moscow, Mir, 1973, 280 p.

9 Novikov N.V., Fedoseyev D.V., Shulzhenko A.A., Bogatyreva, G.P. *Diamond synthesis*. Kiev, Naukova Dumka, 1987, 158 p.

10 Novikov N.V. et al. *Synthetic superhard materials. V. 1. Synthesis of superhard materials*. Kiev, Naukova Dumka, 1986, 175 p.

11 Vityaz P.A., Khefetz M.L., Senyut V.T. *Thermodynamics of processes of synthesis and production technology of nanostructured diamond materials. Chapter 8 in the book: Advanced materials and technologies.* Ed. by V.V. Klubovich. Vitebsk: VSTU, 2013, pp. 152-171.

12 Gamarnik M.Y. Energetical preference of diamond nanoparticle. *Phys. Rev. B.*, 1996, Vol. 54, No.3, pp. 2150 - 2156.

13 Chaikovsky E.F., Rosenberg G.H. The phase diagram of carbon and the possibility to obtain diamond at low pressures. *USSR SA Proceedings*, 1984, Vol. 279, No. 6, pp.1372-1375.

14 Vityaz P.A., Zhornik V.I., Ilyushchenko A.F., Senyut V.T., Komarov A.I., Korzenevsky A.P., Ivakhnik A.V. *Detonation-synthesized nanodiamonds: obtaining and use*. Minsk, 2013, 381 p.

15 Dolmatov V.Yu., *Detonation nanodiamonds. Obtaining, properties and use*. St. Petersburg, SPO "Professional", 2011, 536 p.

16 Fedoseyev D.V., Deryagin B.V., Varshavskaya I.G., Semenova-Tyan-Shanskaya A.S. *Diamond crystallization*. Moscow, Nauka, 1984, 136 p.

Article accepted for publication 21.10.2016

UDC 539.216.2; 541.145

INFLUENCE OF ANNEALING TEMPERATURE ON PHOTOPHYSICAL PROPERTIES OF NANOSTRUCTURED TiO_2 FILMS

N.Kh. Ibrayev[1], T.M. Serikov[1], A.K. Zeinidenov[1], K.A. Kuterbekov[2], K.Zh. Bekmyrza[2]

[1]Institute of Molecular Nanophotonics, E.A. Buketov Karaganda State University, Karaganda, Kazakhstan, niazibrayev@mail.ru
[2]L.N. Gumilyov Eurasian National University, Astana, Kazakhstan

The spectral and kinetic characteristics of the photoluminescence of titanium dioxide films were studied. At ultraviolet excitation of films the luminescence spectrum characteristic of the anatase structure is observed. Heat treatment of the samples at temperature of *1273 K leads to a long-wavelength shift of the photoluminescence band with a maximum wavelength of 850 nm that indicates the formation of the rutile crystal structure. The current-voltage characteristics of titanium dioxide films were measured. It is found that the films with the anatase structure have a higher photocurrent than the films with the rutile structure. The photocatalytic properties of titanium dioxide films were studied. It is shown that titanium dioxide films with anatase structure have the highest photocatalytic activity.*

Keywords: titanium dioxide, anatase, rutile, luminescence, current-voltage characteristics, photocatalysis

Introduction

In recent years the interest in the nanomaterials based on titanium dioxide was steadily growing due to their unique physical and chemical properties. This is due to the widespread use of TiO_2 in a variety of practical problems. Thus, nanomaterials based on titanium dioxide are used in photocatalysis, solar energy, water and air purification from organic impurities, as well as for destruction of bacteria [1, 2].

Electronic structure and the structure of energy bands of crystalline TiO_2 are studied in detail and results were shown in several papers [3, 4]. Titanium dioxide has a wide band gap and its photocatalytic properties begin to appear during irradiation in the ultraviolet region of the spectrum. It is known that powder particles of TiO_2 (P25, Hombikat UV-100) have the highest catalytic activity. It is believed that its high activity is due to an effective separation of charge carriers at the interface of two semiconductors [5]. Despite the fact that the powder particles are highly efficient and inexpensive photocatalysts the work on producing TiO_2 with improved photocatalytic properties is continuing [6]. Therefore, at the present time for expansion of the application of these catalysts the main focus is on creating of thin films based on TiO_2, as in this form it is easier to use TiO_2 for conducting photocatalysis in a variety of conditions.

This paper presents the results of a study of luminescent, electrophysical and photocatalytic properties of nanostructured films of titanium dioxide.

2. Preparation of samples and experimental technique

For obtaining TiO_2 film the solution containing powder of colloidal TiO_2 (Sigma Aldrich) was prepared. The solution was prepared in the following way: colloidal TiO_2 powder was ground in a porcelain mortar with a small amount of deionized water and acetone, taken in a volume ratio of 10:1. Acetone was added to prevent clumping of the particles. After the formation of a homogeneous viscous paste the solution of titanium dioxide nanoparticles was deposited on the surface of the substrate by the method of doctor-blading. Then, the resulting films were subjected to heat treatment at a temperature of 773 and 1273 K during 2 hours.

.

The microstructure and the thickness of the films were studied on the cleaved samples on a scanning electron microscope (SEM) TESCAN Mira 3. The measurements of spectral and kinetic characteristics of TiO_2 films were performed on an automated spectral and kinetic installation with the registration in photon counting mode. Stimulation was performed by a nitrogen laser AIL 3 (λ_{gen}=337 nm, $E=30$ *mJ*, τ_{imp}=10 ns).

Measurement of CVC films formed by NPs and NTs titanium dioxide with the anatase structure and rutile was performed using a potentiostat (ELINS, Russia) in a standard three-electrode cell. The nanostructures of titanium dioxide were used as a working electrode, they were deposited on the surface of the glass substrate with a conductive layer of FTO. The opposite electrode was platinum foil and as a comparison AgCl electrode was used. Measurements were carried out in an electrolyte of 0.1 M NaOH in a quartz cuvette at room temperature. When registering photocurrent titanium dioxide films were irradiated with light from a xenon lamp of 80 W. The long-wavelength part of the spectrum was cut off light filter UFS-6.

Electrical and transport properties of titanium dioxide films were investigated by measurement of the photocurrent and impedance of the electrochemical cell. Measurements by the method of electrochemical impedance spectroscopy were carried out under standard simulated solar radiation (Air Mass (AM) 1.5) at impedancometry Z-500PRO (Elins, Russia). The amplitude of the applied sinusoidal signal was 20 mV and the frequency was varied from 1 MHz to 100 MHz. The absorption spectra of dye of methylene blue films were prepared by a dual-beam spectrophotometer Cary 300 UV-Vis.

3. Results and discussion

The morphology of surface and cross cleavage of TiO_2 films obtained at an annealing temperature of 773 and 1273 K are shown in Figure 1. The figure shows that the surface of the film has a granular structure. Also it is evident that the film annealed at 1273 K (Figure 1 b) has less granular structure than the film that was subjected to thermal annealing at a temperature of 773 K (Figure 1 a). This is probably due to the fact that under the influence of heat some of the particles sintered. From the cross cleavage of samples it is evident that the thickness of the films was 7-8 microns.

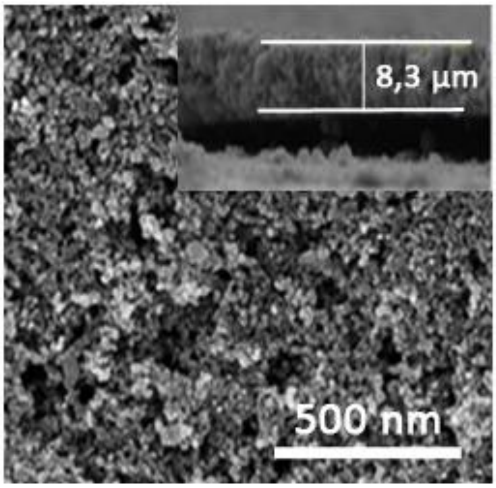

a)

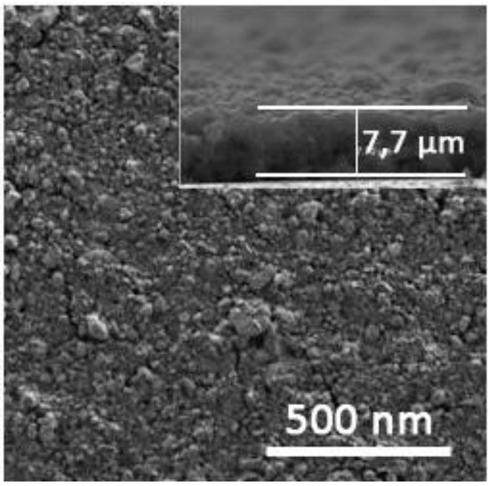

b)

Fig.1. SEM images of TiO_2 films.

It is known that before heat treatment the TiO_2 structure is amorphous. Crystallization of the structure occurs during thermal annealing of the sample starting with the temperature of 553K. At a temperature of 773 K the amorphous phase transforms to the anatase structure. At further annealing to 1273 K anatase structure is completely transformed into the rutile phase [7].

Figure 2 shows the luminescence spectra of TiO_2 films annealed at 773 K. The measurements were performed in an optical cryostat which can cool the sample to the boiling point of liquid nitrogen. Before the measurements the sample was placed in the cryostat, it was pre-evacuated to residual pressure $P=5*10^{-4}$ mbar. When photoexcitation of TiO_2 samples with anatase form of the crystal cell at room temperature luminescence was not observed. After cooling the samples to T=200 K the luminescence with a maximum spectrum at a wavelength of 525 nm is observed. By lowering the temperature of the sample to 80 K the luminescence intensity increases.

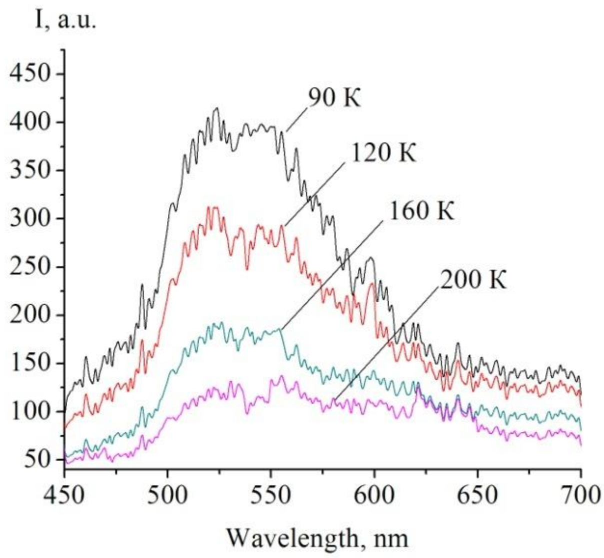

Fig.2. The luminescence spectra of TiO_2 films with anatase structure

Measurements of the kinetics of the luminescence were carried out on the wavelength of 530 nm in the temperature range of 90-200 K. The kinetic curve is generally non-exponential. Lifetimes of excited states, calculated from the exponential part of the decay curves are shown in Table 1.

Table 1. The effect of temperature on the luminescent properties of TiO_2 films with anatase structure.

T, K	I_{max}^{lum}, a.u.	λ_{max}^{lum}, nm	$\Delta\lambda_{1/2}^{lum}$, nm	τ, ms
90	419	525	114	3.19
120	322	525	120	2.77
160	266	525	133	1.26
200	197	525	237	1.18

Figure 3 shows the luminescence spectra of TiO_2 films annealed at 1273 K. It can be seen that the photoluminescence spectra contain a broad band in the region of 750-950 nm that indicates the presence of multiple emission centers. As a result of thermal effects on the films a phase transition of the crystalline cell from anatase to rutile takes place. This leads to the fact that the emission band with a maximum 525 nm disappears, at the same time in the emission spectrum a new band with a maximum 850 nm appears. According to the paper [8] such behavior of TiO_2 luminescence

.

spectrum is due to the formation of additional emission centers associated with oxygen vacancies in different charge states.

Lifetimes of the excited states calculated from the exponential curves of the TiO_2 damping films are presented in Table 2.

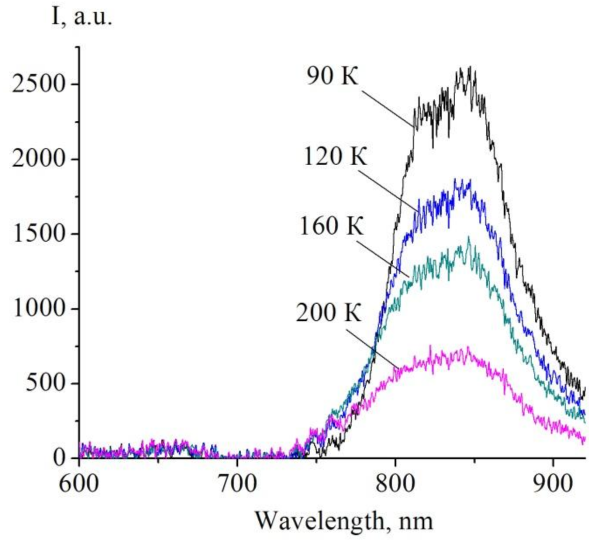

Fig.3. The luminescence spectra of TiO_2 films with rutile structure

Table 2. The effect of temperature on the luminescent properties of TiO_2 films with rutile structure.

	T, K	$I_{\max}^{lum}$, a.u.	$\lambda_{\max}^{lum}$, nm	$\Delta\lambda_{1/2}^{lum}$, nm	τ, ms
1	90	2653	850	78	7.5
2	120	1886	850	87	3.9
3	160	1509	850	88	2.3
4	200	762	850	96	1.7

The current-voltage characteristics of pure TiO_2 films with anatase and rutile structure are presented in Figure 4. The figure shows that for TiO_2 films the value of the photocurrent for anatase is 4 times higher than that for rutile.

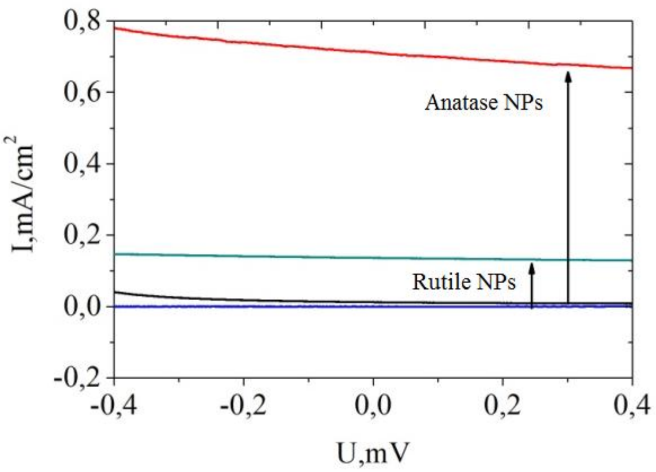

Fig.4. The current-voltage characteristics of TiO_2 films

The studies of electrical and transport properties of TiO_2 films were carried out by measuring the electrical impedance. Figure 5 shows hodographs of impedance in Nyquist coordinates for TiO_2 films with anatase and rutile structure.

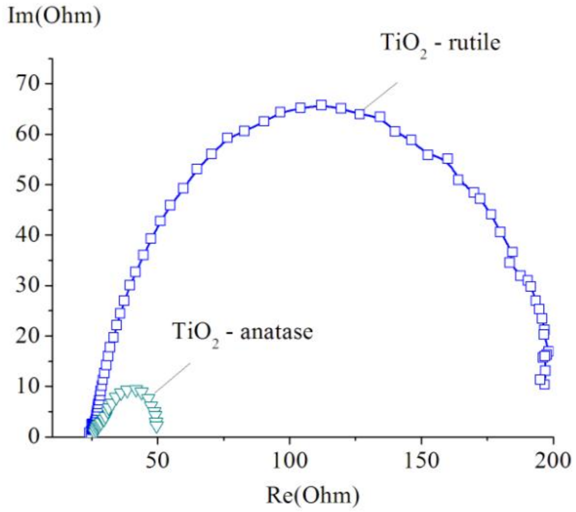

Fig.5. Impedance spectra of TiO_2 films with anatase and rutile structure

From the presented data it is evident that the impedance spectrum is composed of multiple circles. Using the method described in [9, 10] from a central arc of impedance spectra effective diffusion coefficient of electrons D_{eff}, the effective speed of recombination k_{eff} , effective lifetime of electron τ_{eff}, resistance of electron transport in the film of titanium dioxide R_w, charge transfer resistance R_k associated with the recombination of the electron were calculated. The results are shown in Table 3.

Table 3. Electrical and transport options of TiO_2 films

Films	D_{eff}	k_{eff} , (s^{-1})	τ_{eff} , (s)	R_k , (Ohm)	R_w , (Ohm)
TiO_2 (anatase)	$9.9*10^{-5}$	14.0	0.07	22.0	26
TiO_2 (rutile)	$4.7*10^{-5}$	57.0	0.02	175.0	26

From the tabulated data it is evident that the electron transport resistance in TiO_2 (R_w) for films of anatase and rutile structures does not change. At the same time the rate of recombination (k_{eff}) in films with anatase structure is less than k_{eff} films of TiO_2 with rutile structure. The magnitude of the recombination resistance shown in Table 3 indicates a high rate of recombination of charges in films with rutile structure. This is also evidenced by the low efficiency of the electron lifetime in films with rutile structure.

In accordance with the formula $k_{eff}=2N_sk_r$ (N_s - density of electrons at the defect levels of energy (cm^{-3}), k_r - recombination rate constant (cm^3s^{-1}) into electrolyte of electrons from TiO_2 defective levels [10]) it can be concluded that in the rutile films the concentration of defects through which the recombination processes take place is higher than in anatase.

Photocatalytic activity of TiO_2 films with anatase and rutile structures was measured in the model reaction of decomposition of the methylene blue dye under irradiation of UV light from a xenon lamp (Figure 6). Obtained data indicate that TiO_2 films with rutile structure have a sufficiently high catalytic activity in the oxidation reaction of methylene blue. At the same time, when excited by ultraviolet radiation activity is lower than the activity of TiO_2 films with anatase

.

structure. This may be due to the fact that TiO_2 contains the defects which can serve as traps and recombination centers of charge carriers.

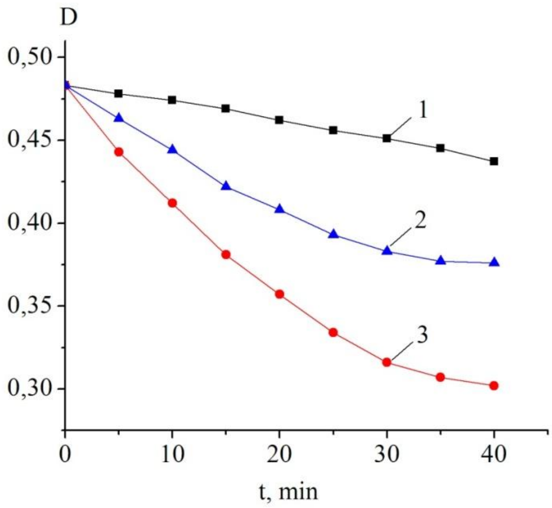

Fig.6. Photocatalytic activity of the samples in the oxidation reaction of methylene blue: 1 - alcoholic solution of methylene blue; 2 - TiO_2 film with rutile structure; 3 - TiO_2 film with anatase structure.

Conclusion

In the paper the luminescence and photovoltaic properties of TiO_2 films were examined. For samples annealed at T=773 K, when excited by a nitrogen laser luminescence is observed with a spectrum characteristic of the anatase structure.

Annealing of the samples at T=1273 K leads to a long-wavelength shift of the photoluminescence band with maximum at 850 nm wavelength which corresponds to the rutile structure. For the anatase the duration of films luminescence of NPs was 3 ms. The lifetime of photoluminescence of rutile films is higher than the lifetime of luminescence of anatase structure.

The current-voltage characteristics of TiO_2 films of different structures were measured from which it follows that the films of anatase structure have a higher photocurrent than films with rutile structure. It is found that the films of anatase structure have higher photocatalytic activity than the films of rutile structure.

ACKNOWLEDGEMENTS

The research was supported by Grant № 303 of 13.05.2016 of the Ministry of Education and Science of the Republic of Kazakhstan within the program target financing scientific and technical programs «The development of hydrogen energy and technologies in the Republic of Kazakhstan», 2015 - 2017.

REFERENCES

1 Abdel-Wahab A.-M.A., Gaber A.E.-A.M. TiO_2-photocatalytic oxidation of selected heterocyclic sulfur compounds. *J. Photochem. Photobiol. A.*, 1998, **V.114,** pp. 213–218.

2 Ollis D.F., Al-Ekabi H. *Photocatalytic purification of water and air*. Amsterdam, Elsevier, 1993, 432p.

3 Mo S., Ching W. Electronic and optical properties of three phases of titanium dioxide: Rutile, anatase, and brookite. *Physical Review* B., 1995, **V.51.** № 19, pp.13023-13032.

4 Landmann M., Rauls E., Schmidt W.G. The electronic structure and optical response of rutil, anatase and brookite TiO_2. *Journal of Physics: Condensed Matter*, 2012, **V.24,** № 19, pp.1-6.

5 Gerischer H., Heller A. Photocatalytic oxidation of organic molecules at TiO_2 particles by sunlight in aerated water. *Journal of the Electrochemical Society*, 1992, **V.139,** №1, pp.113-118.

6 Kaneko M., Okura I. *Photocatalysis: science and technology*. New York, Springer-Verlag, 2002, 134p.

7 Zhang V., Zhou M., Fu Q. et. al. Observation of defect state in highly ordered titanium dioxide nanotube arrays. *Nanotechnology*, 2014, **V. 25,** pp. 275603.

8 Lin J., Chen J., Chen X. Facile fabrication of free-standing TiO2 nanotube membranes with both ends open via self-detaching anodization. *Electrochemistry Communications*, 2010, **V. 12,** pp. 1062.

9 Fabregat-Santiago F., Bisquert J., Garcia-Belmonte G. et. al. Influence of electrolyte in transport and recombination in dye-sensitized solar cells studied by impedance spectroscopy. *Solar Energy Materials & Solar Cells*, 2005, **V.87,** pp.117.

10 Adachi M., Sakamoto M., Jiu J. Determination of parameters of electron transport in dye-sensitized solar cells using electrochemical impedance spectroscopy. *Journal Physics Chemistry* B., 2006, **V.110,** pp. 13872.

Article accepted for publication 11.11.2016

.

UDC 669.539.382.2

ULTRASOUND CONTROL AND STUDY OF PHYSICAL MODEL CONDUCT OF 20 GL STEEL TENSILE

Pavlov A.M., Agelmenev M.E , Zhilkashinova A.M., Pavlov A.V., Satbaeva Z.A.

East Kazakhstan State University named after S. Amanzholov, National scientific laboratory of collective use, East Kazakhstan region, Ust-Kamenogorsk, Kazakhstan, amaxut@mail.ru

One of the most important problems in solid state physics is searching new patterns in the performance of the physical characteristics of metals in the external radiation on them. This research deals characteristics of ultrasonic testing on plastic molded metal, based on the connection speed of ultrasound with elasticity module and the analysis of the stress-strain on the example of steel 20GL brand. According to the results of the experiment there is a new theoretical basis of a physical model of metal pattern in tension. It was found that the previously proposed a parabolic response function is not applicable when there is maximum deformation. It was given an analytical expression for the response function. It is shown that as the response function fits the function displayed in the form of an ellipse. It was found that exactly that function describes the experimental data satisfactorily.

Keywords: elastic constants, elastic modulus, plastic deformation, the longitudinal ultrasonic wave, tensile test, steel 20GL.

Introduction

Today the research and ultrasound technique are used, for example, to detect violations of the metal continuity, it cracks and weld defects etc. Recently, an interest in it has increased even more, as a link between acoustic and strength properties of metals.

Currently, methods of non-destructive testing in toughness and elasticity are considered for structural steels pearlite as a class issued in the form of forgings and rolled [3], for a low-carbon and low-alloy steels after rolling and heat treatment [4]. In this research was [5] made a special study of the correlations between the ultrasonic velocity, hardness and toughness in hot-rolled steel 09G2S. In contrast to the above forgings and rolled, the heterogeneity of cast metal structure reduces the accuracy of ultrasonic testing, therefore, is urgent search for new methods of ultrasonic cast metal control. This subject is partially considered in the research [6], which offers acoustic emission method for non-destructive testing of internal defects in molded parts of rolling stock.

The continuously increasing level of quality requirements for parts involves the development of new physical models of the metals pattern when exposed to shock and tensile loads. In this sense, interesting presentation of JF Bell [1, 2], which proves that the function describing the dependence of the stress-strain in plasticity, is a parabola.

The aim is a relationship of ultrasonic velocity with the plastic properties of cast metal. A new model of destruction of metal samples after stretching was developed.

1. The methodology of the analysis.

The propagation velocity of longitudinal ultrasonic wave generated by the transducer with a frequency of 4 MHz, measured on the device UST A 1209 using a calibration mode on a given metal thickness. For that, we prepared samples with KCU hub, according to GOST 9454 ("GOST" means in Russian “ГОСТ”) [7] with different heats of steel 20GL brand, in the amount of 20 peaces. Then on the sample measured the velocity of propagation of longitudinal and transverse ultrasonic waves at ambient and low temperatures. Static tensile test cylindrical samples 10 mm in diameter was performed on the same samples at room temperature in a car one main static preloading «WAW-600C» with stretching chart entry in accordance with GOST 1497 [8], with the measurement of physical yield strength, ultimate strength, relative uniform elongation and contraction.

2. Results and discussion.

Modulus of elasticity (Young's modulus) can be determined by stretching the diagram and the propagation velocity of ultrasonic waves in the metal [9]. Generally speaking, the velocity of longitudinal sound wave has two meanings. If the wave propagates in a solid medium, from Lame equations an expression for the speed of sound. In fact, the Lame equation is

$$\rho \frac{\partial^2 \vec{\omega}}{\partial t^2} = (\lambda + \mu)\, grad\ div \vec{\omega} + \mu \Delta \vec{\omega}$$

where the vector displacement of the rigid body, λ and μ are Lame coefficients.

In the case of longitudinal wave $rot \vec{\omega} = 0$, a $div \vec{\omega} \neq 0$ and as

$grad\ div \vec{\omega} = rot\ rot \vec{\omega} + \Delta \vec{\omega} = \Delta \vec{\omega}$, so

$$\frac{\partial^2 \vec{\omega}}{\partial t^2} = \frac{\lambda + 2\mu}{\rho} \Delta \vec{\omega}$$

It shows that the longitudinal wave velocity in a solid sample is:

$$C = (\lambda + 2\mu)^{\frac{1}{2}} \rho^{-\frac{1}{2}} = \sqrt{\frac{\lambda + 2\mu}{\rho}}$$

Young's modulus and shear modulus related to the Lame coefficients of relations:

$$E = \frac{\mu (3\lambda + 2\mu)}{\lambda + \mu}; \quad N = \mu$$

So to find E is necessary to know the shear modulus. If the wave travels along a narrow rod, then the equation of wave propagation is:

$$\rho \frac{\partial^2 \omega}{\partial t^2} = E \frac{\partial^2 \omega}{\partial x^2}$$

and the velocity of the wave is equal to:

$$C = (E/\rho)^{\frac{1}{2}}. \qquad (1)$$

According to formula (1)

$$E = C^2 \cdot \rho \qquad (2)$$

.

According to this formula (2) the elastic modulus was determined. After analyzing a large number of heats, empirically obtained values with an accuracy of ± 12%, were compared with the calculated data on the chart stretching. It was found that the accuracy of the result adversely affect the internal defects in the metal, in the form of foreign inclusions, cracks and blowholes, and the grain size of the structural components. For example, in samples from 9 score scale grain GOST 5639 [10], the measurement accuracy is higher than a score of 8 samples.

Let us return to the physical model tests the tensile rupture. In theory, [1, 2] is apparently not considered the maximum voltage and to break the sample. For this reason, the response function, i.e. function in the plastic region is a non-parabola, and an ellipse. Let us consider this statement. The orientation of the ellipse is shown in Figure 1.

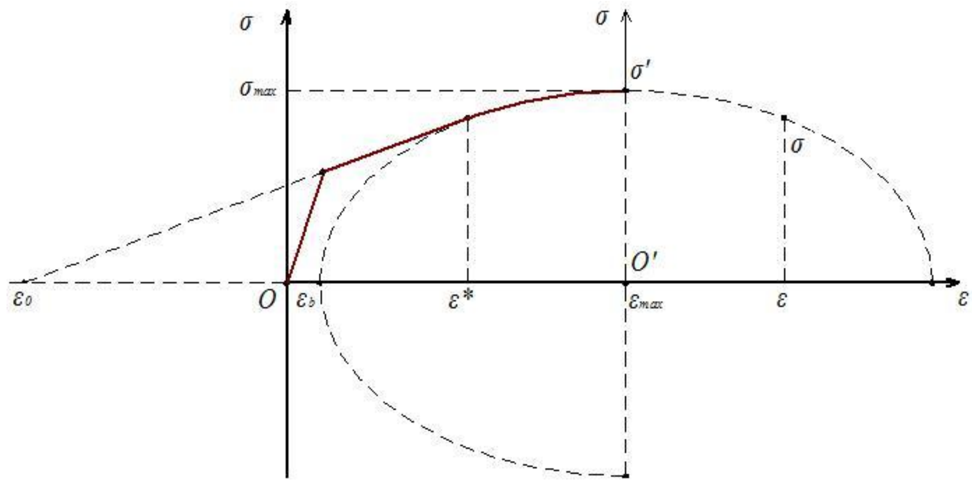

Fig.1. Schematically shows the response ellipse function.

Figure 1 shows that the axes ($\varepsilon'\sigma'$), passing through a point of the ellipse equation is:

$$\frac{\varepsilon'^2}{a^2}+\frac{\sigma'^2}{b^2}=1 \tag{3}$$

It is also easy to see that $a=\varepsilon_m-\varepsilon_b$ и $b=\sigma_m$. Further, $\varepsilon'=\varepsilon-\varepsilon_m$; $\sigma'=\sigma$. Thus, the axes ($\varepsilon\sigma$) function response equation is as follows:

$$\frac{(\varepsilon-\varepsilon_m)^2}{(\varepsilon_m-\varepsilon_b)^2}+\frac{\sigma^2}{\sigma_m^2}=1. \tag{4}$$

Solving this equation for, we obtain

$$\sigma=\sigma_m\cdot\left[1-\frac{(\varepsilon-\varepsilon_m)^2}{(\varepsilon_m-\varepsilon_b)^2}\right]^{0,5}. \tag{5}$$

The meanings ε_b were found by Bella. Point ($\varepsilon^*\sigma^*$) is the beginning of a curvilinear relationship. After the tangent at this point, i.e., extending the linear section, we get the point ($\varepsilon_0 0$). The value is determined by the formula:

$$\varepsilon_b = \frac{\varepsilon_m^* + \varepsilon_0}{2} \qquad (6)$$

As an example, consider the following diagram of stretching, melting № 224 (Figure 2.), Grain size 8, the values of the stress and strain on the calculations according to the chart:

$\varepsilon_m = 16.3 \cdot 10^{-3}$; $\sigma_m = 627.0$ MPa; $\varepsilon_b = -2.74 \cdot 10^{-3}$

$\varepsilon_2 = 11.7 \cdot 10^{-3}$; $\sigma_2 = 609.40$ MPa;

$\varepsilon_3 = 8.379 \cdot 10^{-3}$; $\sigma_3 = 564.78$ MPa;

$\varepsilon_4 = 6.348 \cdot 10^{-3}$; $\sigma_4 = 516.55$ MPa.

Fig. 2. Diagram of the sample stretching 20GL steel, smelting No.224, grain score 8.

Fig.3. Diagram of the sample stretching 20GL steel, smelting No.226, grain score 9

Calculations by the formulas (5) and (6) gave the following voltages: σ_2 = 608.65 MPa; σ_3 = 570.29 MPa; σ_4 = 534.7 MPa. The maximum error of theoretical value does not exceed 3.5 %.
For sample melting №226 (Fig. 3). The following values were obtained σ and ε:

$\varepsilon_m = 14.955{*}10^{-3}$; σ_m = 615.07 MPa;

$\varepsilon_2 = 11.866{*}10^{-3}$; σ_2 = 603.30 MPa;

$\varepsilon_3 = 8.758{*}10^{-3}$; σ_3 = 569.01 MPa;

$\varepsilon_4 = 5.427{*}10^{-3}$; σ_4 = 511.44 MPa.

Calculations by the formulas (5) and (6) give: σ2 = 597.6 MPa; σ3 = 573.3 MPa; σ4 = 515 MPa. The maximum error does not exceed the theoretical values of the order of 1 %. It also follows that the plastic deformation is achieved when the voltage maximum, the response function is an ellipse rather than a parabola.

Conclusion

In the equations (5) and (6), in coupled methods a camera of speed measuring procedure longitudinal ultrasonic wave may well be used in evaluating the properties of plastics become 20GL. The parabolic response function is not able describe the dependence fully of σ on ε when there is a maximum voltage value. In this case, in our opinion, it is the best response function for the equation of the ellipse.

Acknowledgements

The present research is for study the ultrasonic inspection and investigation of the physical model of the pattern of steel 20GL tensile held within state grant project No.118 "Study of the influence of the chemical composition, heat treatment, modification and micro-alloying on the toughness of the steel 20GL at low temperatures for castings of railway transport, and development of methods of non-destructive control of toughness".

REFERENCES

1 Bell J.F. *Experimental foundations of the mechanics of deformable solids. Vol.1. Small deformation.* Science, Moscow, 1984, 598 p.
2 Bell J.F. *Experimental foundations of the mechanics of deformable solids. Vol.2. Finite deformation.* Science, Moscow, 1984, 432 p.
3 Sukharev E.M. *Investigation of the relationship with the ultrasonic velocity impact resistance and the development of quality control methods of structural steels*. Dis. … kand. tech. sciences; 05.02.11, NGTU, Novosibirsk, 2000, 132 p.
4 Kulikov O.A. *Development of the method of ultrasonic testing the toughness of the hot-rolled steel sheet*. Dis. … kand. tech. sciences; 05.16.01, TGPU, Tomsk, 2000, 109 p.
5 Zuev L.B., Poletika I.M., Tkachenko V.V., Gromov V.E. Ultrasonic testing of mechanical properties of the steel in a structurally inhomogeneous state. *Vestnik of Tambov University. Series: Natural and Technical Sciences.* 2000, Vol. 5, Issue 2 – 3, pp. 358 – 360.
6 Beavers A.L. *Increasing the reliability of non-destructive testing of cast parts of rolling stock*. Dis. … kand. tech. sciences; 05.02.11, SGUPS, Novosibirsk, 2000, 142 p.
7 *GOST 9454-78 Metals. Method for testing the impact strength at low, room and high temperature.* Moscow, 1979, 26 p. [in Russian]
8 *GOST 1497-87 Metals. Methods of tension test.* Moscow, 1989, 28 p. [in Russian]
9 Botaki A.A. Ulyanov V.L., Charcot A.B. *Ultrasonic testing of strength properties of structural alloys*. Moscow: Mechanical engineering, 1983, 74 p.
10 *GOST 5639-82 Steels and alloys. Methods for detection and determination of grain size*. Moscow, 1983, 20 p. [in Russian]

Article accepted for publication 11.11.2016

UDC 535.371:535.621:621.373:544.032

INFLUENCE Au NANOPARTICLES ON ABSORPTION AND LUMINESCENT PROPERTIES RHODAMIN C IN ETHANOL

A.K. Aimukhanov, A.M. Esimbek, N.Kh. Ibrayev

[1]Institute of Molecular Nanophotonics, E.A. Buketov Karaganda State University, Universitetskaya Str. 28, Karaganda, 100028, Republic of Kazakhstan Karaganda, Kazakhstan, ash_ok_94@mail.ru

*Au nanoparticles were obtained gold target ablation in ethanol second harmonic of solid state laser 215 LQ. The concentration of nanoparticles (NPs) Au was determined to change the target weight before and after ablation by duration of 30 minutes. Studies have shown that by adding Au nanoparticles by C = 5 * 10-6 mol / l solution of dye, the optical density at the absorption maximum is increased. Fluorescence intensity at the maximum increases 1.2 times. The provisions of maxima of the bands and their half-widths are not changed.*

***Keywords*:** laser ablation, gold nanoparticles, local plasmon resonance, absorption optical density, fluorescence intensit y, stimulated emission, the pulse width generation

Introduction

Many researches related to the excitation of local plasmon resonance (LPR) of metal nanoparticles (NP) [1] are actively conducting now. Among optical appearences of LPR of metal NP the most noble is gigantic Raman scattering [2]. Fluorescence dye molecules placed near the surface of metal nanoparticles are also affected by local electromagnetic fields. At the same time, depending on the distance between the nanoparticles and the molecule, fluorescence of latter either amplified or damped [3]. At close distances and direct contact of nanoparticles to fluorophores, a glow is extinguished due to the prevalence of nonradiative energy transfer from the fluorescent molecules to the nanoparticle.

From a practical point of view, interest in plasmon effect is associated with the possibility to create a highly fluorescent sensors [4], optoelectronic devices [5], nanolasers, efficient photovoltaic cells], and others. One of the promising areas of modern laser physics is creating and investigating of composite media of the laser-active molecules and metal nanoclusters. Addition of metal NP in the active media of dye lasers leads to a decrease in the lasing threshold [6].

In this paper we conduct a study on the impact of metallic gold on the low absorption and luminescence Rhodamin C.

1. Experimental part

Gold nanoparticles were obtained by ablation of a gold target in ethanol, the second harmonic of a solid-state laser Nd LQ - 215 (SOLAR). Au nanoparticles concentration was determined by weight change of the target before and after the ablation and was $3.5*10^{-3}$ mol/l for 30 minutes ablation. The average size of Au nanoparticles were determined by dynamic light scattering on the size analyzer of submicron particles Zetasizer Nano ZS.

Measurements showed that the average size of the nanoparticles is 85 nm (Figure 1) in the test environment. Register absorption and fluorescence spectra of the samples was carried out by the Solar SM2203 spectrometer.

.

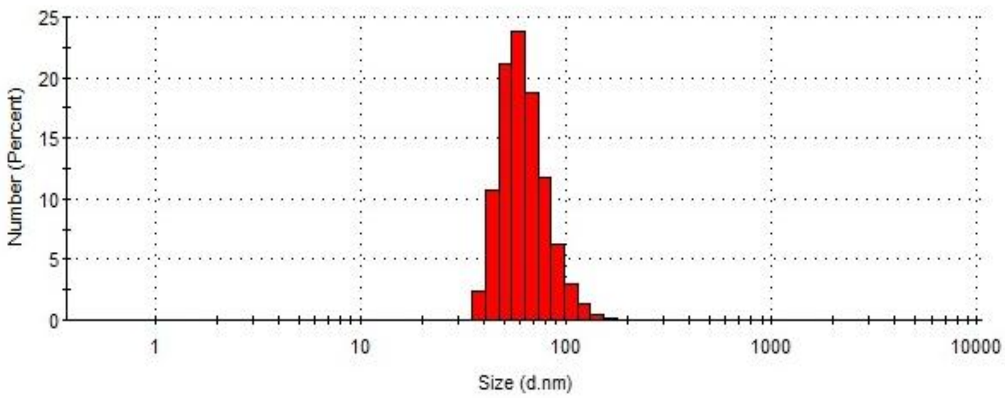

Fig. 1. The average sizes of Au nanoparticles

2. Results and discussion

The absorption spectrum of Au nanoparticles in ethanol (Figure 2) represents a broad band with a maximum at 535 nm. Rhodamin C absorption spectrum in ethanol has a maximum at λ_{abso}^{max} = 558 nm and a half width of the strip $\Delta\lambda_{1/2}^{abso}$ = 45 nm.

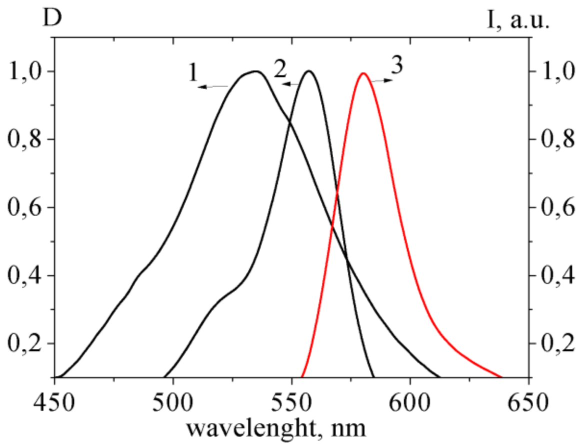

Fig. 2. The relative position of the absorption Gold nanoparticles (1) and fluorescence spectra of the Rhodamin C (2, 3)

Photoexcitation of the ethanol solution at λ_{exci} = 530 nm spontaneous fluorescence spectrum with a peak wavelength λ_{max}= 580 nm and a band-width $\Delta\lambda_{1/2}^{fluo}$= 38 nm observed. Figure 2 shows that the absorption spectrum of Au NP overlaps with the absorption and fluorescence spectra of Rhodamin C, indicating that the performance of the plasmon resonance conditions are fulfilled.

Figure 3 shows absorption spectra of dye molecules in the presence of Au nanoparticles at different concentrations. At low concentrations of nanoparticles slight increase of absorbance of the dye solution in the maximum is observed.

Adding Au nanoparticles with concentration equal to $5*10^{-6}$ mol/l in a dye solution (C_{dye} = 10^{-5} mol/l) absorbance grows 1.2 times at the maximum. Further concentration increase of the nanoparticles in a solution leads to a drop in optical density at the absorption maximum of the dye. The position of the maximum and its half-width do not change.

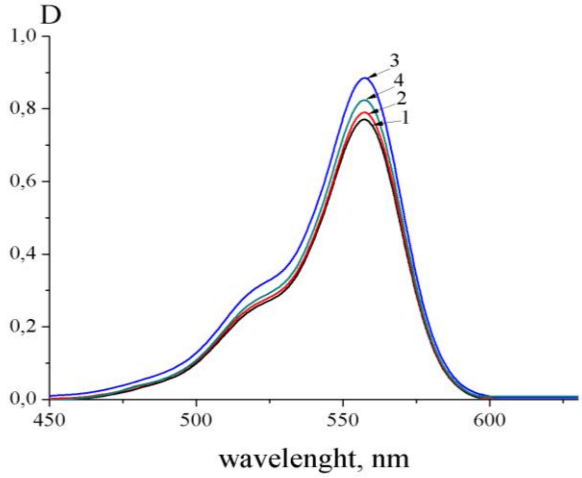

Fig.3. Influence of Au nanoparticles on the Rhodamin C absorption in ethanol:
1 – 0; 2 – $2 \cdot 10^{-6}$ mol/l; 3 – 5 10^{-6} mol/l; 4 – $5 \cdot 10^{-5}$ mol/l.

Reducing optical density of the dye in the presence of metal nanoparticles observed in [7]. Enhancement of absorption of the dye at low concentrations of the nanoparticles connected to the fact that the dye molecules are in the near field of metallic nanoparticles, plasmons in which are excited. Since the field near the nanoparticles significantly enhanced compared with the field of the incident light wave, the dye molecules in the near field absorb more than in the absence of nanoparticles in solution.

NP get closer with each other as their number increases. This leads to increased interaction between them and NP clusters are organising when the distance is of the order of their size or less. Increasing of the size of the nanoparticles leads to an increase in the intensity of scattered light in the media. This may cause a decrease in the number of particles and excited plasmons and, as a result, decrease of absorption of the dye. In addition, strong light scattering can lead to the fact that photons incident on the solution cannot reach dye molecules and translucence will occur.

When photoexcitation wavelength of an ethanol solution of the dye λ_{exci} = 530 nm and concentration equals 10^{-5} mol/l spontaneous fluorescence is observed (Figure 4). Adding gold NP in the alcoholic solution as a dye increases fluorescence intensity.

Rhodamin C, fluorescence intensity becomes 1.2 times stronger at the maximum. The intensity of the luminescence of the dye concentration increases until concentration will equal $C_{Au} = 5*10^{-6}$ mol/l, and further increase C_{Au} leads to quenching of fluorescence (Figure 4). The position of the band maximum and its half-width does not change.

According to [7], greater fluorescence of the molecules near the metal nanoparticles is an increase in the fluorescence excitation rate due to local plasmon resonance. At the same time, the arrangement of molecules near the metal surface or in contact with it, nonradiative energy transfer from the molecules to the nanoparticles occurs, resulting in reduced probability of radiative decay of the excited molecules.

At low concentrations of nanoparticles, when they are far from dye's molecules, increase in fluorescence due to plasmon resonance occurs because of gold nanoparticles. At high concentrations of gold nanoparticles due to the decrease in the distance between the fluorophores and nanoparticles radiationless deactivation of the excited fluorescence state is dominating.

The intensity of fluorescence in solution with silver nanoparticles can be increased due to additional absorption of exciting emission, scattered by gold nanoparticles. However, at high

.

concentrations of nanoparticles non-radiative decay channel of excited molecules is apparently determining.

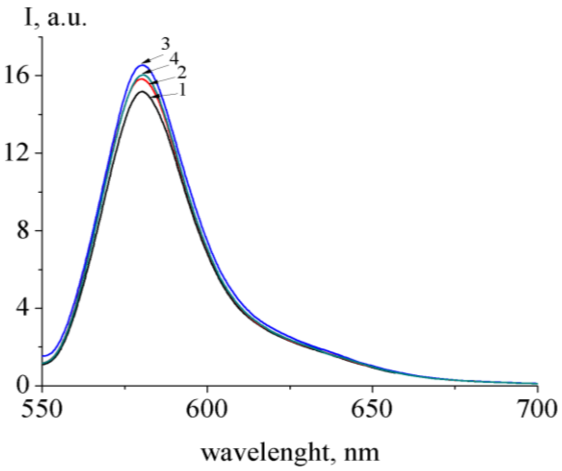

Fig.4. Effect of Au nanoparticles on Rhodamin C fluorescence in ethanol:
1 – 0; 2 – $2\cdot10^{-6}$ mol/l; 3 – 5 10^{-6} mol/l; 4 – $5\cdot10^{-5}$ mol/l.

Conclusion

Thus a result of the researches gold nanoparticles were obtained by ablation of a gold target in ethanol. It is shown, that by adding Au nanoparticles C = 5 * 10^{-6} mol/l in a solution of dye, optical density at the absorption maximum is increased 1.2 times and the fluorescence intensity at the maximum become 1.2 times bigger. At the high concentrations of nanoparticles observed drop in optical density at the absorption maximum and maximum of the spectra emission of the dye. Establishment, enhancement of absorption and emission of the dye at low concentrations of the nanoparticles connected to the fact that the dye molecules are in the near field of metallic nanoparticles, plasmons in which are excited.

ACKNOWLEDGEMENTS

The work was performed as part of the grant № 1124 / GF4 of the Ministry of Education and Science of the Republic of Kazakhstan

REFERENCES

1 Klimov V.V. *Nanoplasmonics*. Fizmatlit, Moscow, 2009, 480 p. [in Russian]

2 Tian Z.Q. Surface–enhanced raman spectroscopy: advancements and applications. *Spect*. 2005, Vol. 36, No. 6, pp. 466 – 470.

3 Lakowicz J.R. et al. Release of the self–quenching of fluorescence near silver metallic surfaces. *Analytical Biochemistry*. 2003, Vol. 320, pp. 13 – 20.

4 Homola J., Yee S.S., Gauglitz G. Surface plasmon resonance sensors: review. Sens *Actuators B* Chem., 1999, Vol. 54, pp. 3 – 15.

5 Oulton R.F. et al. Plasmon lasers at deep subwavelength scale. *Nature*, 2009, Vol. 461, pp. 629 – 632.

6 Kim W., Safonov V.P., Shalaev V.M., Armstrong R.L. Fractals in Microcavities: Giant coupled, multiplicative enhancement of optical responses. *Phys. Rev. Lett*., 1999, Vol. 82, No. 24, pp. 4811–4814.

7 Anger P., Bharadwaj P., Novotny L. Enhancement and quenching of single–molecule fluorescence. *Phys. Rev. Lett*., 2006, Vol. 96, pp. 113002 – 113005.

Article accepted for publication 25.11.2016

UDC 537.311.322; 681.382.473

SPECTRA OF PHOTOLUMINESCENCE OF CARBONCONTAINING NANOSTRUCTURED OBJECTS

S. E. Kumekov[1], N. K. Saitova[1], E. O. Syrgaliyev[2]

[1]Hi-Tech Engineering Institute of Kazakh National Research Technical University named after K.I.Satpaev, Almaty, Kazakhstan, skumekov@mail.ru
[2]University of Power and Communication, Almaty, Kazakhstan

It is discussed the possible mechanism of photoluminescence of such objects as carbon quantum dots, layers of amorphous hydrogenated carbon, and the natural biopolymer – native collagen. Recently in some researches were observed the interesting features of photoluminescence of carbon quantum dots . The features were discovered in comparison of photoluminescence in layers of amorphous hydrogenated carbon and in natural biopolymer – native collagen. This article describes a method of experimental study of the absorption spectra, excitation and photoluminescence characteristics of collagen with using modern measuring devices. Fixed excitation of photoluminescence was carried by an argon laser. A nitrogen laser was used for pulsed excitation. It is found that some properties of the luminescent radiation may be explained by assuming the nature of excimer photoluminescence collagen.

Keywords: quantum dots, carbon, excitation, photoluminescence, collagen.

Introduction

Recently [1-4], there has been discovered an interesting feature of photoluminescence (PL) of carbon quantum dots (CD): a broad structure less band in the visible spectrum whose half width, photon energy at a maximum, and short-wave edge depend on the energy of excitation quantum. The long-wave edge of the band depends neither on the size of a quantum dot [1] nor on the energy of excitation quantum [1-4]. The decay of the luminescence typically follows first-order kinetics. Four respectable PL mechanisms have been confirmed: the quantum confinement effect or conjugated π-domains, which are determined by the carbon core; the surface state, which is determined by hybridization of the carbon backbone and connected chemical groups; the molecule state, which is determined solely by the fluorescent molecules connected on the surface or interior of the CDs; and the crosslink-enhanced emission (CEE) effect.

The similar behavior of photoluminescence spectra has been observed earlier in layers of amorphous hydrogenated carbon and in natural biopolymer – native collagen [5-6]. The present work proposes a unified mechanism for the photoluminescence characterized by the properties of spectrum established in [1-6].

In previous studies [5] the main properties of photoluminescence (PL) of a-C: H films were investigated. The investigation in [5] demonstrated that the spectra of PL of amorphous hydrogenated carbon depend on the position of the energy of the quantum of excitation and show that the temperature dependence of photoluminescence in those matters reveals anti-Stokes radiation at high temperatures. The kinetics of the decay of the luminescence typically is fluorescent. In [5] it was shown that all remarkable PL features, such as, a high emission quantum efficiency which is independent of temperature, electrical field and energy of the exciting light, and an extremely rapid exitonic –like PL decay which is also nearly independent of temperature and energy of both exciting and emitted quanta, are connected with micro- inhomogeniety of the materials. It was suggested that there exist light emitting nanograins of sp2 phase inside a wide gap sp3 and polymer matrix.

.

Earlier O'Reilly and Robertson [7, 8] have theoretically shown that π - bonding in a-C:H favours aromatic 6 - fold rings and clustering of separate rings into compact graphitic sheets. It is also well known that similar aromatic rings are contained in natural polymers. Hence one has to expect similar PL properties. From a-C:H and from such polymers, provided the sextets are the main centers of radioactive recombination.

1. Experimental technique

For the research of absorption spectra, excitation and characteristics of photoluminescence was used spectral, versatile and computing complex KSVU-23 spectro-fluorometer "Hitachi". PL measurements of spectra were performed in two excitation modes: in stationary and pulsed.

The sources of radiation which were used to investigate the photoluminescence excitation spectra were: d - lamp in the region of 250-350 nm, ultrahigh pressure mercury lamp DRSh-500 with lines of emission (254, 303, 312, 365, 405, 436, 546 nm). Stationary excitation of the PL was carried out by lines of an argon laser (459.2 nm, 476.9 nm, 488.2 nm, 496 nm, 502.02 nm, 514.5nm), He-Cd-laser (325 nm, 416 nm) Kr (645, 8 nm and 677.5 nm) and He-Ne (632,6 nm).

To designate the necessary band of the radiation lamps DDS-30 and DRSh-500 and to eliminate the stray light entering into the registering device were used filters: UFS 1-4. Isolation of excitation light lines was produced by using a double monochromatic prism DMR-4.

When measured spectra and kinetics decay of photoluminescence for pulsed excitation was used a pulsed nitrogen laser with a line at 337 nm and a pulse copper laser (510.3 nm and 579.4 nm). PL samples were carried out at three constant temperatures: 300, 70, 4.2 K.

When measuring the photoluminescence excitation spectra was registered the integral intensity of PL in the range of 1.6 to 2.0 eV. To excite the photoluminescence emission line was used a mercury lamp that stood with double prism monochromator DMR-4. Excitation spectra measurements of photoluminescence were performed at 78 and 300 K.

For measurements was used glass helium cryostat at 4.2 K. A sample was placed directly in liquid helium. To study the samples was used a nitrogen cryostat at 77 K: the sample was placed in liquid nitrogen. Experimental determination of the relative position of the photoluminescence spectra, excitation of photoluminescence spectra and absorption spectra is usually give opportunity to establish the nature of the energy levels that form these spectra. To this end, we measured the excitation spectra and absorption spectra.

The absorption spectra of native collagen is difficult to measure because of its optical heterogeneity. Therefore, according to the conventional approach, the absorption spectrum was measured with a model of collagen analogue - gelatin films, which is optically uniform material.

2. Results and discussion

Identical features of PL are characteristic of all objects investigated in [1-6]: shape of structure, dependence of position of a maximum of PL and of half-width of a PL band on energy of quantum of excitation (see Figures 1 and 2).

These features of PL as is well-known are inherent in an excimer luminescence [6, 9, 10]. Excimer in these objects can be formed in the sandwich structures of benzene rings, such as, in crystals of pyrene or naphthalene [9, 10]. In [6] are investigated the PL of the biopolymer – collagen. It is shown the anti-Stokes tail of spectra at high temperatures. The spectra are structure less at all temperatures. The kinetics of decay of PL has fluorescent behavior.

Fig.3 illustrates the spectra of absorption (1) of PL of collagen at excitation by quanta with $h\nu_{exc}$ = 3.68 eV (2) and excitation of PL (3) at room temperature. Overlapping of spectral bands of a photoluminescence and excitation of PL of collagen in a wide interval of wavelengths of light demonstrate that the energy levels determining transitions of electrons in case of light absorption are at the same time levels between which there are radiating transitions.

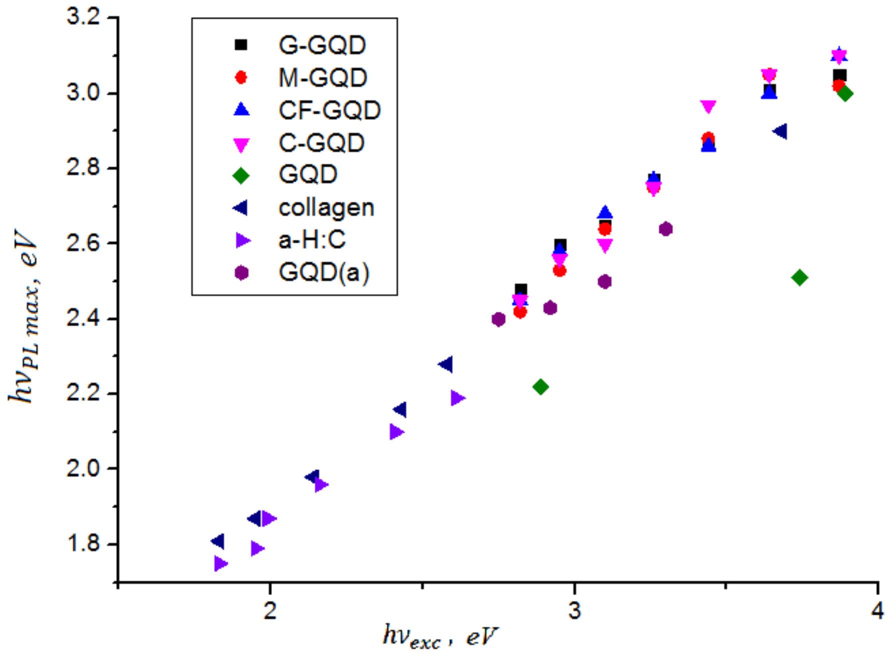

Fig. 1. The dependence of the position of the maximum of spectra of PL of different objects on the energy of quantum of excitation observed in [1-6]. Objects: G-GQD, M- GQD, CF- GQD, C- GQD, GQD are grafen quantum dots performed by different technologies, a-C: H films, collagen.

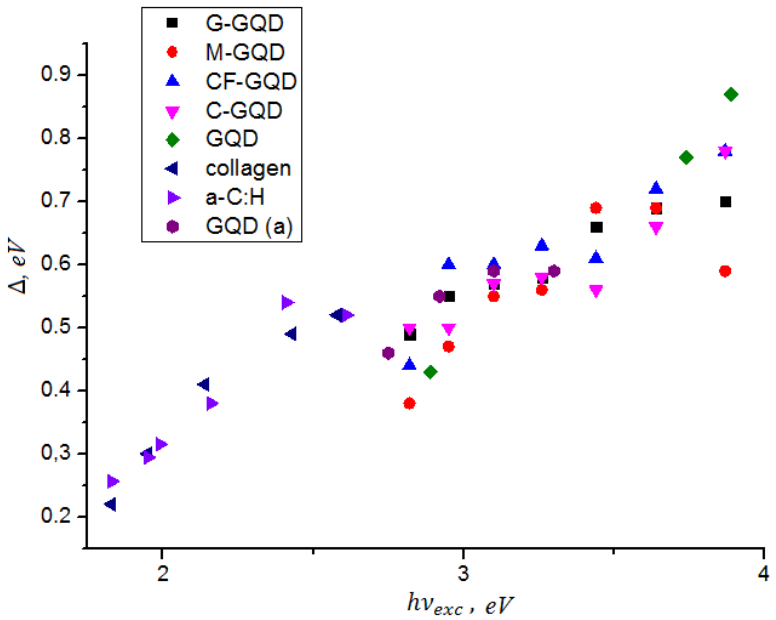

Fig. 2. The dependence of the halfwidth of spectra of PL of different objects on the energy of quantum of excitation observed in [1-6]. G-GQD, M- GQD, CF- GQD, C- GQD, GQD are grafen quantum dots performed by different technologies, a-C: H films, collagen.

This circumstance in a complex with the found and described properties of luminescent radiation can be explained within the assumption about excimer in a complex with the found and described properties of luminescent radiation can be explained within the assumption of the excimer nature of PL of collagen.

.

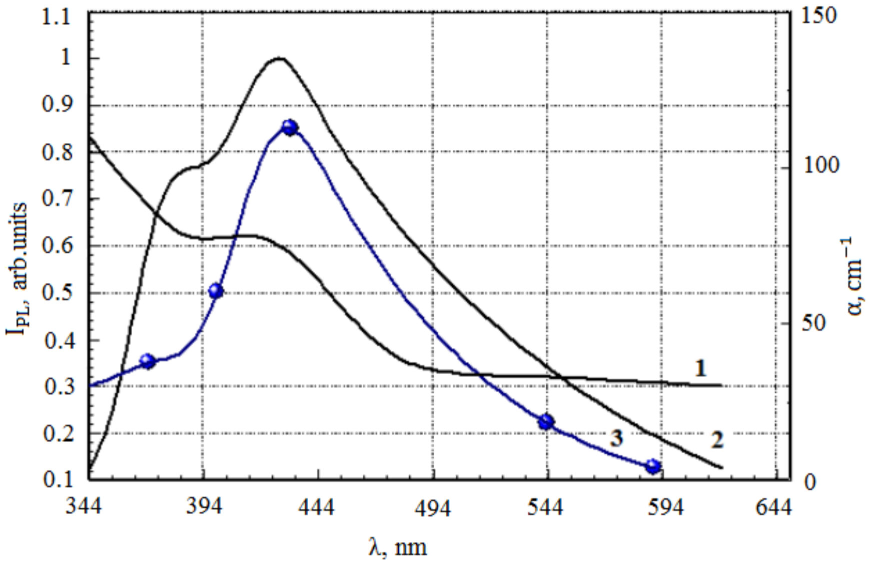

Fig.3. The spectra of absorption (1), of PL of collagen at excitation by quanta with $h\nu_{ex\,c}$= 3.68 eV (2) and excitation of PL (3) at room temperature.

Excimer is the dimer which exists only in an excited state [9, 10]. The main condition of such couple is unstable as in case of distance between molecules of an order of the size of an excimer of force of interaction have repulsive character. For the excimer-forming connections a characteristic sign is that circumstance that features of optical absorption correspond to monomers (molecular bands), and in a range of fluorescence wide structure less bands are found.

Hamiltonian of dimer of two sandwich benzene rings is expressed as [10]: $\mathbf{H=H_1+H_2+\langle V\rangle_{12}}$. $\mathbf{\langle V\rangle_{12}}$ is defined by Coulomb interaction. For ground state of dimer the Coulomb interaction is negative (repulsive interaction) and for excited state of excimer the Coulomb interaction is positive (attractive interaction). Fig.4 illustrates the dependence of ground state of dimer and of excited state of excimer on distance between a benzene rings.

The shape of a band of a luminescence and fast kinetics of decay are caused by nature of electronic terms of the initiated and main conditions a dimer which are schematically represented in the figure 4. Optical transitions in case of absorption and radiation of light in such system happen between two terms.

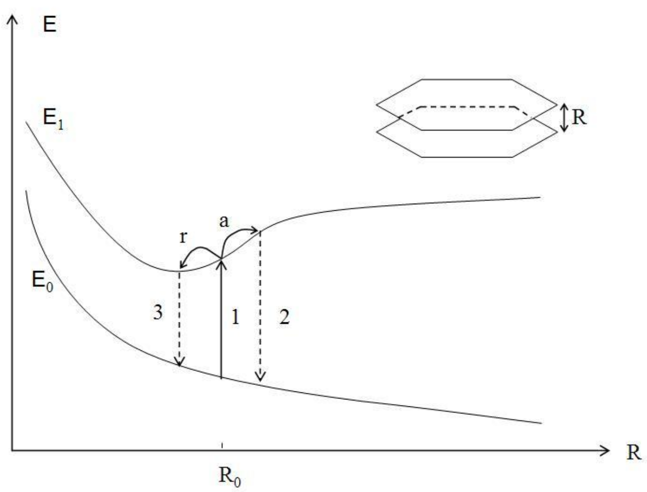

Fig.4. Energetic levels E of dimer-excimer complex as a function of R: 1 – transition of electron at absorption of light, 2 – anti Stokes transition, 3 – Stokes transition; a – termoactivation, r – relaxation.

On fig. 4 the value of R is a distance between two benzene rings. E_0 and E_1 are the terms of graund and excited states of dimer. Excimer radiation of systems of aromatic molecules is well known to [10]. The experiments described in these reviews showed that almost all flat aromatic molecules are formed by excimer. Experiments were conducted in different systems: solutions, liquids, organic crystals, solid polymers.

Mainly eximer in system of flat aromatic molecules spatially represent sandwich structures (see a figure 4 insert) which in case of a crystal are formed along the plane of sliding of dislocations [10], and in case of liquids and solutions are created in case of absorption of light in one of aromatic rings, accidentally appeared at a short distance, sufficient for forming of an excimer.

Conclusion

The features of PL of native collagen are observed: structure less shape at high and low temperatures, great values of halfwidth, and fast kinetic of decay. Experimentally observed the overlapping the spectra of excitation of PL and spectra of PL gave possibility to propose the excimer model of PL. In frame of this model it is shown the create of the anti-Stokes tail of spectra at high temperatures [6]. It is proposed the excimer model of luminescence. Given mechanism will have possible relation to the nature of PL of objects observed in [1-5].

REFERENCES

1 Libin Tang, Rongbin Ji, Xiangke Cao, Jingyu Lin, Hongxing Jiang, Xueming Li, Kar Seng Teng, Chi Man Luk, Songjun Zeng, Jianhua Hao, and Shu Ping Lau. *Deep Ultraviolet Photoluminescence of Water-Soluble Self-Passivated Graphene Quantum Dots. ACS Nano,* **2012**, *6* (6), pp. 5102 – 5110.

2 Juan Peng, Wei Gao, Bipin Kumar Gupta, Zheng Liu, Rebeca Romero-Aburto, Liehui Ge, Li Song, Lawrence B. Alemany, Xiaobo Zhan, Guanhui Gao, Sajna Antony Vithayathil, Benny Abraham Kaipparettu, Angel A. Marti, Takuya Hayashi, Jun-Jie Zhu,and Pulickel M. Ajayan. *Graphene Quantum Dots Derived from Carbon Fibers. Nano Lett.,* 2012, 12 (2), pp. 844–849.

3 Mahasin Alam Sk, Arundithi Ananthanarayanan, Lin Huang, Kok Hwa Lim and Peng Chen. *Revealing the tunable photoluminescence properties of graphene quantum dots. J. Mater. Chem. C*, 2014, 2, pp. 6954 – 6960.

4 Yonghun Shin, Jintaek Park, Daesun Hyun, Junghee Yang, Jae-Hyeok Lee, Jae-Ho Kim and Hyoyoung Lee. *Acid-free and oxone oxidant-assisted solvothermal synthesis of graphene quantum dots using various natural carbon materials as resources. Proc. of the Int. Conf. "Electronic Supplementary Material (ESI) for Nanoscale".* March, 2015, pp. 5633-5637.

5 Vasil'yev V.A., Volkov A.S., Musabekov E., Terukov E.I., Chernyshov S.V. *Antistoksovskoye izlucheniye amorfnykh plenok ugleroda a-C : H. Fiz. Tverd. Tela,* 1990, Vol. 32, No. 3, pp.784 – 788. [in Russian]

6 Volkov A.S., Kumekov S.E., Syrgaliev E.O., Chernyshov S.V. *Polosa fotolyuminestsentsii i antistoksovo izlucheniye nativnogo kollagena v vidimoy oblasti spektra*. Biofizika (Biophysics), 1991, Vol. 36, No. 5, pp.770 – 773. [in Russian]

7 O'Reilly E.P. *The electronic structure of amorphous carbon. J. Non-Cryst. Solids,* 1987, Vol. 97–98, pp. 1095-1102

8 Robertson J. *Amorphous carbon. Adv. Phys.*, 1986, Vol. 35, No. 4, pp.317-374.

9 J. Guillet. *Polymer photophysics and photochemistry*. Cambridge University Press, Cambridge 1985.

10 Martin Pope, Charles E. Swenberg. *Electronic Processes in Organic Crystals.* Clarendon Press, New York: Oxford University, 1982, 821 p.

Article accepted for publication 02.12. 2016

.

UDC 537.533.34

CALCULATION OF THE INSTRUMENTAL FUNCTION OF THE COMBINED ENERGY ANALYZER OF CHARGED PARTICLES BEAM

Saulebekov A.O.[1], Kambarova ZH.T.[2]

[1]Lomonosov Moscow State University, Kazakhstan branch, Kajimukana str. 11, Astana, 010010, Kazakhstan
[2] Ye.A. Buketov Karaganda State University, Universitetskaya Str.28, Karaganda, 100026, Kazakhstan
saulebekov@mail.ru

In this work the model of combined energy analyzer consisting of electrostatic mirror fields was studied by numerical calculations. A trajectory analysis of the motion of charged particles in the given electron-optical system was held. The instrumental function of the device for a case of a point source was first developed in order to optimize the size of output aperture and crossing windows of energy analyzer, what allowed estimating the energy resolution of the instrument. The spectrometer enables to analyze charged particles beams leaving the source at angles about 90^0 *at the instrumental energy resolution of 2%.*

Keywords: hyperbolic mirror, cylindrical mirror, charged particles, the instrumental function, the energy resolution.

Introduction

Earlier [1] we calculated electron-optical characteristics of the electrostatic energy analyzer combined of successive hyperbolic (HM) and cylindrical mirrors (CM). The novelty of the proposed device is a new mutual arrangement of electron mirrors in the two-stage energy analyzer, that allows input charged particles beam to the field of hyperbolic mirror at angles close to a right angle.

The scheme of mirror energy analyzer of combined successive HM and CM is shown in Fig.1 [1]. The figure shows the cross-section of the system by a plane r, z. The analyzer consists of a point source (1), arranged in series with mirrors with hyperbolic (2) and cylindrical (3) distribution of fields and the detector. HM is formed between two conical electrodes (4), which are under the zero potential, and an electrode of a hyperbolic shape (5), having a potential of the same charge as particles.

1. Modeling of electron-optical scheme of combined energy analyzer composed of successive electrostatic HM and CM

In this work the electron-optical scheme of energy analyzer combined of successive electrostatic HM and CM was analyzed, with the using of the "Focus" modeling program of axially-symmetric systems of corpuscular optics [2], in order to validate results obtained by analytical calculation formulas.

Fig. 2 demonstrates the distribution of the electrostatic field in the energy analyzer combined of successive electrostatic HM and CM. Fig.3 shows a three dimensional image of cross section of the electrostatic field in the combined system of mirrors. Here we calculated values of potentials at nodes of the mesh of the partition area and also painted the output field with colours, corresponding to value of potential at each point - the greater the potential, the "warmer" is the colour.

Fig. 4 presents trajectories of charged particles in the electron-optical scheme of combined energy analyzer of successive HM and CM. The total length of the electron-optical system is equal to 12.1. Radii of inner (3) and outer (4) electrodes of CM are equal to 1 and 2.5 respectively. Potentials of hyperbolic electrode (2) and the outer electrode CM are equal to 1. The inner electrode CM (3) and conical electrodes (1) are at a zero potential.

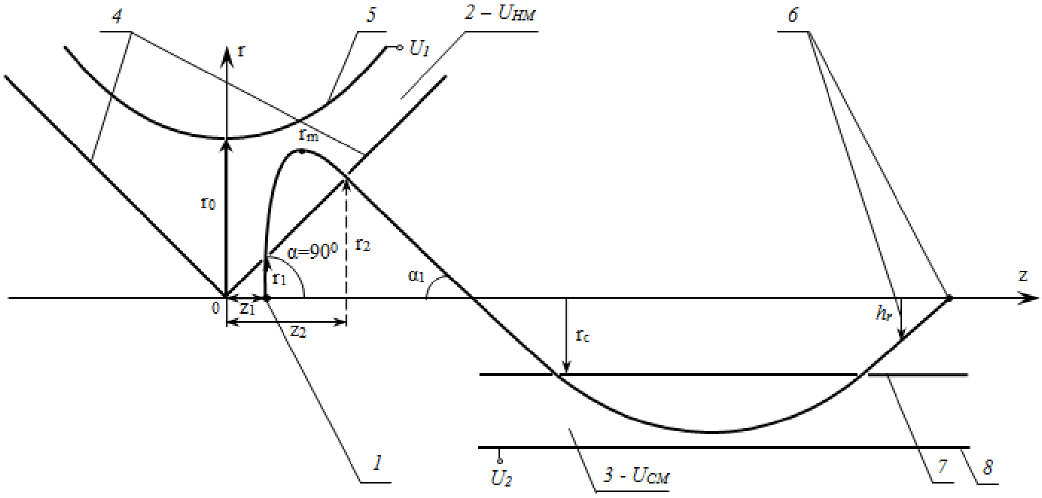

1 - the source of charged particles beam, 2 - HM, 3 – CM, 4 - conical transparent electrodes,
5 – the hyperbolic electrode, 6 - image of source, 7 - inner cylindrical electrode,
8 – the outer cylindrical electrode

Fig.1. Scheme of energy analyzer combined of successive HM and CM
(in cross section by plane r, z)

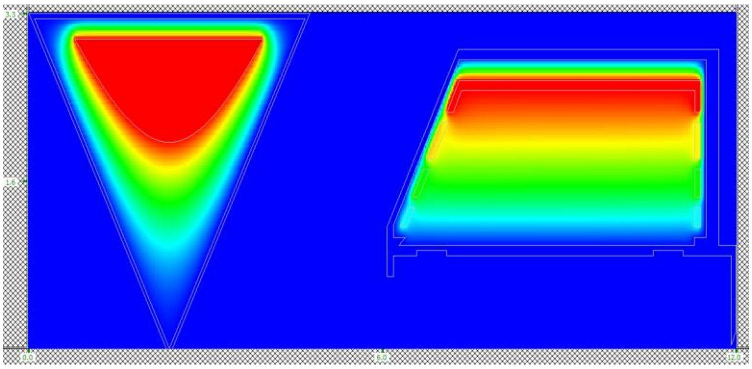

Fig.2. The distribution of the electrostatic field in the combined energy analyzer

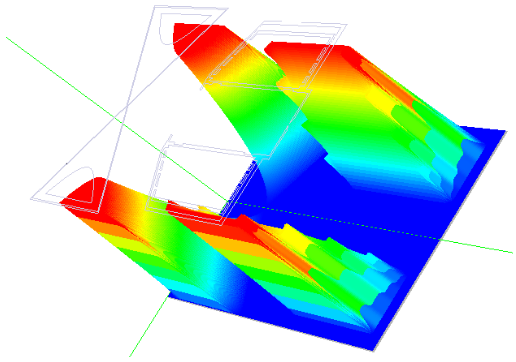

Fig.3. Three-dimensional image of cross section of the field in the combined energy analyzer

Asymptotes of hyperbolic electrode have an angle β=arc tan √2=54.4^0. All dimensions are expressed in relative units. Marked parameters are crucial to setting geometric parameters of electrodes.

Main elements of CM are two coaxial cylindrical electrodes with different radii. To correct the boundary field at butt ends of cylindrical electrodes corrective rings under potentials (in fractions of the outer cylinder’s potential *V*) are placed in accordance with logarithmic law of variation of a cylindrical field with radius. For example, in the case of three pairs of adjusting rings their potentials have the following values are 0.25*V*, 0.5*V* and 0.75*V*. Thus, the analyzing field is formed between cylinders. Widths of input and output slits in the inner cylindrical electrode are equal to 0.5 respectively. By changing the potential *V* we can analyze the whole spectrum of energy *E* of charged particles. Electrodes of HM are chosen to be transparent for passing of charged particles. Opaque segments of electrodes are coloured in red in the program.

.

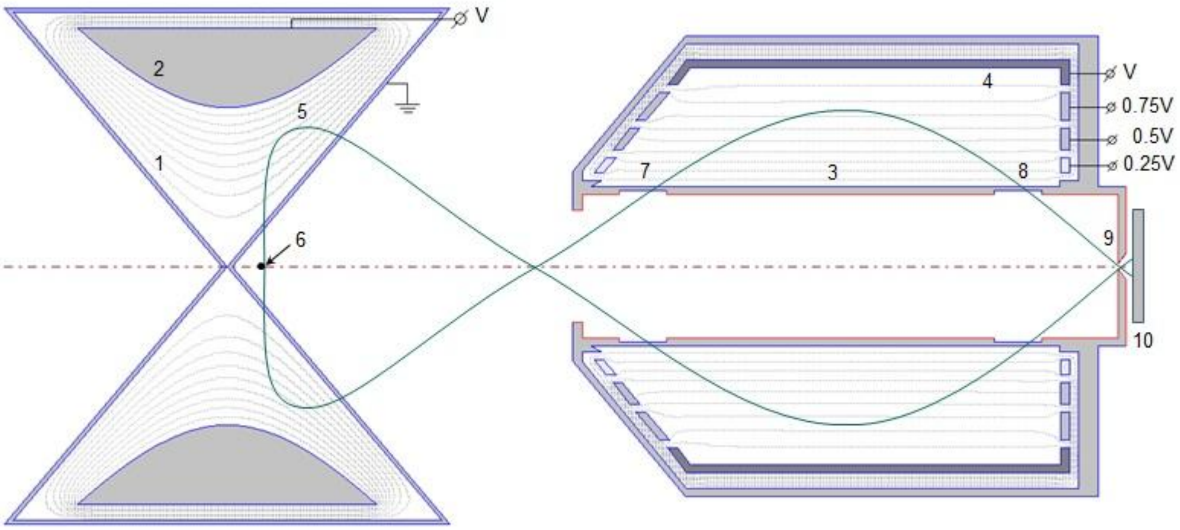

1 - conical electrodes , 2 - hyperbolic electrode, 3 - inner cylinder,
4 - outer cylinder, 5 - charged particles, 6 - point source,7 - input window of CM,
8 - output window of CM, 9 - circular output aperture, 10 – the detector

Fig.4. Trajectory of charged particles in the electron-optical scheme of combined energy analyzer of successive HM and CM

Fig. 4 shows the case characterized by large values $\alpha = 90^0$. The energy of the particle or rather the ratio of the energy of a charged particle to the potential of the electrode is 1. A point source is located on the symmetry axis of the energy analyzer in a distance from the hyperbolic mirror equal to x=1.13. Referring to Fig. 4, charged particles (5) from the point source (6) through the conical transparent electrode (1) of HM are reflected from hyperbolic electrode (2), then enter the field of CM. Charged particles, which passed through the output aperture (9), fall onto the position-sensitive detector (10), and thus are recorded. As a result of the focusing effect of two mirrors on the charged particles beam, a point image of source on the symmetry axis of the analyzer is produced. Thereby, the "axis -axis" type focusing is performed in the system.

The instrumental function is one of the main characteristics of both axial electrostatic energy analyzers and many other electron and ion-optical devices [3-5]. Instrumental function (transmission curve, instrument line, apparatus function, response function) of axial electrostatic energy analyzer is proportional to dependence of monoenergetic electron beam passing through the exit slit of the energy analyser from energy of electrons [3,4]. If instrumental function is known, it is not difficult to identify a resolution and transmission capabilities of a device. In electron optics there is a method called "trajectory". Applying of this method can give you new basic characteristics of studied energy analyzer.

The following algorithm can construct instrumental function for the energy analyzer based on axial-symmetric fields. Firstly, the range of variation of the charged particles' initial angles and energies are determined. The instrumental function of energy analyzer is determined by calculating a large number of charged particle trajectories for initial conditions, varying in width (radius) of circular output diaphragm. To simplify calculations, it was considered a motion of charged particles in one of planes passing through the mirrors axis, i.e. the device's instrumental function was determined excluding non-axial trajectories of charged particles. Thus, in the numerical calculations additional "broadening" of the instrumental function by non-axial energy analyzer "rays" was not taken into account. Motion trajectories of charged particles in this energy analyzer were found by numerical solution with the "Focus" program.

2. Results and discussion

For calculation of the instrumental function of electron-optical system in the case of the point source, initial conditions are given in the program, i.e. charged particles with the initial angle of 90^0 and having initial energy within the emission range (more precisely *E/V*) equal to 0.9-1.1 *eV/V* are launched from the point source.

Figures 5.1 and 5.2 present instrumental functions of the combined energy analyzer in the case of a point source with a small (R_d = 0.025 R_{in}; 0.05 R_{in}) and large (R_d = 0.075 R_{in}; 0.1 R_{in}) radii of the output aperture.

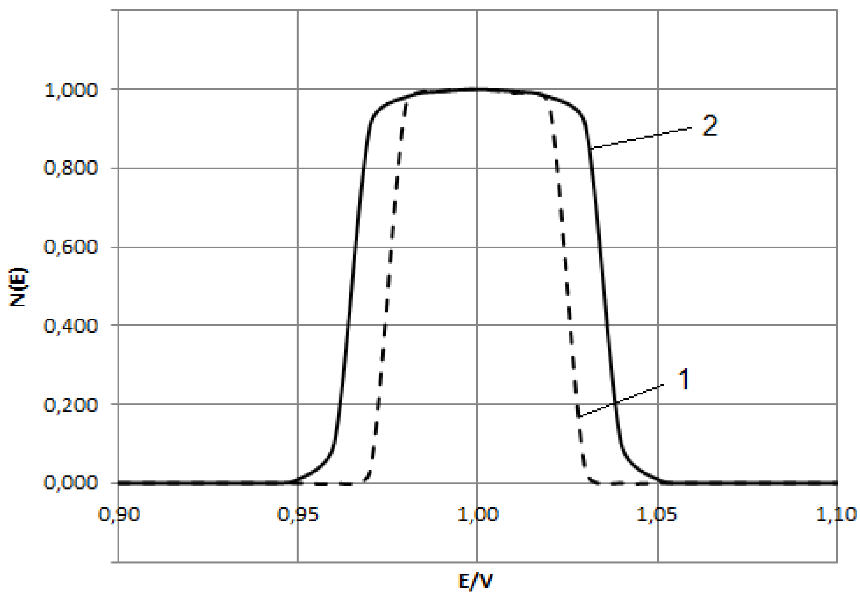

Fig. 5.1. The instrumental function of analyzer with small radii of the output aperture.
The radius of the output aperture: 1 – 0.025 R_{in} ; 2 – 0.05 R_{in}

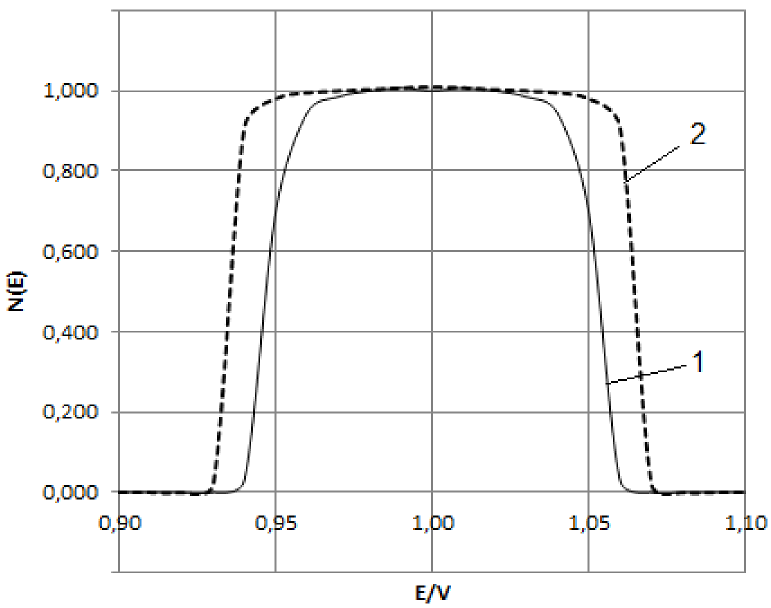

Fig.5.2. The instrumental function of analyzer with large radii of the output aperture.
The radius of the output aperture: 1 – 0.075 R_{in} ; 2 – 0.1 R_{in}

On graphics of instrumental functions for combined energy analyzer with small (R_d = 0.025

.

R_{in}; 0.05 R_{in}) and large (R_d = 0.075 R_{in}; 0.1 R_{in}) radii of the circular output aperture (Fig. 5.1 and 5.2) can be seen that the width at half-height increases with increasing of the output aperture radius. Fig. 6 shows the dependence of the width of the instrumental function $\Delta E_{1/2}$ at half-height from the output aperture radius. Fig. 6 shows that it is a linear relationship.

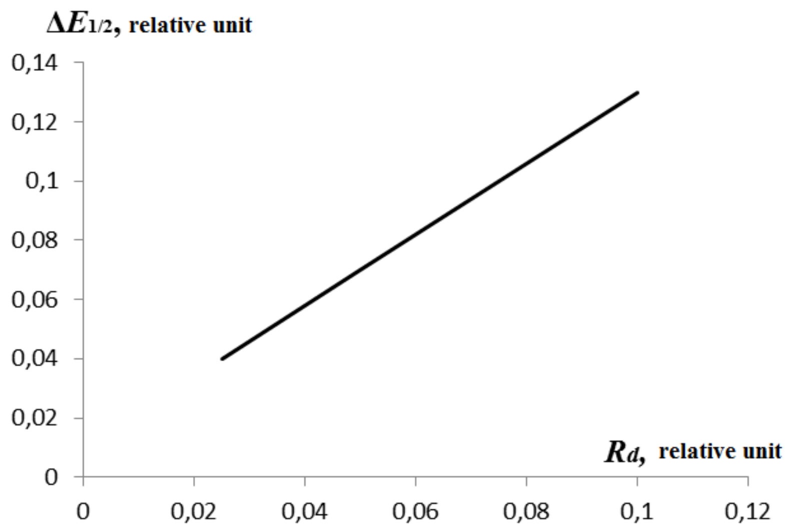

Fig.6. The dependence of the instrumental function width at half-height from the radius of the output aperture

From results of numerical calculations it was determined that the optimal radius of output aperture is R_d=0.02 R_{in}. Fig. 7 shows the instrumental function of the combined system based on electrostatic HM and CM with optimal radius of output aperture.

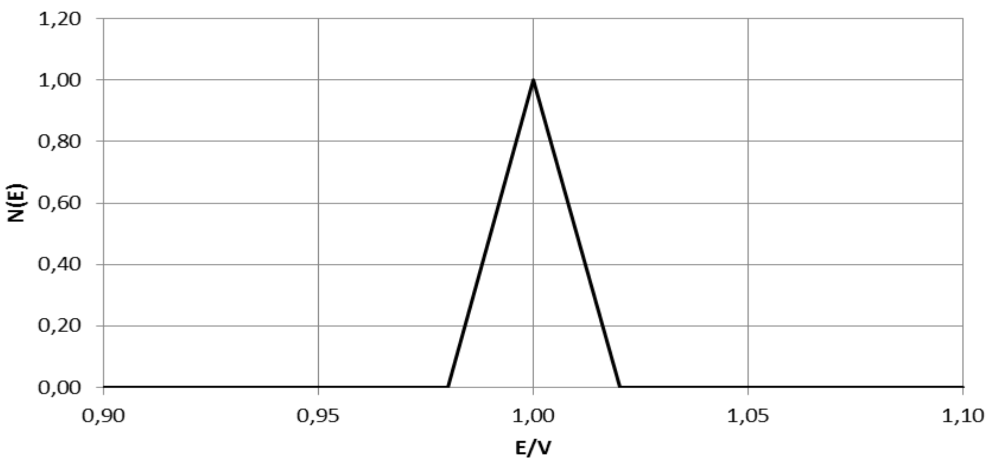

Fig. 7. The instrumental function of the combined system of successive HM and CH at optimum output aperture radius R_d = 0.02 R_{in}

Graphics of instrumental function (Fig.7) shows that the instrumental function is the combined energy analyzer at the optimal radius of the circular output aperture is a symmetrical curve close to an isosceles triangle. As it seen in Fig.7, only charged particles with energy *E/V*=1 *eV/V* pass through the output aperture and reach the detector. The aperture truncates particles of the same energy differing by 1% or more.

Thus, the relative energy resolution at half-height of instrumental function of the combined energy analyzer with optimal output aperture radius 0.02 R_{in} is 2% of the case of a point source.

Conclusion

Thereby the numerical model of the combined energy analyzer of electrostatic mirror fields has been obtained. The instrumental function of energy analyzer in the case of a point source at different radii of the circular output aperture was calculated. The dependence of instrumental function width for combined energy analyzer at half-height from the radius of the output aperture has been studied. The optimum radius of the output aperture was determined.

The spectrometer allows analyzing beams of charged particles leaving the source at an angle close to 90^0 and the instrumental energy resolutions of 2%.

REFERENCES

1 Ashimbaeva B.U., Chokin K.Sh., Saulebekov A.O., Kambarova Zh.T. The combined energy analyzer composed of electrostatic mirror fields. *J.of Electron Spectrosc. Relat. Phenom*, 2012, Vol. 185, No. 11, pp.518 – 522.

2 Trubitsyn A.A. The sofeware «FOCUS» to simulate axi-symmetrical and planar electron (ion) optical systems. *Handbook of the 8^{th} Intern. Conf. «Charged Particle Optics».* Singapore, 2010, 208 p.

3 Afanassyev V.P., Yavor S.Ya. Electrostatic energy analyzers (Review). *Tech. phys. J.*, 1975, Vol.45, No. 6, pp. 1137 – 1169.

4 Kozlov I.G. Modern problems of Electron spectroscopy. Moscow, Atom publ., 1978, 248 p.

5 Yavor M. *Optics of Charged Particle Analyzer. Advances in Imaging and Electron Physics*. Elsevier, 2009, Vol. 157, 677 p.

Article accepted for publication 02.12. 2016

.

UDC 544.33; 544.34

SOME ASPECTS OF THE THEORY AND PRACTICE OF CORROSION AND THERMAL DESTRUCTION OF METAL MATERIALSAND OF METAL COATINGS

Platonova E.S.[1], Yurov V.M.[2], Eremin E.N.[3], Buchinskas V.[4], Guchenko S.A.[2], Laurynas V.Ch[2]

[1]Karaganda StateTechnical University, Karaganda, Kazakhstan, danilina1969@list.ru
[2]KaragandaState University named after E.A Buketov, Karaganda, Kazakhstan, exciton@list.ru
[3]Omsk State Technical University, Omsk, Russia, weld_techn@mail.ru
[4]Vilnyussky Technical University named after Gediminas, Vilnius, Lithuania, Vytautas.Bucinskas@vgtu.lt

On the basis of the statistical approach to the formation of corrosion spots obtained an expression that shows the logarithmic dependence of the corrosion spot area of "defects" of the metal surface or coating. On the basis of a thermodynamic model obtained relationship between corrosion rate, the surface tension of a metal surface and their melting point. A method for determining the thermal stress in the coating on the basis of experimental values of microhardness, measured along and across the sample. On the basis of thermodynamic model derived relationship between the heat resistance of coatings and surface energy. A formula that is suitable for qualitative analysis and forecasting of metal fracture rate and coatings deformation and thermal influences.

Keywords: corrosion, thermal stability, metal, metal coating, a statistical model, thermodynamic model, microhardness

Introduction

Issues of metal corrosion devoted a huge amount of work, of which only work note [1-7], where an extensive bibliography. Despite this, in the field of corrosion theory continues to grow with the growth of various types of structural metallic materials used in various areas of industrial production.

In the most general case, corrosion of the metal can be present as the nucleation and growth of the new phase (oxidized metal). A critical new phase nuclei are formed sequentially in a series of random acts of attachment and detachment of atoms (molecules) from each other. Therefore, nucleation - random process in time and space. It determines the probabilistic nature of the parameters that describe the kinetics of formation of nuclei in the process of corrosion, or crystal growth [1]. A quantitative description of random process is given by its distribution function satisfies the kinetic equation. In general, the kinetic equation is a complex integral-differential equation, which cannot be solved. However, when viewed as a Markov random process, the kinetic equation becomes a differential, which has a simple form [2].

In the particular case of a Poisson process, birth and death with a finite number of states, a system of differential equations [8, 9]:

$$\begin{cases} dp_0(t)/dt = -\lambda_0 p_0(t) + \mu_1 p_1(t), \\ \ldots\ldots\ldots\ldots\ldots\ldots\ldots\ldots \\ dp_\kappa(t)/dt = \lambda_{\kappa-1} p_{\kappa-1} - (\lambda_\kappa + \mu_\kappa) p_\kappa(t) + \mu_{\kappa+1} p_{\kappa+1}(t) \\ \ldots\ldots\ldots\ldots\ldots\ldots\ldots\ldots\ldots\ldots\ldots\ldots\ldots\ldots\ldots\ldots \\ dp_n(t)/dt = \lambda_{n-1} p_{n-1}(t). \end{cases} \quad (1)$$

Here λ_0 – is the likelihood of transition from state E_0 to E_1, etc.; μ_1 – is the probability of transition from the state E_1 to E_0, etc.

The probability of transition from E_n to E_{n-1} is assumed to zero ($\mu_n = 0$), i. e, E_n condition for such a system - an absorbent; p_i (t) - the probability of finding the system in state E_i. The system of equations (1) is a system of Kolmogorov equations [10]. The general solution is so cumbersome that does not allow for even the numerical analysis methods.

In this paper, we make a generalization of our work on some issues of corrosion and thermal resistance of metallic materials and coatings [11-16].

1. Statistical model for the formation of corrosion spots

The most common case of metal corrosion is its interaction with the oxygen molecules. It is obvious that this interaction begins with a "weak" places the metal surface or its defects. We present our model for the formation of corrosion spots from a position of statistical physics.

Consider the number of the metal surface defects m. Let the distance between the defects and the same is equal to R. We describe around each defect 0 circle of radius R. Let the number density of defects in the circle is equal to n_0, then the probability $W_0(r)$ the fact that the nearest particle of oxygen gets to the distance r from the particle 0, it is easy to get on the basis of statistical physics, and it is equal to:

$$W_0(r) = \pi n_0 r^2 \exp[-\pi n_0 r^2]. \tag{2}$$

The probability of finding the particle N_0 oxygen defect in the area of radius r is equal to 0, it is obvious:

$$W_{N_0}(r) = \prod_{k=1}^{N_0} W_k(r) = (\pi n_0)^{N_0} r^{2N_0} \exp[-\pi N_0 n_0 r^2]. \tag{3}$$

The probability of (3) define on the other hand as the ratio of the number N_0 of the defect particles to the total number of particles in the selected circle - Q_0:

$$p_0 = \frac{N_0}{Q_0} = (\pi n_0)^{N_0} r^{2N_0} \exp[-\pi n_0 r^2]. \tag{4}$$

For a system of m defects we have:

$$\begin{aligned} p_0 &= (\pi n_0)^{N_0} r^{2N_0} \exp[-\pi N_0 n_0 r^2] = \frac{N_0}{Q_0}, \\ p_1 &= (\pi n_1)^{N_1} r^{2N_1} \exp[-\pi N_1 n_1 r^2] = \frac{N_1}{Q_1}, \\ &\ldots\ldots\ldots\ldots\ldots\ldots\ldots\ldots\ldots\ldots\ldots\ldots \\ p_m &= (\pi n_m)^{N_m} r^{2N_m} \exp[-\pi N_m n_m r^2] = \frac{N_m}{Q_m}. \end{aligned} \tag{5}$$

For all of the metal to the number of defects 0,1,2, ..., m, we have:

$$P = \prod_{i=0}^{m} p_i = \prod_{i=0}^{m} (\pi n_i)^{N_i} r^{2N_i} \exp[-\pi N_i n_i r^2] = \frac{\prod_{i=0}^{m} N_i}{\prod_{i=0}^{m} Q_i}. \tag{6}$$

The system of equations (5) and (6) is a system of transcendental equations that can be solved only by numerical methods or approximate.

.

Therefore, it is possible to make a numerical estimate based on the actual situation of the system 1 and equation (5):

$$\ln N_0 - \ln Q_0 = N_0 \ln(\pi n_0) + 2N_0 \ln r - \pi N_0 n_0 r^2.$$

An assessment shows that the first term on the left side of the equation and the first two terms of the right - are negligible. The result:

$$N_0 = \frac{\ln Q_0}{\pi n_0 r^2}. \qquad (7)$$

Given that $\pi r^2 = S$ - the area of corrosion spots and $n_0 N_0 = const$, (7) we have:

$$S = \cos t \cdot \ln Q. \qquad (8)$$

The last expression shows the logarithmic dependence of the corrosion spot area of "defects" of the metal surface or coating. The probability of (3) can be determined, on the other hand, as the ratio of the binding energy of oxygen molecule E_0 to the metal atom to the total energy of formation of corrosion spots E. Given that [5]:

$$E_{общ.} = \Delta \mathbf{G}_{\mathbf{T}}^{\mathbf{0}} = -RT2{,}303 \lg K_p, \qquad (9)$$

where Kp - the constant of chemical equilibrium.

For the area of corrosion spots get:

$$S = \cos t \cdot \ln K_p \qquad (10)$$

Despite the simplicity of the formulas (8) and (10), they may be useful for the study of the processes of any corrosion of structural materials, because include easily experimentally determined parameters.

2. Thermodynamic model of corrosion and mechanical failure of metals, alloys and coatings.

Considering the elementary carriers of corrosion or mechanical damage as a subsystem of non-interacting particles immersed in a thermostat, it is possible on the basis of quantum statistical thermodynamics to obtain the response function of this subsystem to the external action [13]. If the response function to take the area of corrosion spots S, we obtain:

$$S = \frac{kT}{C} \cdot \frac{A}{G^0} \cdot \overline{N} \cdot t, \qquad (11)$$

where A is the work of "external forces" and T is temperature, G^0 is Gibbs potential of a bulk sample of metal - the average number of points of corrosion, t - is time of corrosion, k - is Boltzmann constant, C - is constant.

The work of "external forces" equal to the change of the standard thermodynamic potential ΔG_T, which is the basis of thermodynamics and corrosion can be determined through the chemical equilibrium constant Kp according to the formula [5]:

$$\Delta G_T^0 = -RT2{,}303\lg K_p, \tag{12}$$

Corrosion starts from the surface layer and therefore in the formula (11) to make the substitution $G^0 = \sigma \cdot S_0$ - where σ - the surface tension, S_0 - specific surface. As shown in [17], the surface tension of the metal is related to its melting point ratio $\sigma = 10^{-4} \cdot Tp$.

Taking as a response function in (11) the thickness of the corrosion layer h, for corrosion rate $(V_c = h/t)$, which is determined experimentally, we finally obtain the following expression:

$$v_{кор.} = C_1 \frac{T^2 \lg K_p}{\sigma S} = C \cdot \frac{T^2 \lg K_p}{T_{пл.}}, \tag{13}$$

where the constant *C* includes all the constants of the previous formulas.

Formula (13) can be used to predict the corrosion rate of newly synthesized coating and selection of their elemental composition. For thin films and coatings surface tension value is the value of σ and additive may be determined experimentally as described in [17]. Similarly, the speed of the mechanical or thermal destruction of the coating will have the following relationships:

$$v_p = C \cdot \frac{E_F}{T_{пл.}}. \tag{14}$$

$$v_p = C_1 \cdot \frac{\mu}{\sigma}. \tag{15}$$

Equation (14) is valid for pure metals. Using the experimental values of the Fermi energy E_F, melting and corrosion rates for ten metals Au, Ag, Al, Cu, Fe, Ni, Pb, Pt, Sn, Zn, we calculated the constant C. Up to 20% of it was constant and equal to (2,5-3,0) 10^{-4}. Equation (15) is valid for multiple and multi-coatings. In this case, better experimentally determine the corrosion rate and the amount of tension as described in [17].

3. The corrosion resistance of components of mining equipment.

To determine the corrosion resistance of the coatings used the method of anodic polarization initiation defects (APID). For quantitative evaluation of the integral quality coatings using the integral quality parameter K = (Q-Q_1) / Q_0, wherein Q_0 and Q_1 - amount of electricity passed through the cell when electrical polarization uncoated surface of the sample and in the potential range covering from the start of the dissolution potential of the substrate material to the potentials on the (10-40)% less capacity starts dissolving coating material

Typically, the upper limit is selected from the interval (3-5) B. The parameter K is dimensionless and normalized. Higher quality coverage corresponds to the value K = 1 and K = 0 the lowest. The coating is applied to the following items of mining equipment: rod (steel 40X); pin 12 (steel 35); with sleeve 12 (steel 35); RU11.008-01 coupling (steel 35); cork GVU 30.002 (steel 35); gon 10NG12 (steel 35); right cheek G9.00.18 (steel 3).

However, the calculation of economic efficiency of the entire production cycle of the application of titanium nitride coatings showed that the price of the above items of mining equipment increased by approximately 20% compared to the galvanized coating applied electrolytically factory RGTO Coal Department of JSC "ArcelorMittal". It should be noted that despite the increase in the cost of coverage, galvanized coating plant RGTO obtained substandard.

.

Table 1 - The corrosion rate of titanium nitride coatings technological environment

technological environment	concentration (mass)%	temperature, ºC	corrosionrate mm / year
nitricacid	80	20	0.01
sulfuricacid	52	20	0.03
hydrochloricacid	80	20	0.05

Nitriding was conducted for parts described above. Table 2 shows the comparative analysis. From Table 2 that the technology of vacuum nitriding, though inferior in corrosion resistance of titanium nitride coatings, but is much greater than the zinc coating. At the same time, the cost of nitrided parts on (10-15) % lower zinc.

In the case of small lots of parts, and also to make better use of critical parts of titanium nitride coatings which enhance corrosion resistance in addition have high strength. Vacuum nitriding is a cheaper way to increase corrosion resistance. It has distinct advantages over electrolytic zinc and chrome finish. We applied the method of ion plasma coating Fe-Al-Ti, Zn-Al-Ti, Zn-Cu-Al-Ti. Table 3 are represented by their corrosive characteristics.

Table 2 - Characteristics of various coatings

namedetails	anti-corrosioncoating	coefficient K
Coupling RU 11.008-01,steel 35	Zinc	0.15
Coupling RU 11.008-01,steel 35	Nitrated	0.40
Coupling RU 11.008-01,steel 35	Titaniumnitride	0.75

Table 3 - Characteristics of various coatings

namedetails	anti-corrosioncoating	coefficient K
Nipple 12, steel 35	Fe-Al-Ti	0,47
Coupling 12 c, steel 35	Zn-Al-Ti	0,57
CorkGVU 30,002, steel 35	Zn–Cu-Al-Ti	0,61

As can be seen from Table 3, the proposed coating are second only to the titanium nitride coating, but they are much cheaper than all the coatings shown in Table. 2. The manufacture of such cathodes without difficulty. The coating thickness is from 2 to 4 microns, so that a cathode is enough for about 12 thousand. Parts such as coupling 12 c.

4. Anti-corrosion wear-resistant coatings on parts of oilfield equipment

The problem of corrosion and protection against oil and gas and oil field equipment is becoming more urgent and acute. This is due, primarily, the increase in the number of acceding to the development of oil, gas and gas condensate (especially sea), containing corrosive components, and secondly, the increasing intensity of work of oilfield equipment under intensive production methods, transport and processing.

The high efficiency of the existing corrosion protection technology makes introduce other, more efficient technologies to reduce the corrosive wear and thereby increase the terms of use and other downhole oilfield equipment.

At present, all industrial countries are not on the path of anticorrosive steel and alloys and application technology developed by modern anti-corrosion coatings for cheaper grades of steel [18-25].

In recent years, attracted the interest of researchers high entropy alloys and coatings based on them [26-29]. In this case, the coating obtained with high performance.

This paper discusses the results of a study of the structure and properties of coatings Cr-Mn-Si-Cu-Fe-Al and Cr-Mn-Si-Cu-Fe-Al + Ti. We used methods Cr-Mn-Si-Cu-Fe-Al, produced by induction melting. The coatings were deposited by ion-plasma method on the vacuum unit HHB-6.6I1 on a sample of steel 12X18H10T. Coatings Cr-Mn-Si-Cu-Fe-Al+Ti were obtained while spraying a cathode Cr-Mn-Si-Cu-Fe-Al and a titanium cathode. Electron microscopic study was performed on a scanning electron microscope MIRA 3 firms TESCAN. Research carried out at an accelerating voltage of 20 kV and a working distance of approximately 15 mm. Each sample was done by 4 shots at 4 points on the surface at different magnifications: 245-fold, 1060-fold, 4500-fold and 14600-fold. And power dispersive analysis conducted at 4 points each specimen. The thickness of the coatings and their elemental composition is measured using an electron microscope 200 Quanta 3D. The phase composition and structural parameters of the samples was performed on diffractometer XRD-6000 X in the CuKα-rays. An analysis of the phase composition, the size of coherent scattering regions, the internal elastic stresses (Δd/d) carried out with use of databases PCPDFWIN and PDF4 +, as well as programs POWDER CELL 2.4. For samples nanohardness coatings was determined using the method of Oliver nanoindentation system and headlamp using a Berkovich indenter with a load of 1 g and a dwell time of 15 sec. The corrosion resistance of the coatings was determined in accordance with GOST 9.908-85.

On the stainless steel substrate was coated with Cr-Mn-Si-Cu-Fe-Al in gaseous nitrogen for 40 min. Fig. 1a shows an image of the coating obtained in an atomic force microscope. Fig. 1b shows a cross section of 1 micron coating produced a focused ion beam.

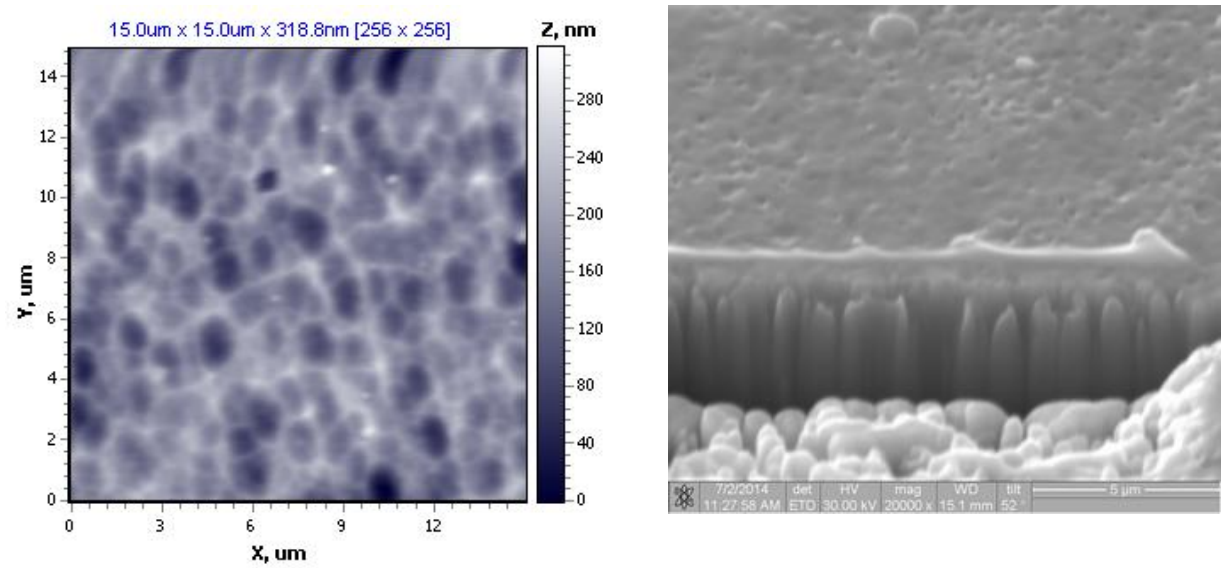

a) b)

Fig.1. AFM image of the coating Cr-Mn-Si-Cu-Fe-Al (a) andcross section (b)

The results of the study of the phase composition of the sample are shown in Table 4. It was determined on the hardness of the coating Cr-Mn-Si-Cu-Fe-Al nitrogen gas, which is equal to 7.413 GPa. It was determined: modulus of flow coating which is equal to 169.5 GPa, fluidity is 0.68%, and the coating is 0.05% relaxation.

.

Table 4 - Phase composition of Cr-Mn-Si-Cu-Fe-Al in nitrogen gas

Coating	Phase detection	Phasecontent, vol.%	Thelatticeparameters, Å	The size of CSR, nm	Δd/d $*10^{-3}$
Cr-Mn-Si-Cu-Fe-Al	$FeN_{0.0324}$	60.6	a=3.598	103.4	3.46
	$TiN_{0.31}O_{0.31}$	39.4	a=4.211	25.6	5.14

To determine all the above parameters were determined by Poisson's number to coating the Cr-Mn-Si-Cu-Fe-Al nitrogen gas equal to approximately 0.30. The corrosion rate in sulfuric acid (53 wt.%) was about 0.02 mm/year. Coating structure Cr-Mn-Si-Cu-Fe-Al+Ti, while spraying the resulting composite and titanium cathodes is shown in Figure 2. It is similar to the structure of the coating Cr-Mn-Si-Cu-Fe-Al. Nanohardness coating Cr-Mn-Si-Cu-Fe-Al+Ti equal to 14.2 GPa. The corrosion rate in sulfuric acid (53 wt.%) was less than 0.01 mm/year.

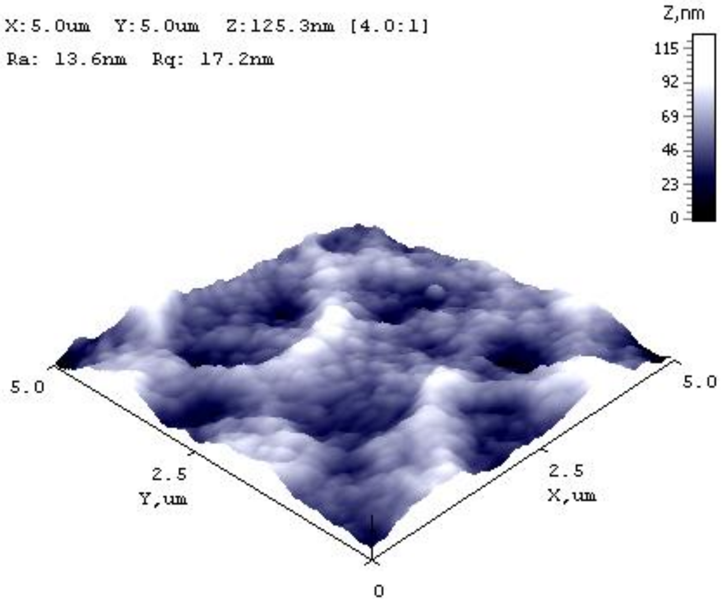

Fig.2. AFM image of the coating Cr-Mn-Si-Cu-Fe-Al+Ti under nitrogen

Figure 1b shows that the coating Cr-Mn-Si-Cu-Fe-Al is a columnar structure, which is characteristic of single-phase coatings and described by the model Thornton [30]. Single-phase structure observed in the coatings V-Zr-Nb-Hf in [31]. However, in this case there are two phases (Table 1). This suggests that the mechanism of columnar structure is not described by the model of Thornton. Below we will look at different mechanisms of such structures. It is interesting to compare the results with the known data on the nanoindentation other materials. These data are presented in Table 5.

Comparing the result obtained by us (7.413 GPa) with Table 2 shows that the nanohardness coating Cr-Mn-Si-Cu-Fe-Al almost 2 times higher nanohardness titanium and close to the Ti/α-C:H multilayer film. However, the preparation of such a film is much more difficult than coating Cr-Mn-Si-Cu-Fe-Al composite cathode via. Nanohardness coating Cr-Mn-Si-Cu-Fe-Al+Ti (14,2GPa) is nearly amorphous ribbon nanohardness Zr-Cu-Ti-Ni (14,5 GPa) or silicon (100) (14.8 GPa).Thus, the connection between the coating reveals the structure and its hardness. For ordered structures coating hardness increases. The relationship between the hardness of the coating and its structure was discussed in [33].

Table 5 - Properties of the materials according to the calculated nanoindentation [32]

Material	H, GPa	E, GPa	R, %
Copper	2.1	121	14
Titanium	4.1	130	19
The multilayer film Ti/α-C:H	8.0	128	34
The amorphous ribbon Zr-Cu-Ti-Ni	11.5	117	42
Silicon (100)	11.8	174	62
Thin film Ti-Si-N	28.4	295	62

5. The thermal resistance of multi-coating

Under the thermal resistance means the ability of a material to resist chemical degradation at high temperatures. Already in the 80s of the last century it became clear that you must not go towards the creation of special heat-resistant alloys and application technology to create various heat-resistant coatings on parts of machines and mechanisms operating under extreme conditions [34-36]. In subsequent years, interest in the thermally resistant materials and coatings continued to grow with the development of rocket and space technology, energy, etc. [37-39].

This paragraph is not intended to produce heat-resistant coatings. Using multi-element coverage, we would like to show the relationship between the thermal resistance and the surface energy of the coating, as well as to the method of calculating the surface energy (surface tension) of the deposited coating, using the results obtained in our work [17].

Thermal stability tests were carried out in electric furnaces resistance type G-30 in an atmosphere of air, with automatic temperature control to within ± 10 ° C. In tests we used special ceramic crucibles. The samples were placed in a crucible, which is then sent to the furnace.

Heat resistance was evaluated by weight of oxidized material. Weighing the samples before and after heat treatment was carried out on an analytical balance to the nearest 0.1 mg. Table 6 shows test results for heat resistance of the coatings.

Table 6 - The weight loss of the coating after heat treatment at 600 ° C for 100 hours

Coating	Oxidized coating weight, mg
Uncoated sample	56.8
Cr-Mn-Si-Cu-Fe-Al	4.2
Zn-Al	5.6
Mn-Fe-Cu-Al	6.8
Fe-Al	14.2

From Table 6 it follows that the highest thermal stability of the investigated coatings has a coating Cr-Mn-Si-Cu-Fe-Al, and the lowest - Fe-Al. However, any of the above coating greatly increases the thermal resistance substrate (metal substrate). If the response function F from [15] to take the thermal resistance χ, we obtain:

$$\chi = \frac{kT}{C_1} \cdot \frac{A}{G^0}, \tag{16}$$

.

where A - work of "external forces", T - temperature, the G^0 - Gibbs potential bulk metal sample (pure metal - is the Fermi energy E_F), k - Boltzmann constant, C_1 - constant.

The work of "external forces" for surface and thin films is equal to the energy of their destruction, i.e., $A = \sigma \cdot S$, where σ - surface tension, S is the specific surface. Thus, the thermal resistance is greater the greater their surface energy (surface tension). Table 7 shows the values of the investigated surface tension coatings obtained as described in [17]. CorrelationbetweenTables 6 and 7 there.

Since $G_0 = a + bT + cT^2$, the temperature dependence of χ can be neglected and the record (16) for one-component coating in the form of:

$$\chi = C \cdot \sigma / E_F, \tag{17}$$

where C - a constant.

For a multiple-coating, when there is no separation of the individual phases, we have:

$$\chi = C \cdot \left(\sum_i X_i \cdot \sigma_i / E_{F_i} \right), \tag{18}$$

where X_i - the mole or atomic fraction of the respective element in the coating.

Table 7 - The surface tension of multi-coating

Coating	The surface tension, j/m^2
Cr–Mn–Si–Cu–Fe–Al	1.019
Zn–Al	0.594
Mn–Fe–Cu–Al	0.446
Fe-Al	0.314

Multi-element, single-phase coatings are obtained, for example, in [31]. In the case of the individual phases in the coating (nitride, sulfide, etc.), the formula (3) can not be used. In this case we can use in our work [40], where the values of surface tension for nitrides, sulfides, oxides, etc. most of the elements of the periodic table. Determination of the surface tension of solids - a difficult task, so you can use a universal relation [17]:

$$\sigma = 0{,}7 \cdot T_{\text{пл.}}, \tag{19}$$

where T_m - the melting point of the metal, which is defined with great precision for all elements.

These formulas allow purposefully synthesize coating with desired thermal properties. The main problem is the generation of multi-element plasma flows. In most cases, this problem is not fundamental problems.

6. Thermomechanical destruction of metals, alloys and coatings

The destruction of the metal at the supply of thermal energy is accompanied by the accumulation of thermal stress, leading to an increase in the dislocation density, various defects (dilatons, frustrons etc.) [41-44].

Most of the existing mechanical systems in nature with the free movement of scatter ordered kinetic energy of its movement and turn it into a random thermal motion of the molecules. Such systems are usually called dissipative systems. Sometimes the flow of energy supplied to the system can reach such intensity that the old dissipation mechanism cannot cope with it. The system threatens the destruction. Then it can produce an internal reorganization of its elements in such a way that the energy dissipation process would go more intensively. This internal change occurs at phase transitions in the volume of metals and alloys [45], at the grain boundaries [46], on the surface [47]. On the basis of the theory of phase transitions attempt to combine different mechanisms of destruction processes [48]. In [49] proposes a mechanism of destruction of solids, not associated with the presence of defects in their original condition.

The theory of thermoelasticity of thin plates, and in this case coatings, as well as the corresponding isothermal theory is based on the hypothesis of the immutability of the normal element, and on the assumption of a two-dimensional stress state, a similar plane stress. The most complete questions thermoelasticity of thin plates described in [50].

In the formation of thermal stresses are distributed coating on some periodic (autowave) law [51]. Experimentally, it is shown in a periodic variation of the coating microhardness measured the length and breadth of the sample. Here we want to show the methodology for calculating the thermal stress on the experimental values of the microhardness. For this we use the heat equation for an infinite plate (cover), obtained in [52] for the radial μ_r and axial μ_z microhardness components:

$$\mu_r = A_r \frac{\partial T}{\partial r} = \frac{2}{z} \frac{A_r T_0}{\sqrt{\pi}} I_1\left(\frac{2r}{R}\right), \tag{20}$$

$$\mu_z = A_z \frac{\partial T}{\partial z} = \frac{R A_z T_0}{\sqrt{\pi} z^2} I_0\left(\frac{2r}{R}\right). \tag{21}$$

In these expressions A is a constant value with small thermal strains. The metal bodies of the effect of connectedness strain field and temperature field usually has little effect on the thermal perturbation and distribution of thermal stresses. In this case, you can use the known solutions for a circular plate of constant thickness [50]. And the stress component record:

$$\sigma_r = -2G \frac{1}{r} \frac{\partial T}{\partial r}. \tag{22}$$

$$\sigma_z = -2G \frac{\partial T}{\partial z}. \tag{23}$$

Here G is the shear modulus is given by:

$$2G = \frac{E}{1+\varepsilon}, \tag{24}$$

where E - Young's modulus, ε - Poisson's ratio.

We experimentally determined the radial component of the microhardness. Comparing (20) and (22) we obtain:

$$\sigma_r = -2G \frac{1}{r A_r} \mu_r. \tag{25}$$

Formula (25) is the basis for calculating the thermal stress in the coating on the experimental values of the microhardness.

.

Conclusion

Based on the analysis of the current state of destruction theories, corrosion, thermal and deformation of metals loading and coatings, as well as based on the proposed model, we can draw the following conclusions:

- in the most general case, corrosion of the metal can be present as the nucleation and growth of the new phase (oxidized metal). This is the approach used in the present study when discussing theoretical aspects of metal corrosion;

- formal description of the probabilistic nature of the new phase of the process as a random Markov stationary or non-stationary Poisson process requires a rigorous justification, as a number of assumptions (no aftereffects, ordinary, etc.) Does not stem from the physical picture of the phenomenon of corrosion;

- on the basis of a statistical approach to the formation of corrosion spots obtained an expression that shows the logarithmic dependence of the corrosion spot area of"defects" of the metal surface or coating;

- on the basis of non-equilibrium quantum statistical thermodynamics of a formula for the defects of the system response function (corrosion centers) to the external field;

- on the basis of a thermodynamic model obtained relationship between the corrosion rate, the surface tension of a metal surface and melting them;

- the theory of thermoelasticity of thin plates, and in this case coatings, as well as the corresponding isothermal theory, based on the hypothesis of the immutability of the normal element, and on the assumption of a two-dimensional stress state, a similar plane stress;

- proposed method of determining the thermal stress in the coating on the basis of experimental values of microhardness, measured the length and breadth of the sample;

- on the basis of thermodynamic model derived relationship between the heat resistance of coatings and surface energy;

- obtain a formula which is suitable for qualitative analysis and forecasting of metal fracture rate and coatings deformation and thermal influences.

REFERENCES

1 Strutt I.E., Nicholls and Barbier B. The prediction of corrosion by statistical analysis of corrosion profiles. *Corrosion science*. 1985, Vol. 25, No. 5, pp. 305 – 3l6.

2 Provan J.W., Rodriguez E.S. Development of a Markov description of pitting corrosion. *Corrosion (USA)*, 1989, Vol. 45, No. 3, pp. 178 – 192.

3 Baroux B. The kinetics of pit generation on stainless steel. *Corrosion science*, 1988, Vol. 28, No. 10, pp. 969 – 986.

4 Kondo J. Prediction of fatigue crack initiation life based on pit growth. *Corrosion science*, 1989, Vol. 45, No. 1, pp. 7 – 11.

5 Azarenkov N.A., Lytovchenko S.V., Nekludov I.M., Stoev P.I. *Corrosion and protection of metals. Part 1. Chemical corrosion of metals.* Kharkiv, 2007, 187p.

6 Park J.K., Baik Y.J. Increase of hardness and thermal stability of TiAlN coating by nanoscale multi-layered structurization with a BN phase. *Thin Solid Films*, 2008. Vol. 516, pp. 3661 – 3664.

7 Verma N., Cadambi S., Jayarama V., Biswas S.K. Micromechanisms of damage nucleation during contact deformation of columnar multilayer nitride coatings. *ActaMaterialia*, 2012, Vol. 60, pp. 3063 – 3073.

8 Skripov V.P. *Metastable liquid*. Nauka, Moscow, 1972, 312 p.

9 Kidyarov B.I. *The kinetics of formation of crystals from the liquid phase*. Nauka, Novosibirsk, 1979, 134 p.

10 Dynkin E.B., Yushkevich A.A. *Theorems and problems on Markov processes*. Nauka, Moscow, 1967, 426 p.

11 Platonova E.C., Buchinskas V., Yurov V.M. Statistical model for the formation of corrosion spots on

the metal. *Fundamental Research*, Russia, 2015, No.2, pp. 3048 – 3051.

12 Platonova E.C., Buchinskas V., Yurov V.M. Thermodynamic model of the formation of corrosion spots on the metal. *Fundamental Research*, Russia, 2015, No. 2, pp. 3281 – 3284.

13 Platonova E.C., Buchinskas V., Yurov V.M. Some questions of the theory of metal corrosion. *Bulletin of the University. Physics,* Kazakhstan, 2015, No.1 (77), pp. 21 – 30.

14 Yurov V.M., Guchenko S.A., Laurynas V.Ch. The role of the surface tension in the formation of plasma coatings. *Scientific Review. Technical science*, Russia, 2016, No. 4, pp. 124 – 139.

15 Platonova E.S.,Zhetesova G.S., Yurov V.M., Guchenko S.A. Anticorrosion and strengthening coatings for mining equipment. *Naukova News of the National Mining University*, Ukraine, 2016, No. 2, pp. 55 – 59.

16 Eremin E.N., Yurov V.M., Ibatov M.K., Guchenko S.A., Laurynas V.Ch. Anti-corrosion wear-resistant coatings on parts of oil field equipment. *Procedia Engineering,* 2016, Vol. 152, pp. 594 – 600.

17 Yurov V.M., LaurynasV.Ch.,Guchenko S.A., Zavatsky O.N. The surface tension of hardening coatings. *Reinforcing technology and coating*, Russia, 2014, No.1. – pp. 33-36.

18 Lorpez D., Alonso Falleiros N., Tschiptschin A.P. Effect of nitrogen on the corrosion–erosion synergism in an austenitic stainless steel. *Tribology International*, 2011, Vol. 44, pp. 610–616.

19 Liu R., Li X., Hu X., Dong H. Surface modification of a medical grade Co-Cr-Mo alloy by low-temperature plasma surface alloying with nitrogen and carbon. *Surface and Coatings Technology*, 2013, Vol.232, pp. 906 – 911.

20 Lv Jinlong, Luo Hongyun. Effect of surface burnishing on texture and corrosion behavior of 2024 aluminum alloy. *Surface and Coatings Technology*, 2013, Vol. 235, pp. 513 – 520.

21 Lee Y.J., Lee T.H., Kim D.Y.et. al. Microstructural and corrosion characteristics of tantalum coatings prepared by molten salt electrodeposition. *Surface and Coatings Technology*, 2013, Vol. 235, pp.819 – 826.

22 Castillejo F.E., Marulanda D.M., Olaya J.J, Alfonso J.E. Wear and corrosion resistance of niobium–chromium carbide coatings on AISI D2 produced through TRD. *Surface and Coatings Technology*, 2014, Vol. 254, pp. 104 – 111.

23 Klemm J., Klemm S.O., Duarte M.J. et. al. Multi-element-resolved electrochemical corrosion analysis. Part I. Dissolution behavior and passivity of amorphous Fe50Cr15Mo14C15B6. *Corrosion Science*, 2014, Vol. 89, pp. 59-68.

24 Alvarez-Asencio R., Sababi M., Pan J. et. al. Role of microstructure on corrosion initiation of an experimental tool alloy: A Quantitative Nanomechanical Property Mapping study. *Corrosion Science*, 2014, Vol. 89, pp. 236 – 241.

25 Skliarova H., Renzelli M., Azzolini O. et. al. Niobium–niobium oxide multilayered coatings for corrosion protection of proton-irradiated liquid water targets for [^{18}F] production. *Thin Solid Films*, 2015, Vol. 591, pp. 316 – 322.

26 Otto F., Yang Y., Bei H., George E.P. Relative effects of enthalpy and entropy on the phase stability of equiatomic high-entropy alloys. *ActaMaterialia*, 2013, Vol. 61, pp. 2628 – 2638.

27 Tsai M.H., Yeh J.W. High-entropy alloys: a critical review. *Mater. Res. Lett*., 2014, Vol. 2, pp. 107-123.

28 Pogrebnyak A.D., Baghdasaryan A.A.,Yakushchenko I.V., BeresnevV.M. Structure and properties of alloys and high-entropy nitride coatings on their basis. *Russian Chemical Reviews*, 2014, Vol. 83, No.11, pp. 1027 – 1061.

29 Schuh B., Mendez-Martin F., Vulker B. et. al. Mechanical properties, microstructure and thermal stability of a nanocrystalline Co Cr Fe Mn Ni high-entropy alloy after severe plastic deformation. *ActaMaterialia*, 2015, Vol. 96, pp. 258 – 268.

30 Thornton J.A. Structure and topography of sputtering coatings. *Ann. Rev. Material Sci*., 1977, Vol. 7, pp. 239 – 260.

31 Sabol O.V., Andreev A.A., Gorban V.F. and others. On the reproducibility of single-phase structural state multi element high entropy system Ti-V-Zr-Nb-Hf and high hard nitrides based on it as they are formed by vacuum arc method. *Technical Physics Letters*, Russia, 2012, Vol. 38,No.13, pp. 40 – 47.

32 Golovin Y.I. Nanoindentation and mechanical properties of solids in submicro volumes, thin surface layers and films. *Solid State Physics*, Russia, 2008, Vol. 50, No.12, pp. 2113 – 2142.

.

33 Musil J., Polakova H. Hard nanocompositeZr-Y-N coatings, correlation between hardness and structure. *Surface and Coatings Technology*, 2000, Vol. 127, pp. 99 – 106.

34 Movchan B.A., Malashenko I.S. *Heat-resistant coating is deposited in a vacuum*. Kiev: Naukova Dumka, 1983, 232 p. [in Russian]

35 Muboyadzhyan S.A., Lesnikov V.P., Kuznetsov V.P. *Integrated protective coating of turbine blades for aircraft GTE*. Ekaterinburg: Publishing house "Kvist", 2008, 208 p.

36 Davis J.R. (Ed.) *Heat Resistant Materials*. ASM International, 1997, 591 p.

37 Reed R.C. *The Superalloys: Fundamentals and Applications*. Cambridge Univ. Press, 2006, 372p.

38 Gao W., Li Zh. (Eds.*) Developments in High Temperature Corrosion and Protection of Materials*. - Woodhead Publishing Ltd, 2008,658 p.

39 Madhusudana Chakravarti V. *Thermal Contact Conductance*. Springer Intern. Publishing Switzerland, 2014, XVIII, 260 p.

40 Yurov V.M., Portnov V.S., Laurynas V.Ch. et al. *Size effects and physical properties of small particles and thin films*. Karaganda: Publ. house of the Kazakh-Russian University, 2013, 116 p.

41 Petrov V.A. Dilaton model of thermal fluctuations of crack. *Solid State Physics*, Russia, 1983, Vol.26, No. 11, pp. 3124 – 3127.

42 Zhurkov S.N.Dilaton mechanism of strength of solids.*Solid State Physics*, Russia, 1983. Vol. 25, №10 – pp. 3119-3123.

43 Kulikov D.V., Mekalova N.V., Zakirnichnaya M.M. *Physical nature destruction*. Ufa: UFGU, 1999, 240 p. [in Russian]

44 Olemskoy A.I., Katznelson A.A. *Synergetics of condensed matter*. Moscow, URSS, 2003, 336 p.

45 Christian J. *The theory of transformations in metals and alloys*. Moscow, Mir, 1978, 808 p.

46 Straumal B.B. *Phase transitions in the grain boundaries*. - Moscow, MISiS, 2004, 65 p.

47 Zenguil E. *Surface Physics*. Moscow, Mir, 1990, 536 p. [in Russian]

48 Botvina R.L. *Destruction: kinetics, mechanisms, general laws*. - M.: Nauka, 2008 – 334 p.

49 Panin V.E., Egorushkin V.E., Makarov M.P. et al. *Physical mesomechanics and computer construction materials*. Novosibirsk, Nauka, 1995, Vol. 1, 298 p. [in Russian]

50 Zarubin B.C., Kuvyrkin G.N. *Mathematical models of thermal mechanics*. Moscow, FIZMATLIT, 2002, 168 p. [in Russian]

51 Yurov V.M., Laurynas V.Ch., Guchenko S.A., Zavatsky O.N. Autowave processes in the formation of ion-plasma coatings. *Bulletin of the University. Physics*. Kazakhstan, 2013, No. 1 (69), pp. 56 – 66.

52 Yurov V.M., Laurynas V.Ch.,Guchenko S.A., Zavatsky O.N. The stationary thermal field of endless metal plates nanometer thickness. *International Journal of Applied and Basic Research*, Russia, 2013, No.10, pp. 514.

Article accepted for publication 02.12. 2016

UDC 532.525.6

HEAT TRANSFER IN THE PRESENCE OF TRANSITION INDUCED BY WAKES OF HESITATING CYLINDER

Suprun T.T.

Institute of Engineering Thermophysics National Academy of Sciences of Ukraine (IET NASU), 2a Zhelyabova str., 03057, Kiev, Ukraine, suprun@biomass.kiev.ua

Experimental investigations of a flat plate heat transfer in the presence of transition induced by wakes after still and hesitating cylinder were carried out. Analysis of distributions of local heat transfer coefficients, temperature and velocity profiles, their fluctuations and other characteristics of boundary layers permits to determine the length of wake-induced transition and its location. On the basis of study of wakes characteristics in the free-stream the reason of heat transfer intensification in pre-transitional boundary layer was determined. Under influence of periodic unsteady wakes transition region shits upstream in comparison with the case of steady wake.

Keywords: *heat transfer, laminar-turbulent transition, wakes, hesitating cylinder, dynamic and thermal boundary layers*

Introduction

Unsteady flows after moving and still obstructions are widely spread in various technical applications such as turbomachinery, thermal power installations, and internal flow in technological equipment. Unsteady flow initiates special type of laminar-turbulent boundary layer transition: wake-induced transition. Successful prediction of transition induced by wakes would help in designing efficient equipment. It concerns first of all gas turbine engines. The aerodynamic performance of turbines is dependent on the nature of boundary layer development on the blades. It is known that a considerable area of the blade surface can be covered by transitional boundary layer (BL). This is especially true at the low Reynolds numbers typical for the low-pressure stages in gas turbines. The blade boundary layers are subjected to a combination of variables including free-stream turbulence, pressure gradient, unsteady periodic wakes of the upstream blade rows. These conditions have a significant influence on the BL transition process.

During the last years many researchers experimentally and theoretically investigated the effect of unsteady wakes on the characteristics of thermal and dynamic BL transition. The unsteady wake exhibits mean velocity defect with a high level of turbulence intensity. Just the last is primarily responsible for transition under the influence of periodic unsteady wakes [1, 2]. So such transition has common features with bypass transition at Tu >0 as noted in [3].

The present investigation focuses on the effect of periodic unsteady wakes on heat transfer and internal structure of the thermal and dynamic boundary layers in the presence of laminar-turbulent transition. In order to study the influence of periodic instability experimental investigation with still cylinder situated on the distance from the plate equal to the amplitude of hesitating cylinder was conducted.

1. Experimental technique

The experiments were carried out at velocity 9 m/s in a wind tunnel T-5 of IET NASU with working section 120x120x800 mm. A heated flat plate (2) was mounted in working section (3) asymmetrically at h =90 mm from top wall (Fig.1). For generating periodic unsteady wakes single hesitating at f =4.4 Hz cylinder (1) d =3 mm was located upstream of the plate at x =-15 mm. The amplitude of cylinder motion was 20 mm from the axis of the leading edge of the plate. Steady wake was produced by the same still cylinder which is situated also at x=-15 mm and y_c=20 mm.

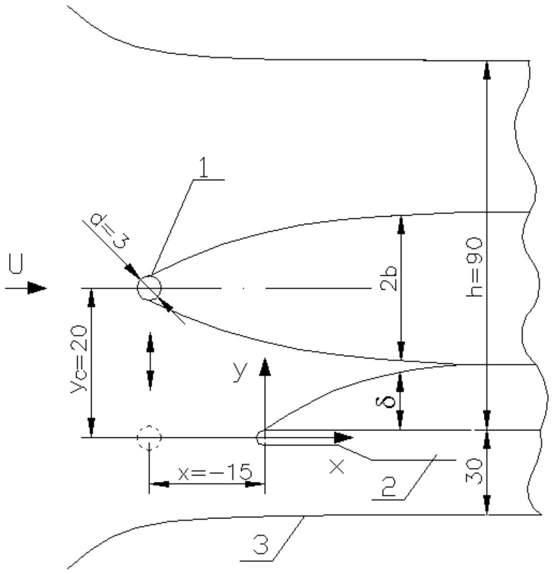

Fig. 1. Sketch of the experimental installation

Heat transfer was explored by electrocalorimetry. The parameters of the internal structure of the dynamic and thermal boundary layers and external flow were measured by DISA-55M hot-wire system with 5μ and 1μ probes. It is necessary to remark that in periodically disturbed flow total turbulence intensity was measured including periodic and turbulent fluctuating components.

2. RESULTS AND DISCUSSION

Heat transfer

For estimating the influence of the wakes on the characteristics of the thermal transition the results of heat transfer investigation without cylinder with natural transition at Tu=0.2-0.4% were used (Fig.2, symbol 3). In case of steady wake generation after still cylinder (Fig.2, symbol 4) the distribution of local heat transfer coefficients along the plate is changed: the start of wake-induced transition is shifted upstream relatively natural transition which occurred without wakes and heat transfer in the pre-transition boundary layer is increased.

In the presence of hesitating cylinder (Fig.2, symbol 5) the distribution $St = f(\mathrm{Re}_x)$ became smoother than in previous case but remained non-monotone. Intensification of heat transfer in the pre-transition boundary layer in cases of steady and periodic wakes was correspondingly ~20% and 38% at Re_x=$4 \cdot 10^4$ relatively laminar boundary layer (Fig.2, line 1).

The increase of heat transfer in the pre-transition boundary layer allows one to treat the latter as an analog of the pseudolaminar boundary layer [4]. The reason of pseudolaminar boundary layer origin consists in the presence of elevated free-stream turbulence. As shown in [5] under influence of other moving obstructions organised by still and rotating “squirrel cage” the distribution of local heat transfer coefficients along the plate is also changed relatively natural transition: the start of wake-induced transition is shifted upstream which occurred without wakes and heat transfer in the pre-transition boundary layer is also increased. But after still and rotating “squirrel cage” the distribution $St = f(\mathrm{Re}_x)$ became monotone and approach to the turbulent BL from “above”. In this case the existence of wake-induced laminar-turbulent transition of upper type is confirmed.

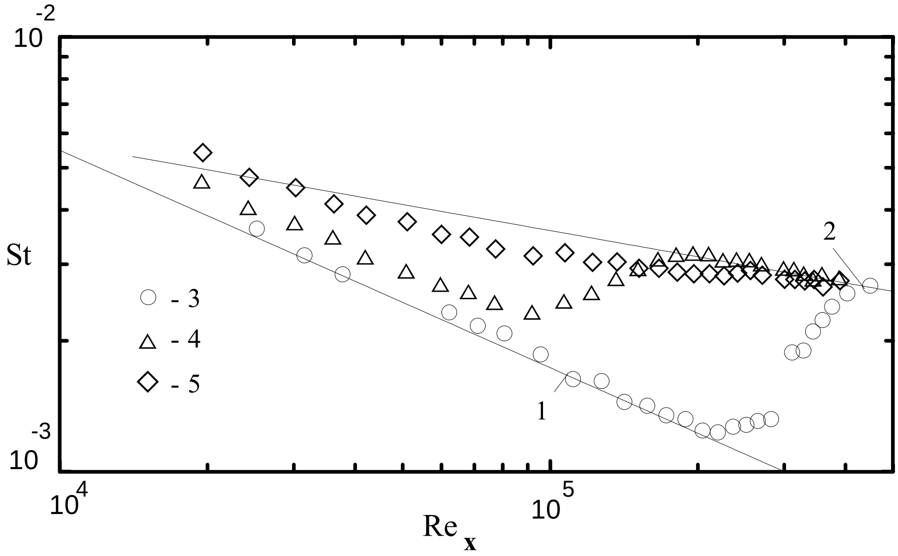

Fig.2. Heat transfer distribution: 1- $St = 0.55\,\mathrm{Re}_x^{-0.5}$; 2 - $St = 0.036\,\mathrm{Re}_x^{-0.2}$;
3 – without cylinder; 4 - still cylinder; 5 - hesitating cylinder

Characteristics of wakes

The analysis of distributions of time-averaged velocity (Fig.3a, 3b, symbol 1) and its longitudinal fluctuation (Fig.3a, 3b, symbol 2) in the free-stream ($y > \delta$) showed that wakes change the uniformity of the velocity distribution because of the presence of defect and generate a nonuniform turbulence field.

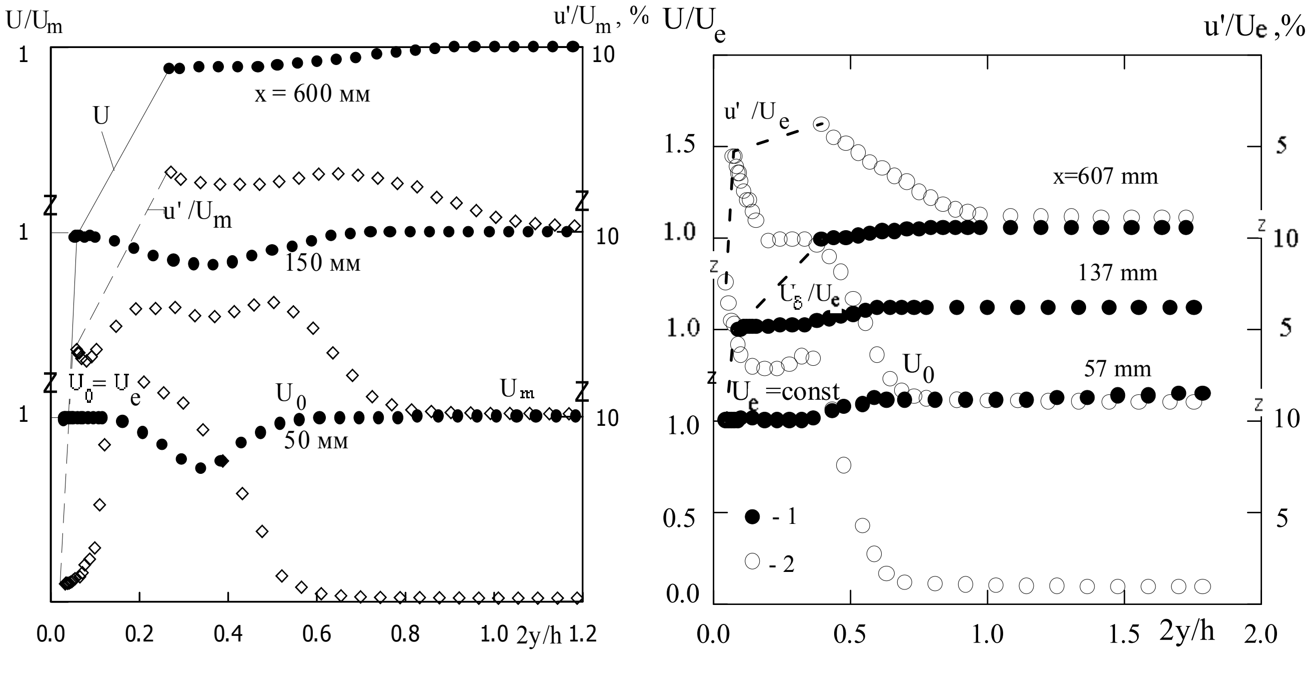

a) b)

Fig.3. Characteristics of wakes after still (a) and hesitating (b) cylinder

However the interaction between shearing motion in the wake and boundary layer leads to formation the region close to BL with the uniform field of the velocity U_e=const in cases of still (Fig.3a) and hesitating cylinder (Fig.3b). The value U_e is taking as a velocity of free-stream at forming of BL. In the region U_e=const at x<150 mm longitudinal fluctuations of velocity changed substantially (for example, from u'_δ/U_m=1% up to 8.5% (Fig.3a, x=50 mm) and from u'_δ/U_e=15.8% up to 12% (Fig.3b, x=57 mm), where U_m - maximal velocity out of the wake. As seen from Fig.3a and 3b, total intensity of turbulence in case of hesitating cylinder is higher than for still one. Such increased level of turbulence in free-stream causes the increase of the local heat transfer and friction coefficients in pre-transitional boundary layer.

Features of dynamic and thermal boundary layers

The analysis of dynamic and thermal boundary layers characteristics in the presence of still and hesitating cylinder confirmed the origin of pseudolaminar boundary layer before wake-induced transition. The profiles of velocity and temperature in BL that precedes wake-induced transition are characterized by the elevated gradients at the wall. At the same time the BL thicknesses δ and δ^{**} increase at conservative displacement thickness δ^{**}, what leads to reduction of shape parameter H in comparison with laminar BL. Distinguishing feature of pseudolaminar BL is also the appearance of maximum of turbulence kinetic energy at y/δ=0.2-0.3. Distributions of the longitudinal velocity fluctuations in BL disturbed by the wake of still cylinder (Fig.4a) demonstrated such peak at x=50 and 150 mm. This peak shifts in direction of the wall in the process of transition.

One of the important features of longitudinal velocity fluctuations in BL disturbed by the wakes of hesitating cylinder is appearance of two peaks (Fig.4b). The amplitude and the location of these peaks vary with the development of transition.

Thus, the amplitude of the first near the wall peak increases upon approaching the transition and its location is shifted to the wall. The location and amplification of this peak is similar to that observed in bypass transition. The second peak located closer to the outer edge of the boundary layer arises as a result of wakes interaction. The energy of secondary peak decreases with distance from the wake generator. The observed features of velocity fluctuation profiles are in good agreement with results of investigation carried out in Institute of Fluid-Flow Machinery PASci. (Gdansk), when boundary layer affected by the wakes of two different wake generators: single moving cylinder [3, 6] and rotating “squirrel cage”.

At the same time profiles of temperature fluctuation have only one peak near the wall (Fig.4b, dashed line 1) like the first peak in velocity fluctuation profiles but located closer to the wall.

Coordinates of wake-induced transition

The analysis of mentioned above specific features of pseudolaminar BL and bypass transition permitted to determine coordinates of wake-induced transition using special diagnostics methods developed in IET NASU [7]. At presence of still cylinder the start and the end of transition are located at $\mathrm{Re}_{xst}=9\cdot10^4$ and $\mathrm{Re}_{xend}=2.65\cdot10^5$ correspondingly; for hesitating cylinder $\mathrm{Re}_{xst}=8.5\cdot10^4$ and $\mathrm{Re}_{xend}=2.4\cdot10^5$. In both cases wake-induced transition transformed into turbulent boundary layer (Fig.2, line 2). Thus the start and the end of wake-induced transition were shifted upstream relatively natural transition which occurred without wakes ($\mathrm{Re}_{xst}=2\cdot10^5$, $\mathrm{Re}_{xend}=4.5\cdot10^5$).

As mentioned above total turbulence level in free-stream for hesitating cylinder was higher than for still one (Fig.3a and 3b). So comparison of heat transfer distributions in cases of steady and periodic unsteady wakes showed that when total turbulence intensity increases intensification of heat transfer in the pre-transition BL also increases. Region of transition induced by hesitating cylinder shifts upstream relatively steady case.

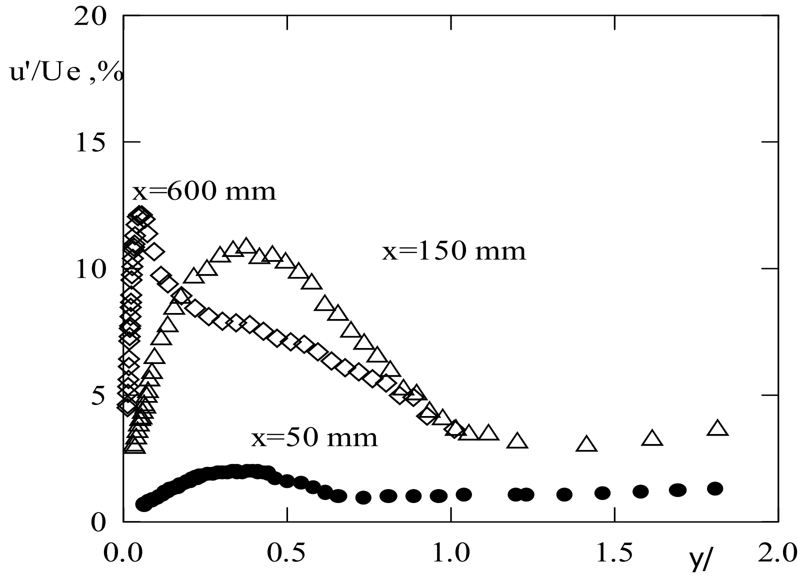

a)

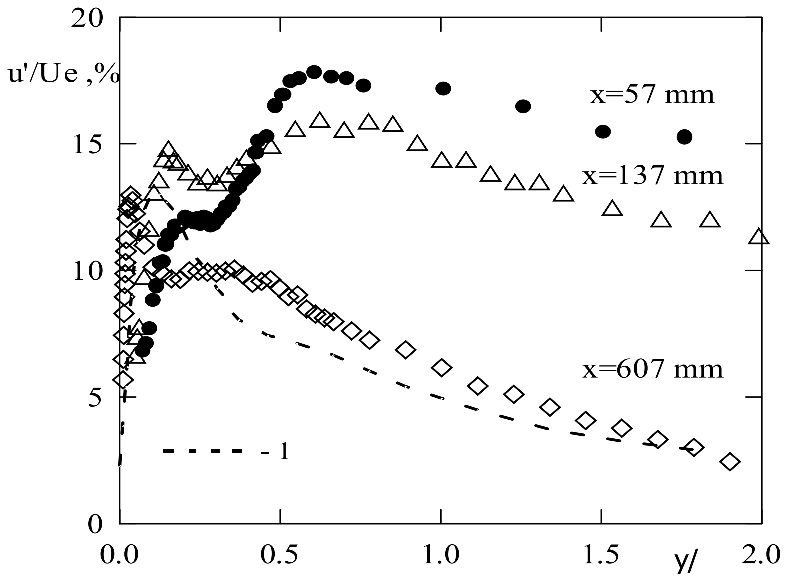

b)

Fig.4. Distributions of the longitudinal velocity fluctuations in the presence of still (a) and hesitating (b) cylinder: 1 - $t'/(t_w - t_e) = f(y/\delta_t)$ at x =50 mm

Comparative length of transition ($\mathrm{Re}_{xend}/\mathrm{Re}_{xst}$) in both cases is practically constant ($\pm$5%). At the same time the absolute length of wake-induced transition ($\mathrm{Re}_{xend} - \mathrm{Re}_{xst}$) for periodic unsteady wakes decreases in comparison with the steady ones.

Conclusion

Experimental investigations of a flat plate heat transfer in the presence of laminar-turbulent transition induced by wakes after still and hesitating cylinder were carried out.

It has been shown that wake-induced transition shifts upstream relatively natural transition without wakes. In both cases of wake-induced transition pre-transitional BL was pseudolaminar and characterized by substantial heat transfer growth in comparison with laminar boundary layer. Taking into account that under influence of hesitating cylinder total turbulence intensity of free-stream is higher than in the presence of steady wakes, intensification of heat transfer in pre-transitional BL at $\mathrm{Re}_x = 4 \cdot 10^4$ increased from ~20% for steady wakes to 38% for periodic ones. Due to increasing turbulence intensity wake-induced transition shifts to lower Reynolds numbers, its comparative length ($\mathrm{Re}_{xend} / \mathrm{Re}_{xst}$) remains unvarying and absolute length ($\mathrm{Re}_{xend} - \mathrm{Re}_{xst}$) decreases.

Obtained results of experimental study of thermal transition induced by wakes should provide test cases for improving the heat transfer modelling and enhancing the accuracy of thermal load prediction.

REFERENCES

1 Schobeiri M.T., Chakka P. Prediction of turbine blade heat transfer and aerodynamics using a new unsteady boundary layer transition model. *Int. J. Heat and Mass Transfer.* 2002, Vol. 45, pp. 815 – 829.

2 Orth U. Unsteady boundary-layer transition in flow periodically disturbed by wakes. *ASME J. of Turbomachinery.* 1993, Vol. 115, pp. 707 – 713.

3 Wiercinski Z.et al. Characteristics of the laminar-turbulent transition induced by wake of a single moving cylinder. [in Russian] *Industrial Heat Engineering*. 2001, Vol. 3, N 3-4, pp. 16 – 23.

4 Dyban Ye.P., Epik E.Ya. The Structure of Boundary Layers in a Bypass Laminar-Turbulent Transition. [in Russian] *Industrial Heat Engineering.* 1999, Vol. 1, N 1, pp. 22 – 30.

5 Epik E.Ya., Suprun T.T. Influence of unsteady flow structure on heat transfer in transitional boundary layer. [in Russian] *Proc. of XIX school-seminar of young scientists and specialists under the leadership of the academician, professor A.I. Leontiev "Problems of heat and mass transfer and gas dynamics in energy plants"*. Moscow. 2013, pp. 42 – 45.

6 Epik E.Ya. et al. Some features of mechanism of laminar-turbulent transition induced by wakes. *Eurasian Physical Technical Journal*. 2006, Vol.3, No. 1(5), pp. 54 – 58.

7 Epik E.Ya., Suprun T.T. Heat Transfer and Diagnostics of Bypass Laminar-Turbulent Transition. *Proc. of the 3rd Int. Symp. "Turbulence, Heat and Mass Transfer"* Nagoya. 2000, pp. 1-8.

Article accepted for publication 11.11.2016

UDC 621.311.24

ANALYSIS OF DEVELOPING WIND POWER APPARATUS IN KAZAKHSTAN

Yershina A.K., Nursadykova Zh.K., Borybaeva M.A.

Kazakh State Women's Teacher Training University, Almaty, Kazakhstan,
meruert_b@mail.ru

The article is devoted to problems of wind energy. Data growth rate of the installed capacity of wind power plants in the world are shown. The authors analyzed the technical and economic performance of wind power systems developed by Kazakhstan scientists. The technical characteristics of Darrieus type wind turbines have been described. The advantages of the Bidarrieus wind turbine were studied.

Keywords: wind power apparatus, Betz-Zhukovsky postulate, Bidarrieus wind turbine, coaxial shaft, usage coefficient of wind energy

Introduction

Today one of the most promising directions in alternative energy is - wind energy. In recent years, wind energy has become a truly thriving industry of "pure", or as it is called "green" energy. Means of converting the kinetic energy of the wind flow into the mechanical, thermal and electrical forms of energy are taking a greater share in the global energy industry.

Based on the report of the development of the global wind energy industry for 2016 by the World Wind Energy Association (World Wind Energy Association - WWEA) [1], it is shown that the power of the global wind power industry has reached 456,486 MW in 2016 (Figure 1). 21,714 MW from total were added during the first six months of 2016. This increase was added similarly as in the first half of 2015, when 21.6 GW. All wind turbines installed worldwide by the middle of 2016 could generate about 4.7% of the world's electricity demand.

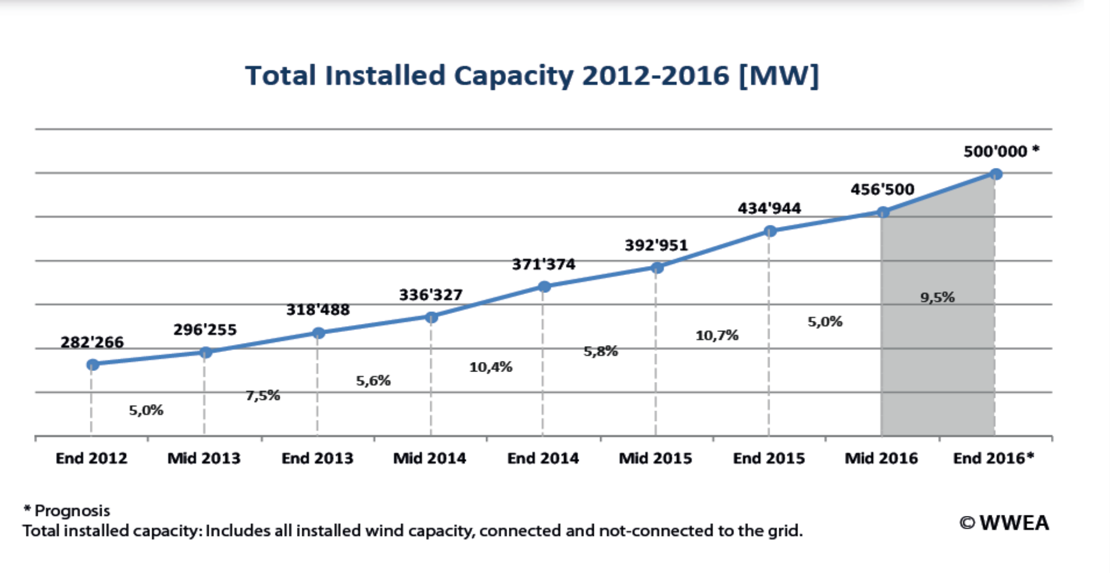

Fig.1. Worldwide power of wind energy installations 2012-2016 years

Overall, 103 countries and regions use wind energy for electricity production. Kazakhstan became the eighty-fourth country in the world using 2 MW wind energy technology in 2014[1]. According to estimates of experts [2, 3] the potential of renewable energy resources (hydro, wind and solar energy) in Kazakhstan is very significant and estimated at over $ 1 trillion kWh / year.

1. Overview of the wind turbine developed in Kazakhstan

Depth study of the problems of wind energy in Kazakhstan started in the last 15-20 years by works of academician of the National Academy of Sciences of Kazakhstan Sh.A. Yershin (Kazakh National University, Almaty) academician of the National Academy of Engineering A.V. Bolotov (AUPET, Almaty), prof. N.S. Buktukov (Institute of Mining, Almaty), Doctor of Technical Sciences (DofTS), H.Zh. Bayshagirov (Scientific Production Association-Wind Energy Apparatus with Diffuser(WEAD), Kokshetau), O.Bayaliev (IE "Innovative bureau of Bayaliev"), prof. A.K. Kusainov (Asiamontazhengeneering, Almaty), M.M. Maylibaev (Almaty), DofTS, prof M.B. Koshumbayev (Kazakh Research Institute of Energy of Sh.Ch. Chokina.), DofTS, prof. G.B. Nurpeisova (Kazakh Research Institute of Energy mechanisation and electrification of agriculture), Ph.D., prof. K.Kussaiynov (Institution of Applied Math, Karagandy) et al. with the lack of financial support from government and UNDP [4 - 16].

The first development and use of wind power plants owned by professor of Almaty University of Energy and Communications A.V. Bolotov, the foundation of which was model of the device Savonius based on the principle of the sailing type wind turbines [4]. Kazakhstan has about 50 stations with wind rotor turbine. Vertical Axis Turbine rotor consists of several individual modules (Figure 2) and the power can be increased by the increasing of their number. The parameters of Bolotov Wind Rotor Turbine (BWRT): weight is 750 kg, temperature range of is (-40) - (+40) Celsius, power is 3-10 kW, nominal speed is 12.3 m / s, features are high security (no vibration open moving parts), available resources, reliability, endurance is more than 10 years, does not depend on wind direction, works in conditions of turbulence, modularity, low operating costs, a synergistic effect in combination with solar panels.

Unfortunately, this type of wind turbine has low technical and economic indicators with high costs of material and cannot compete with modern wind turbines. Wind turbine developed by M.M. Maylibaev has the same features with some changes. Such wind turbine with some changes and development relates M.M. Maylibaev (Figure 3). Apparatus of professor N.S. Buktukov (Institute of Mining MES) can work in any wind direction and speed, from 3 m/s up to 60-80 m / s, all 300-330 days in a year, and its price is only 5000$.

Fig.2. Wind rotor turbine of A.V. Bolotov

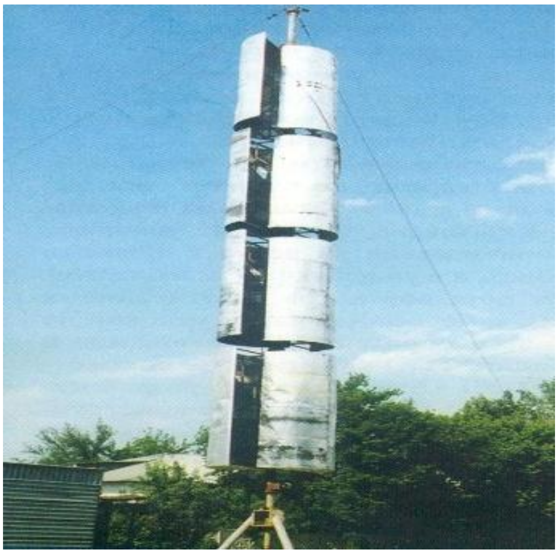

Fig.3. Wind turbine of M.M. Maylibayev

Additionally, in contrast to the expensive foreign wind plants it has a complete generator, multiplexer equipment control device, charging and battery protection device [4, 5]. There is no tower in Buktukov's apparatus and it is easy to produce. Furthermore, the invention simultaneously can be as a beacon in the steppes of Kazakhstan, as well as in the islands. Another advantage is that with increasing of wind speed blades are compressed and acquire a tubular shape. This invention of professor N.S. Buktukov has not found sufficient development and application yet (Fig. 4).

Fig.4. N.S. Buktukov's wind turbine

Fig.5. Wind energy apparatus with diffuser (WEAD), developed by professor H.Zh. Bayshagirov

Professor H.Zh. Bayshagirov (Director of LLP Research and Production Association, WEAD) uses the original proposal to increase wind energy utilization, (Fig. 5) [4, 15]. The idea of creating a device called WEAD is in the fact that the wind turbine installed in the narrow part of the considerable dimensions of the diffuser. It is expected that improvements in energy efficiency of ratio propeller of wind turbines will be determined by the ratio of the sizes of the wide input portion of the diffuser and narrow output portion of this system by accelerating the wind flow in a diffuser.

Prototype of wind energy plant with a diffuser (WEAD) created by professor H.Zh. Bayshagirov gave positive results. WEAD made from fiberglass is environmentally friendly, easy to use and portable power source. Tests have shown that WEAD is twice more powerful than the wind turbine without the diffuser. Main theoretical idea that diffuser is effective was confirmed. Parameters of WEAD: weight is 95 kg, height of the tower is 4 m, design capacity is 1 kW, temperature ranges from -50 ° C to + 80 ° C, the duration of operation is 20 years, produces a current at a wind speed of 4-25 m/s. Installation (dismantling) can be done by the 3 employees in 2-3 hours without lifting devices. Core nodes and the diffuser were manufactured from fiberglass with the use of resource-saving technology of the processing of composite materials; through this method increases the duration of turbine's operating mode and the geography of its use. High mobility, ease of maintenance, increased serviceability, resistance to various manifestations of climate, security in the broadest range of use, quiet operation, small metal content, design appeal, the absence of interference can be highlighted as well. WEAD covers costs of building in 4-5 months when it is used in conjunction with the pump "Vodoley-3" to supply drinking water from the well (Fig. 5).

Professor M.N. Kambarov (LPP "Ecowatt") proposed new model of wind turbine called "Kazkanat" (Fig.6) [4]. Assumed parameters are the following: power is max.15 kW, nominal is 5 kW, wind speed is (3 – 40) m / s, the voltage is (380 – 200) V; the number of blades is 2, the bottom chord of the blade is 1m, the upper chord is 0.5 m, radius of the blades is 1.8 m, the number of poles is 2, height is 2.4 m, height above the shaft ground is 2.4 m. It orientates to the wind through vane blades effects and 4 flat supports (without special arrangements); the angle of attack of the blades is

8 degrees (without regulation). The effort to develop a sailing type machine specifically for the Zhungar Gates ended unsuccessfully.

Fig.6. «Kazkanat» wind turbine, developed by professor M.N. Kambarov

Professor M.B. Koshumbaev from Kazakh Research Institute of Energy developed vortex wind power apparatus with flow concentrator [16]. Improving the efficiency and reliability of wind machine is achieved by generation of swirling motion of the air flow, which occurs due to the curved guiding walls and the tangential air supply to the exhaust pipe. The curvature of the walls and the blade are described by a logarithmic dependence. Furthermore, concentrator consists of a marquee and a cone, which is located between the curved guiding walls. The outer parts of the marquee and black exhaust pipe are heated by solar energy, which also increases the exhaust thrust.

Another feature of the Wind Energy Plants (WEP) is wind wheel, designed as shell of generator which on the outer side curved blade is installed, wherein one end of the generator's shaft fixed in the center of the cone, and another end to the top of the chimney. After entering of airflow to the concentrator it is heated; due to curved guiding walls it receives a rotational movement. An increase in temperature and decrease in effective cross-section of flow also contributes to its stable accelerated rotational motion. The swirling airflow causes the rotation of the blades and generator; additionally, when the blades return, they do not experience resistance. The new WEP allows achieve the technical result that gives increased efficiency by eliminating the heating system, optimization of tangential flow entering to the pipe, assembly reliability by eliminating the effect of the flow on the return stroke of the blade, improving aerodynamic operation [16].

In Figure 7 schematics illustrate the structure of the proposed wind machine. In Fig.7a is shown a side view and a section along A-A, sectional view of an image of the propeller blades of the generator is reflected. In the center of the tent (1) the exhaust pipe (2) is installed. Inside of the tube wind wheel generator (3) is placed, on the outer side of which is rigidly fixed curved blades (4). Shaft generator (5) is fixed on the center of the cone (6) and on the top of the tube. In flow concentrator between the tent and cone curved guide walls (7) are arranged, which curvilinear tapered air passages provide a tangential inlet air flow in the chimney.

Since 90s Kazakh Research Institute of Mechanization and Electrification of Agriculture has been actively working on the development of wind power plants and water lifting machines by wind. The result of researches are standard series of apparatus such as VV-3T, VV-5T, VE-2T, VGE-2.7T, VE-5T, VGE-5T and VE-5T-2M, according to the wind characteristics in Kazakhstan they are slow multi-bladed settings (Fig. 8).

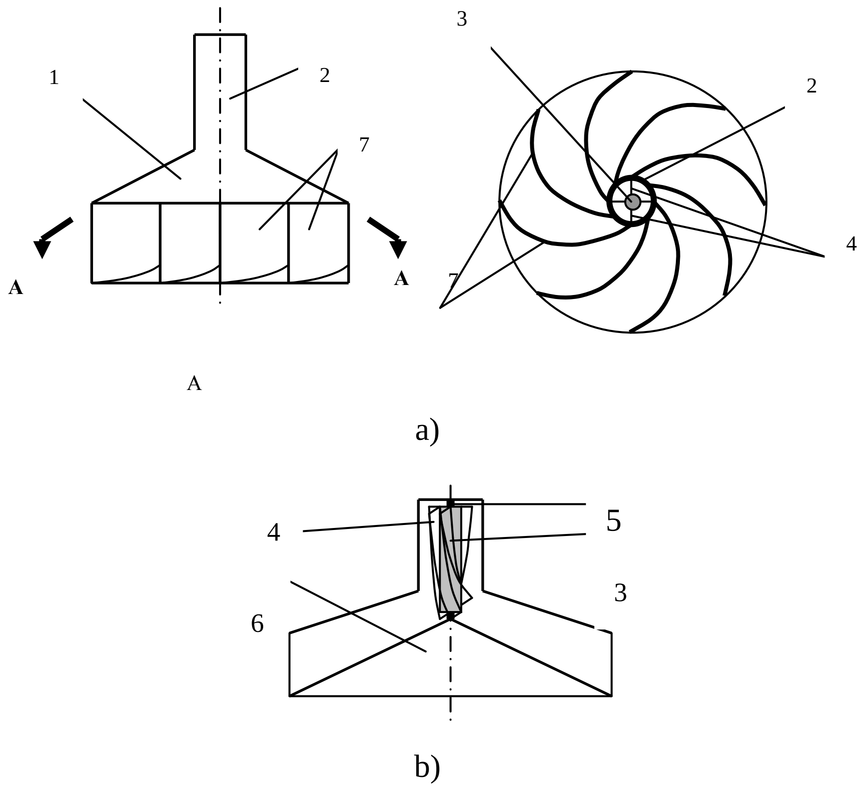

Fig.7. Structure of the wind machine:
a) scheme of wind turbine; b) sectional view of an image of the propeller.

In the laboratory (Institute of Applied Mathematics, Karaganda) professor K. Kussaiynov conducted a research named "Development of a wind turbine for small wind speeds based on variable cross-section of the rotating cylinder" (Fig. 9) [4]. In the wide range of the incoming flow rate (3 - 15) m/s and changes in geometrical parameters the lifting force was generated by the Magnus effect is investigated.

Fig.8. Slow multi-bladed installation of Kazakh Research Institute of Mechanization and Electrification of Agriculture

Fig. 9. Wind turbine model, developed by professor K.Kussaiynov

The dependences of the coefficients of aerodynamic lift force from the wind speed, from the speed of rotation of the cylinder with spherical ends, from the diameter of the test body were found. The range of optimum parameters, providing a stable maximum lift force coefficient, was determined. Sample model of two-bladed wind turbine with car generator as a source of 700 watts was designed and manufactured.

2. Wind turbines Darrieus and Bidarrieus

Last years The Kazakh National University developing promising two-rotor machines (Bidart, HBI-rotor, etc.) under the leadership of Sh.A. Yershin [6-14]. Design of Darrieus apparatus with two coaxial shafts was named Bidarrieus. To some extent, this wind turbine can be considered as unit of two Darrieus rotor deployed in 90^0, so that swings perpendicular to each other. Carousel wind turbine can operate in normal Darrieus mode and Bidarrieus mode (Fig.10). The shafts are separated by a bearing and they can work autonomously and independently from each other. There is a special correcting device (retainer) which supports an angle $\alpha = 90^0$ between the swings of the Bidarrieus.

Fig.10. Sh.A.Yershin's wind turbine

The rotational energy is transferred to the two different current generators, in other words, each shaft runs in its own generator. Then electricity produced by them is summed. Design of semi-industrial sample of Bidarrieus allows coaxially disposed shafts to rotate in the opposite directions. In this case, a dual circuit electric generator can be used. Thus, the advantage of this design is increased obtain of wind energy by the two independent shafts with the same swept area. Therefore, efficiency value of the wind energy in high production can be increased to 0.65.

Bidarrieus Wind Turbine provides power generation at a speed of 5-15 m/s. The total height of the wind turbine is 10.6m, weight is 800 kg. The turbine mounted on a lightweight foundation and additionally secured by a rope. Size of rotors: swing of the outer rotor - 2 m, the length of blade - 4.5 m, swing of inner rotor - 1.7 m, the length of blade - 4 m. Profile of blades is NASA-0021, chord of blades is 0.3 m. Testing of Bidarrieus wind turbines showed that utilization of wind energy ξ is 40% higher than the Darrieus wind turbine with the same capacity (shaded area in Fig.11). Thus, the value ξ reaches the max of the value limited by Betz postulate. The invention protected by patents of the Republic of Kazakhstan.

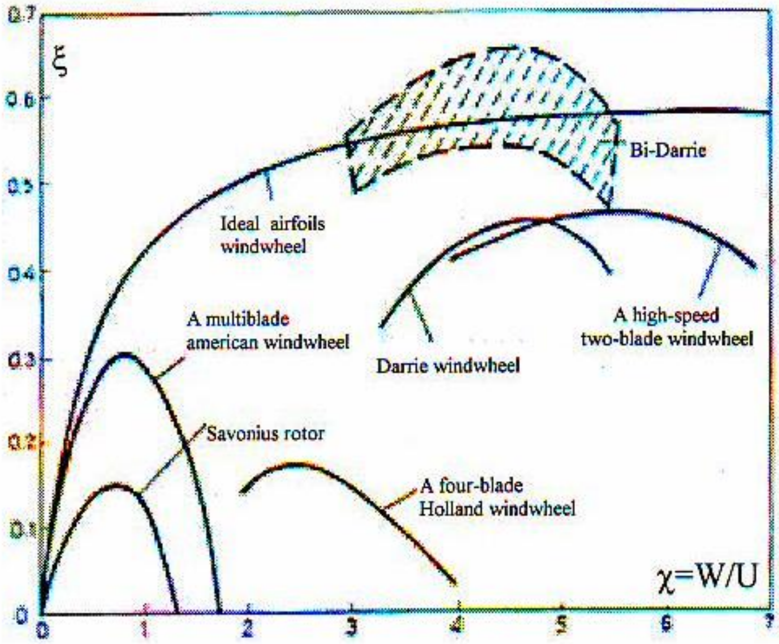

Fig.11. Dependencies of wind energy utilization factor ξ for different types and constructions of wind turbine on their degree of their specific speed χ [7].

Conclusion

In recent years, wind energy has become a truly thriving industry of "pure", or as it is called "green" energy. Based on the report of the development of the global wind energy industry for 2016 by the World Wind Energy Association, it is shown that the power of the global wind power industry has reached 456.486 MW in 2016.

Due to lack of wind machine industry and import substitution, all devices that created by scientists from Kazakhstan have not found its application yet. It seems that the most promising invention from Kazakhstan's scientists is twin-rotor machines carousel developed in the Kazakh National University under the leadership of Sh.A.Yershina. Twin-rotor wind turbine with high technical and economic indicators Bidarrieus does not have analogue.

REFERENCES

1 World Wind Energy Association, October 10, 2016 | Available at: http://www.wwindea.org

2 The Kazakhstan Electricity Association Committee on Renewable Energy Sources. February 24, 2016 [electronic source]. Available at: http://www.windenergy.kz

3 Satkaliev A. Development of electricity industry in Kazakhstan: Sustainable improvement and effectiveness. *Energetics Journal*, 2013, Vol. 44, No. 1, pp.23 -28

4 Bayshagirov H.Zh., Esdavletova K.D., Kazieva D.B. About development of small wind turbines in Kazakhstan. *Kokshetau State University named after Sh. Ualikhanov*,Kokshetau, 2013, pp.14-22.

5 Bayshagirov H.Zh. Have an idea, Innovation in Kazakhstan, Inventions in Kazakhstan. *Kazakhstan innovation magazine*, 2012, No. 19, pp 31-36.

6 Yershina A.K., Yershin S.A., Zhapbasbayev U.K. *The Theory Basic of Darrieus Wind Turbine*. Almaty, 2001, 104 p. [in Russian].

7 Yershina A.K., Yershin Sh.A. et al. *Bi-Darrieus wind turbine*. *Preliminary patent No. 19114 RK, F03D 3/06 (2006/01)*. Published on 15.02.2008, Bull. No. 2, 48p.

8 Yershin Sh.A. et al. *Vertical axial compound wind turbine of carousel type*. *Preliminary patent No.20748 RK, F032D 9/00 (2006/01).* Published on 16.02.2009, Bull. No. 2, 59 p.

9 Yershina A.K., Yershin Sh.A., Tulepbergenov A.K., Manatbayev R.K. Bi – Darrie windturbine. *Proc. of the Int. Conf. on Thermal and Environmental. ASME – ATI – UIT 2010. Issues in Energy Systems*. Sorrento, Italy, 2010, pp. 615 – 619.

10 Yershina A.K., Yershin Sh.A. Vertical – axial compound wind turbine of rotor type. *Proc. of the Int. Conf. on Thermal and Environmental. ASME – ATI – UIT 2010. Issues in Energy Systems*. Sorrento, Italy, 2010, pp. 621 – 625.

11 Yershina A.K. Rotary - type windturbine. *Eurasian Physical Technical Journal*, 2011, Vol. 8, No.2 (16), pp. 28 – 35.

12 Yershina A.K., Yershin Sh.A, Manatbayev R.K. Determination of the Aerodynamic Characteristics of Darrieus Wind Turbine System of Troposkein. *World Applied Sciences Journal*, 2013, Vol. 24, No. 8, pp.94 – 103.

13 Yershina A.K. New perspective version of Bi-Darrieus wind turbine. *Journal of International Scientific Publications: Materials, Methods and Technologies*. *IAEA INIS*, 2014, Vol. 8, pp. 465 – 472. Available at: www.scientificpublications

14 Yershina A.K. *Theory and practice of using renewable energy sources*. Textbook. Almaty, 2015, 216p.

15 Bayshagirov H.Zh., Karimbayev T.D. et al. *Development and creation of compound wind turbine with diffuser*. Report. Almaty, 2004, 91p.

16 Koshumbayev M.B. *Wind turbine*. *Preliminary patent No.20243 RK.* Published on 17.11.2008. Bull. No. 11, 4p.

Article accepted for publication 25.11.2016

UDC 621.314; 537.39

INFLUENCE OF PULSE ELECTRICAL DISCHARGES ON THE MICROSTRUCTURE OF THE ELECTRODE SYSTEM DRILL

Shuyushbayeva N.[1], Altayeva G.[1], Stoev M.[2], Akhmadiev B.[3]

[1]Kokshetau State University named after Sh. Ualikhanov, Kokshetau, Kazakhstan, nn_shuish@mail.ru
[2]South West University of "Neofit Rilski", Blagoevgrad, Bulgaria
[3]Karaganda State University named after Buketov, Karaganda, Kazakhstan

The paper is considered practicalities of the electro-hydraulic drilling. The basis of this method is a unique phenomenon - a method of directly transforms of electrical energy into mechanical energy of the shock waves that accompany electrical discharges in conditions a limited spatial volume of water in the bottom of the well. The power a shock wave is allows to effectively disruption is not only the solid rocks but also influences the condition of the drilling system. Study the structure and quality of the surface of the electrode system of the drill, and the character of the changes after the electrohydropulse of processing. Conducted spectral analysis of the microstructure of the melted portions of the surface drill electrodes resulting from the impact of underwater spark discharge. Experimentally are installed regularities of erosive of wear the metal electrode from the energy parameters and the number of electro-impulses.

Keywords: *electrode, electrohydraulic pulse, energy, discharge.*

Introduction

Electrohydraulic drilling is a basically new method that has not been used in industry as of yet. The electric-pulse treatment developed here is based on the Yutkin electrohydraulic effect [1–3]. The main advantage of the proposed technology is its reliability due to the absence of friction and wear parts in the equipment, as well as the simplicity in operation and maintenance. However, the wide implementation of this technology in practice is hampered by undesirable effects and consequences. The processes occurring on the surface of the electrodes subjected to erosion and action of high-power underwater spark discharges require additional investigations. In electrohydraulic well-drilling, the cable of the positive electrode is also subjected to wear (is consumable). Melted regions appear on the surfaces of the positive and negative electrodes; their effect on the strength of the electrode system has not been studied comprehensively. In this connection, this study aims at experimental investigation of the degree and rate of electrode wear depending on the energy parameters and the number of electro hydraulic pulses.

The electrohydraulic setup with a working cell for testing and studying various processes accompanying electrohydraulic drilling was designed and assembled at the Laboratory of Hydrodynamics and Heat Transfer of the Buketov State University (Karaganda). The operation principle of the electrohydraulic drill can be described as follows: first, the pulse capacitor is charged from a high-voltage generator. When a preset voltage is attained, the breakdown of the discharge gap occurs, and the entire energy stored in the pulse capacitor is transferred to the working gap via the cable-electrode. A pulsed electric discharge occurring in a fluid is a source of high-intensity mechanical shock waves, which are reflected from the bore bit and produce a focused action on the medium being processed, crushing it into small pieces [4–7].

In the system for well-drilling, RK-75-9-12 bared cable core connected to the positive terminal of the pulsed current source is used in the working cell for the central electrode, while the negative terminal is connected with the electrohydraulic bore bit. Such a design of the electrode is convenient in well-drilling for installing heat-exchange pipes. As a result of the redistribution of velocities, the forces emerging during the discharge due to a hydraulic shock and the hydrodynamic force facilitate self-centering of the cable-electrode. During prolonged operation, the central bared core of the cable-electrode becomes shorter due to erosion, and the insulation of its end part is damaged. The insulation is mainly cut along the central core, and efficiency of drill operation becomes lower. For this reason, after electrohydraulic crushing of hard rocks, it is necessary to replant insulation by baring the working end of the cable-electrode from the insulating layer.

3. Experimental technique

To form a pulse with a short front of the voltage applied to the discharge gap in a liquid the authors used a discharge gap in the air that is an air discharger; and to generate a pulse of certain energy they used energy storage electrical capacitor. In the laboratory the authors have developed and tested an electro-hydraulic plant and a working area for drilling (Fig. 1).

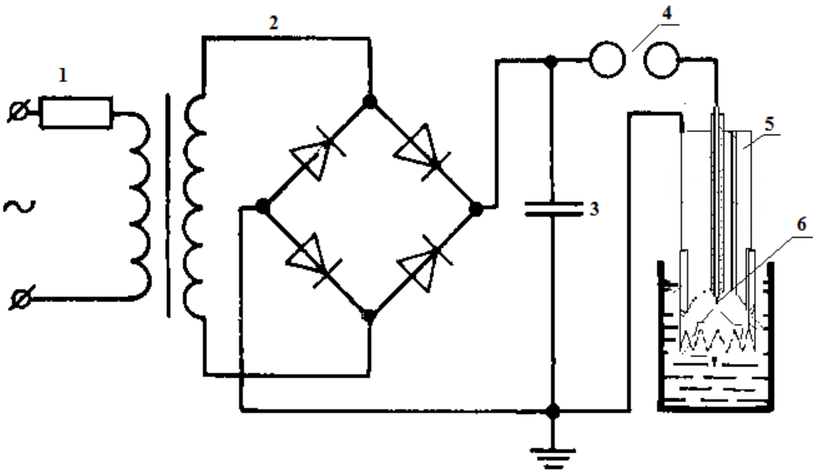

Fig.1. Scheme of electro-hydraulic apparatus and electro-hydraulic drill
1 – power supply, 2 – high-voltage generator, 3 – pulse capacitor, 4 – discharger, 5 – electrohydraulic drill, 6 – centre electrode

As a result of the experimental study the authors defined the optimal values of time and the number of spark discharges in electro-hydraulic drilling the stones, and determined the time at which destruction of stones and hard rock occurs during the drilling.

Forces caused by discharge due to hydraulic impact and flow force, as a result of redistribution of velocities, stimulate self-centering of the electrode cable. During continuous operation the central bare cord of the electrode cable is shortened due to erosion, and the insulator of its end breaks down. Insulation is basically breaks down along the central cord and the device loses its efficiency. In this case, after the solid rocks fracture it is necessary to periodically tinker the operating tip of the electrode cable giving it original shape.

4. Results and discussion

During operation, each discharge is accompanied with erosive wear of the electrodes, which depends on the voltage and energy per pulse, the electrode material, etc. As a result, the cable-electrode of the electrohydraulic drill fails.

It is well known that during electrohydraulic drilling, spark eroding occurs, which is associated with emission of particles from the metal surface by the electric discharge pulse [8, 9]. If the distance between the electrodes immersed into a liquid medium is preset, the decrease in the spacing between the electrodes initiates the breakdown, and the electric discharge occurs with the formation of a high-temperature plasma in the discharge channel. This property is used in electroerosive processing of materials, which is usually carried out by electric pulses with a duration not exceeding 0.01 s so that the released heat has no time to propagate to the bulk of the material. In addition, the pressure of the plasma particles during their impacts against the electrode facilitates erosion of not only the melted, but also of the heated substance.

The electric breakdown always propagates via the shortest route; for this reason, the closest regions of the electrodes are first to erode. The nature of changes and the quality of the surface after the treatment depend on the duration, frequency, and energy of electric pulses. It was found from the results of experiments change of the length wear of the working electrode the depend on the number of pulses and various discharge energies (Table 1).

Table 1 - Change of the length wear of the working electrode at discharge energies from 600 J to 1350 J.

Voltage, kV	Energy, J	Change of electrode’s length, mm	Number of electropulses
20	600	0.1	55
		0.5	98
		1.0	121
		1.5	225
25	938	0.5	50
		1.0	100
		1.5	150
		2.0	254
30	1350	1.0	50
		1.5	102
		2.0	154
		2.5	255

It can be seen from the curves that with increasing discharge energy, the working electrode is worn faster for the same number of pulses. Figure 2, 3 show the microphotographs of the central cable-electrode before and after electrohydraulic treatment, obtained using the MIRA3 TESCAN microscope.

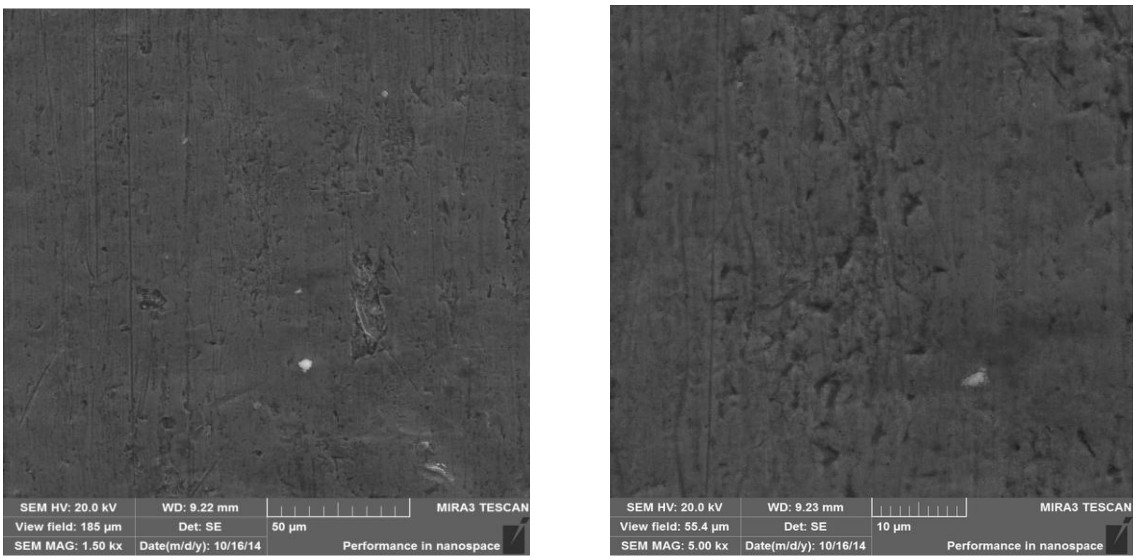

× 1.50 kx × 5.00 kx

Fig. 2. Microphotograph of the central cable-electrode obtained with different magnifications before electrohydraulic treatment

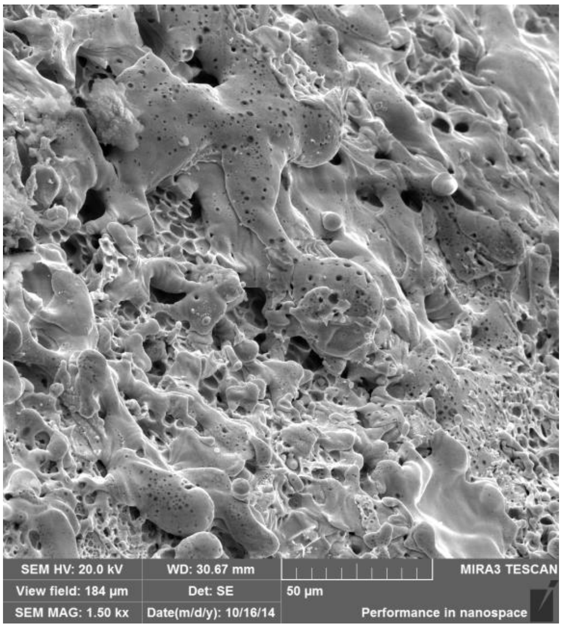

× 1.50 kx

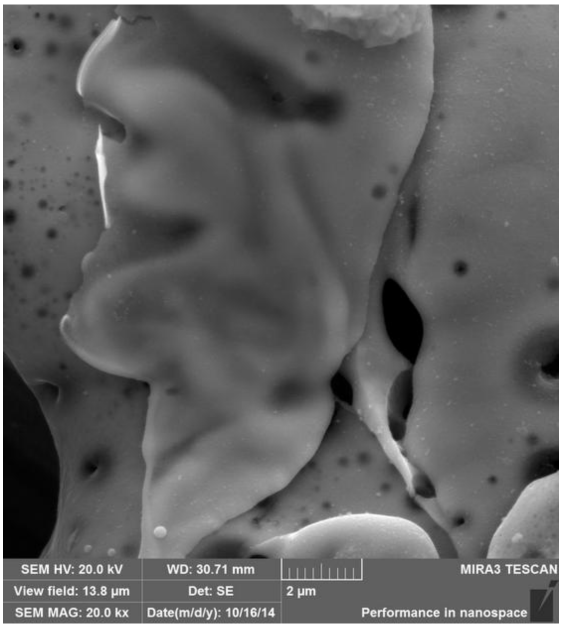

× 20.0 kx

Fig.3. Microphotograph of the central cable-electrode obtained with different magnifications after electrohydraulic treatment

The photographs obtained with the help of the electron microscope with different magnifications help to trace in detail the changes in the microstructure of the positive electrode.

Analysis of the photographs of the surface of the cable-electrode obtained after electrohydraulic treatment shows that the microstructure of the entire surface changes significantly, and large melted regions including spots with different densities and structures as well as voids are observed. However, investigation of longitudinal and transverse metallographic sections using a microscope with 20000-fold magnification showed no traces of cracks in the metal.

Conclusion

In our experiments, we studied erosion in the metal part of the electrode system of the electrohydraulic drill. We investigated melted regions of the surface by analyzing the microstructural changes of the electrode surfaces before and after electrohydraulic action for various parameters of electric discharges. Analysis of characteristic changes in the cable-electrode during electrohydraulic well-drilling shows that erosive wear of metals occurs in different ways depending on the electric parameters, frequency, and duration of discharges.

The inner surface of the tubular shell of the electrohydraulic drill serving as the negative electrode is not torn and is not subjected to mechanical wear. Substantial wear occurs only in the central cable electrode, which is the only consumable material.

Thus, the electrohydraulic pulsed method of well-drilling for heat-exchangers makes it possible to attain high efficiency of crushing with low energy expenditures as compared to mechanical methods.

REFERENCES

1 Yutkin L.A. *Electro-effect and its application in promyshlennosti*. Mechanical Engineering, Moscow, 1986, 253 p. [in Russian]

2 Malyushevsky P.P. *Basics of Running-pulse technology*. Kyiv, 1983. 272 p. [in Russian]

3 Kussaiynov K., Nusupbekov B.R. *Destruction of materials underwater electrical explosion*. Izdatservis, Karaganda, 2010, 250 p. [in Russian]

4 Kusaiynov K., Turdybekov K.M, Kuzhuhanova J.A., Shuyushbaeva N.N. Development of electro-drilling technology for the installation of heat pumps teplosemnyh elements. *Modern science: research, ideas, results and technologies*. Dnepropetrovsk, Ukraine, 2013, No. 2 (13), pp. 420 – 425.

5 Stoev M., Kussaiynov K., Shuyushbayeva N.N., Nussupbekov B.R., Karagaeva M.B. Electrohydraulic drilling of rocks and research of processes of an erosion of metal part of electrode system of the drill. *Bulletin of the Karaganda University*. *Physics Series*. 2014, No. 3, pp.68 – 74.

6 Kussaiynov K., Shuyushbaeva N.N., Kuzhuhanova J.A., Ahmadiev B.A. Development of electro-hydraulic pulse technology of drilling wells for installation of heat exchange elements of heat pumps. *Mathematics and natural science*. Blagoevgrad, Bulgaria, 2013, Vol. 3, pp. 51 – 56.

7 Kussaiynov K., Nussupbekov B.R., Sakipova S.E., Shuyushbayeva N.N., Khassenov A.K. Investigation of the wear of the metallic part of electrode system of electrohydraulic drill. *Metallofizika i Noveishie Tekhnologii*. Kyiv, 2015, Vol.37, No. 3, pp. 397 – 407.

8 Guly G.A. *Equipment and technical processes using electrohydraulic effekta*. Kiev, 1977, 324 p.

9 Mazurovskii B.J., Sizev A.N. *Electro effect in sheet forming*. Naukova. Dumka, Kiev, 1983, 192 p.

Article accepted for publication 25.11. 2016

UDC: 533.6.01; 621.548

STUDY OF AERODYNAMIC CHARACTERISTICS OF THE MODEL OF A WIND TURBINE WITH ROTATING CYLINDERS

Sakipova S.E., Tanasheva N.K., Kivrin V.I., Kussaiynova A.K.

E.A. Buketov Karaganda State University, Karaganda, Kazakhstan, sesaule@mail.ru

The paper discusses problems of alternative energy sources uses, particularly wind energy utilization. The results of an experimental study of the aerodynamics of wind turbines using Magnus effect are considered. To carry out testing, a model of a three-blade wind turbine with rotating cylinders of various cross-sections was made. Aerodynamic testing of the wind turbine model at various airflow conditions was performed. Dependencies of drag force, tractive force and rotation frequency of the wind wheel on the flow rate at different yaw angles of the flow were found. It is shown that the use of rough-surfaced rotating cylinders of various cross-sections makes it possible to use an additional moving force resulting from the Magnus effect.

Keywords*:* wind turbine, aerodynamics, Magnus effect, rotating cylinder, drag force, traction force, angle of attack.

Introduction

One of the most important features of the modern world is the increased attention of the international community to the problems of expediency and efficiency of energy utilization, the implementation of energy-saving technologies and search for renewable energy resources. The increasing demand of the humanity for energy resources necessitates search and increased use of alternative sources of energy supply. Therefore, the development of methods and technologies using renewable sources are important and relevant not only in Kazakhstan, but also throughout the world [1-3].

Issues of meeting the ever-increasing demands for all types of energy, the natural resources depletion, the harmful environmental impact, the danger of global warming, etc. are increasingly discussed at highest national and international levels. In Kazakhstan, these issues become even more urgent in view of preparation for the world exhibition of science and technology achievements "World Expo-2017", the main topics of which are "Energy of the future" and "Ecologically clean energy" [4].

The potential of renewable energy resources such as hydro-energy, wind and solar energy is very significant in Kazakhstan. It should be noted that wind energy does not pollute the environment and it is possible to produce clean, inexhaustible energy in local areas or sites remote from centralized electric networks using the wind. Despite all the advantages, in Kazakhstan the share of wind energy conversion is only 0.4% of the total production of electricity. On the one hand, this is due to the fact that the major part of Kazakhstan are the areas with low annual average wind speeds in which the use of industrially-produced wind turbines is economically unsound. In this regard, construction of wind power plants, effectively operating in low average wind speeds, is highly relevant and meets the basic priorities of the development of science and technology in Kazakhstan.

The paper presents the results of experimental research of aerodynamic characteristics of a three-blade wind turbine with rotating cylinders of various cross-sections at different airflow conditions.

1. The application of Magnus effect in wind turbines

The developed plant makes use of the Magnus effect, i.e. the physical phenomenon that results when fluid flows past a rotating body. The main point of this phenomenon is in the fact that in the flow past a rotating body there arises a force acting on the body and directed perpendicularly to the flow as a result of combined effects of the Bernoulli effect and the formation of a boundary layer in the medium around the streamlined object [5]. The rotating object makes a turbulent motion in the environment around it. On the one side of the object, the vortex direction agrees with the direction of the streaming flow and, respectively, the medium motion rate increases on this side. On the other side of the object, the direction of the vortex is opposite to the flow direction and the medium motion rate decreases. Because of the rate difference there is a pressure difference causing a lateral force on that side of a rotating body where the direction of rotation and flow direction are opposite to the side where the directions are the same [5-8].

It is the Magnus effect that causes curved motion of a rotating sphere. It is established that the effect of force action of air flow on the rotating cylinder is almost 10 times greater than that on the sail of the same streamlined surface [5, 6]. This phenomenon of the origination of great force action on the rotating cylinder is used in some aircraft. In the invention of Bolotov A.V. et al., the Magnus effect made it possible to increase the capacity of wind engines with rotary turbines. [9] The papers of Japanese scientist N. Murakami [10, 11] show that the Magnus effect makes for effective electric power generation at wind speeds over a wide range of the incident airflow rate. A scientist from Novosibirsk Professor N.M. Bychkov developed a wind turbine, each rotor of which is made of non-rotating root and rotating end portions, and a disk at the end [12].

It is not possible to describe all devices and wind turbines using the Magnus effect in a single paper. However, studies show that origination of an incremental lift due to the Magnus effect reduces induced drag, providing higher efficiency relative to traditional bladed wind machines.

2. Test technique in a wind tunnel T-M-1.

The authors made experiments to study the effect of the rate and direction of air flow on aerodynamic characteristics of a three-bladed wind turbine model with blades in the form of rough-surfaced rotating cylinders of various cross-sections. Wind tunnel experiments were based on the principle of reversibility of motion positing that displacement of a body relative to air can be replaced by the motion of the air incident to a motionless body [5, 6, 13]. The testing was conducted on a big open-jet wind tunnel T-1-M, Fig. 1b. Details of the characteristics of the working section of T-1-M are described in [6]. An air flow with a uniform rate field ranging from 3m/s to 25m/s is formed in the working part of the wind tunnel T-M-1.

For aerodynamic testing, a model of a wind turbine with rotating cylinders of variable cross-sections was developed and made, Fig. 1. A wind wheel is designed as a system of three rotating impermeable rough-surfaced cylinders with horizontal axes of rotation. The authors had previously found that the use of cylindrical blades of porous material with end discs at the tops could increase the efficiency of wind energy conversion into mechanical energy of wind-wheel rotation by (15-20)% [8].

The aerodynamic testing showed that the porous surface of the cylinder makes for active trapping of the air. In order to reduce excessive flow turbulence due to the partial migration of the air current into the pores, and accordingly, reduction in aerodynamic drag, in the test model the cylinder surface was covered with impermeable rough layer.

The wind wheel diameter was D=0.4 m, the length of each cylinder was L_c=0.15 m, the cylinder base diameter was d_{c1}=0.08 m and the neck diameter of the cylinder was d_{c2}=0.05 m [14]. The shaft speed of the wind turbine was (40-60) r/min, the axial rotation frequency of cylinders was (500-900) r/min, and the minimum threshold of operating wind speed was equal to 3 m /s.

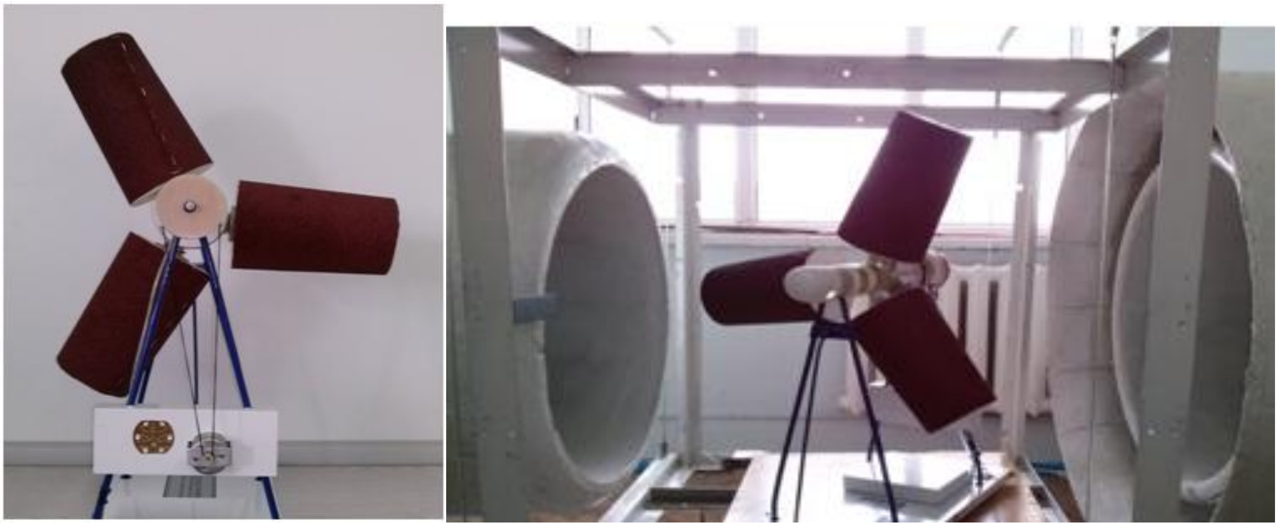

Fig.1. The model of the wind turbine with rotating cylinders of various cross-sections:
a) a general view; b) in the working section of the wind tunnel.

To measure the components of the aerodynamic forces and moments acting on the model, a three-component aerodynamic balance of mechanical type was used. Through special-purposed tailings, the mechanical aerodynamic balance was attached to a rigid cubic frame, within which the model of the wind turbine was placed. The flow of air coming on the frontal part of the cylinder exerted forcing, so that the balance indicator deviated from equilibrium. Independence of measurements of the aerodynamic balance in mutually perpendicular directions made it possible to measure the value of the lift force F_l and drag force F_d at various flow regimes. Using a special-purposed device the wind turbine model was turned by predetermined angle α relative to the direction of air flow, thus providing flow past the model at different angles of attack (yaw angles of the flow). The traction force F_t at different rates and directions of air flow was measured using dynamometers. Measurements of aerodynamic forces were repeated at least 5 times, the measurement error did not exceed (4-5) %.

To measure the angular rate of the rotating cylindrical blades, a contact-contactless digital phototach AT-8 was used, which provided measuring frequency in the 0.1 r/min to 10,000 rev/min range.

3. Discussion of tests results

Figures 2 and 3 show the curves obtained by measuring dependencies of drag forces on the rate of flow at different yaw angles. The yaw angle of the flow α is the angle between the direction of the air flow rate and the direction perpendicular to the plane of the wind wheel.

Fig. 2 shows that the drag force increases with growing air flow rate, however, the greater is the yaw angle of the flow, the less are the values of drag forces.

Figure 3 shows that within the range of yaw angles of the flow $\alpha=(0\div15)$ degrees the drag force of the wind turbine remains substantially constant; in the 15 degrees to 40 degrees range the drag force reduces, and then within the range (45-60) degrees an increase in drag force is observed. This change in the drag force value is due to the fact that with increase in deviation of the flow direction from perpendicular to the plane of the wind wheel the mid-section area reduces. When the angle of attack is over than 60 degrees, all flow rates grow due to the flow past the wind wheel at the backside.

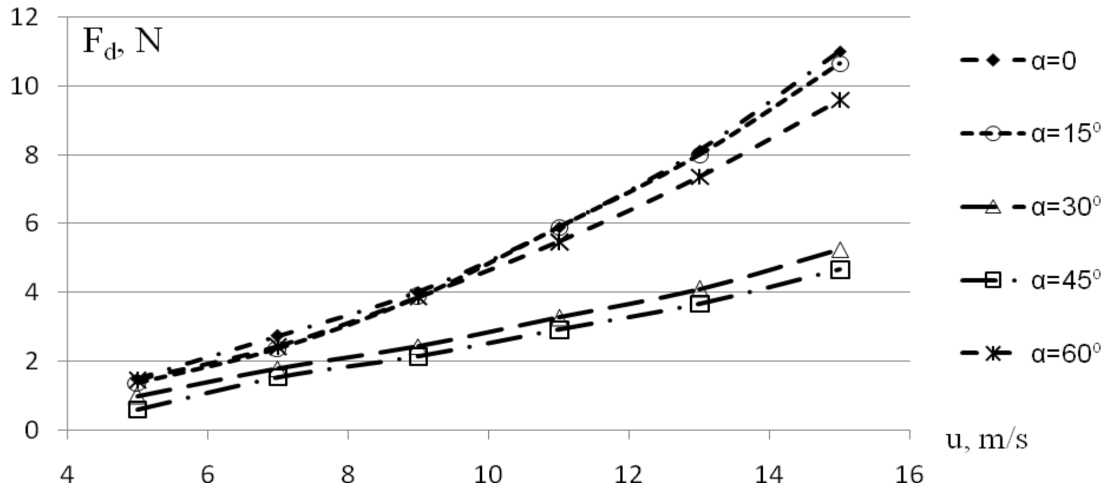

Fig.2. Dependence of the drag force on the flow rate at different yaw angles of the flow α

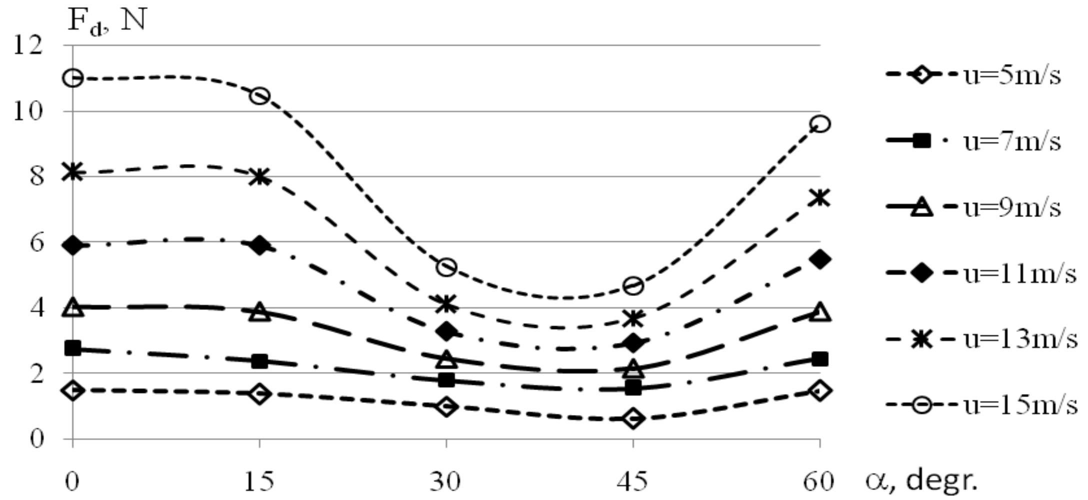

Fig.3. Dependence of the drag force on the yaw angle of the flow α at different flow rates.

Fig. 4 shows the results of experiments on the effect of flow direction on the rotation rate of the streamlined wind wheel with rotating cylindrical blades of variable cross-sections. From these graphs it follows that with an increase in the yaw angle of the flow the rotation frequency of the wind wheel of a three-bladed wind turbine model decreases, which can be explained by the decrease in the total pressure on the wind wheel due to reduced mid-section area, and consequently, lowered rotation rate of the wind wheel. The tractive force generated by the wind turbine is considered a useful effect in the conversion of wind energy.

Figures 5 and 6 show dependences of the tractive force of the wind turbine model with cylindrical rotating blades on the air flow rate at different yaw angles of the flow. Fig. 5 shows that with the rise in the air flow rate the value of the tractive force of the wind turbine model grows. At the yaw angle of 0 degrees when the air flow rate is 15 m/s, the maximum tractive force of 612.6 H is achieved. However, with increasing yaw angle of the flow the value of the tractive force of the three-bladed wind turbine model decreases, Fig.6. With the increase in air flow rate, the value of the tractive force of the three-bladed wind turbine model increases, this is also due to an increase in the pressure force on the wind wheel. This is explained by the fact that with rise in the flow rate, pressure force on the wind wheel increases, and when the yaw angle of the flow increases it decreases with reduction in the mid-section area.

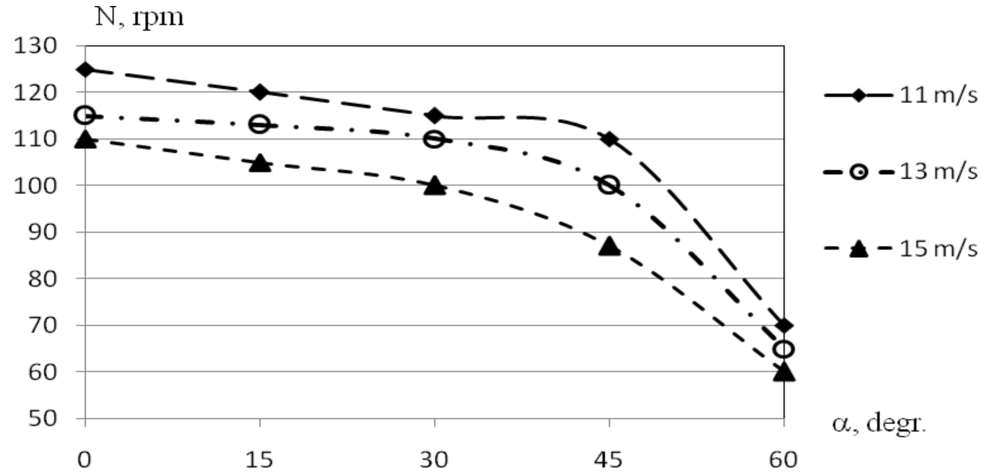

Fig.4. Dependence of rotation frequency on the yaw angle of the flow α at three different flow rates

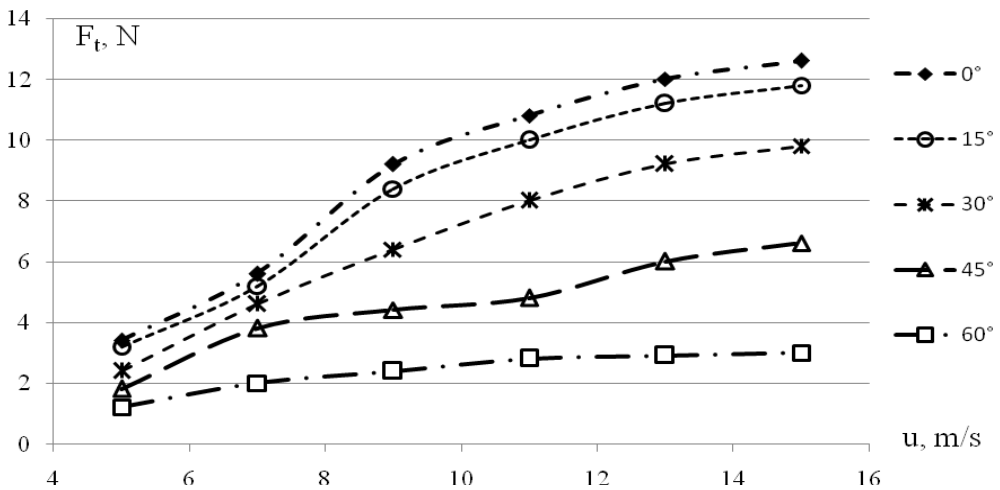

Fig.5. Dependence of the tractive force of wind turbine model at different yaw angles of the flow

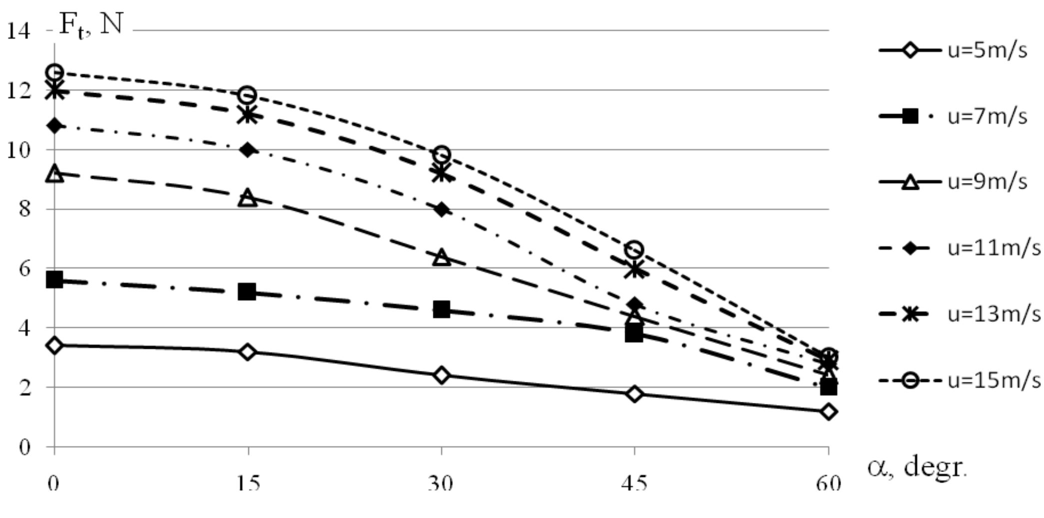

Fig.6. Dependence of the tractive force of the wind turbine model on the yaw angle of the flow at different flow rates

Conclusion

The present level of technological development and high technology makes for the use of a rotating cylinder to generate arising incremental lift force directed across the flow. As a result of the aerodynamic testing of a wind turbine model with blades in the form of three rotating cylinders of variable cross-sections, dependences of drag and tractive forces on the flow rate at different yaw angles of the flow were found. The frequency of rotation of the wind wheel of the model at different flow conditions was studied.It had been previously found that by using porous cylinders with end discs at the tops it's possible to increase efficiency of wind energy conversion into mechanical rotation energy of a wind wheel (15-20)% [8]. In the experiments cylindrical rough- surfaced blades were used. Aerodynamic testing showed that the model of the wind turbine also carried out active trapping of the air flow due to the rotating cylindrical rough-surfaced elements. Obviously, that was caused by the additional force arising due to the Magnus effect.

A further analysis of the aerodynamic characteristics of three-blade models with rotating cylinders of porous material and coated with an impermeable rough-surfaced layer at different flow conditions will be carried out. Various cross-sections of the cylinders provide the rotating elements optimal aerodynamic drag and sufficiently high tractive force within a wide range of rates. However, when a yaw angle of the flow is above 45 degrees the value of the tractive force sharply drops. In practice, it is desirable to use a special-purposed device to keep the angle of attack from rise over 45°. The quoted results valid for the above mentioned model of the wind turbine at the indicated conditions of aerodynamic testing are quite applicable and can be used in practice.

REFERENCES

1 Abdrakhmanov R.S., Yakimov V.V. The effectiveness of the use of wind energy resources at low wind speeds. *Proceedings of the Russian Academy of Sciences. Energy* 2010, No.5, pp. 54-57. [in Russian]

2 Karatayev M., Clarke M. A review of current energy systems and green energy potential in Kazakhstan. *Renewable and Sustainable Energy Reviews*, Vol. 55, March 2016, pp. 491–504.

3 Marinushkin B., Trofimov A. To the general scheme of development of wind power engineering in Kazakhstan. Available at: http://www.windenergy.kz/rus/articles/1/page/1/28

4 Mukasheva A., Sharapatova G.S. Problems of the use of renewable energy sources in the Republic of Kazakhstan (in the framework of EXPO 2017). *Eurasian Law Journal*, 2013, No. 4 (59), pp. 96 - 99.

5 Schlichting H. Boundary layer theory. Moscow, Nauka, 1974, 712 p. [in Russian]

6 Kussaiynov K., Sakipova S.E. *Boundary layer theory*. Textbook. Karagandy, 2002, 220p. [in Kazakh]

7 Kusaiynov K., Sakipova S.E., Nikitina L.A. Aerodynamics of the transversally streamlined rotated

8 barrel. Methods of aerophysical research. *Proc. of the 12th international conference. ICMAR-2004*. - Novosibirsk, 2004, pp. 195 – 198.

9 Kussaiynov K., Sakipova S.E., Tanasheva N.K. et al. *A wind turbine based on the Magnus effect*. RK innovative patent of invention No. 30462. Published: 15.10.2015, 3 p.

10 Bolotov S.A. *A rotary vortex wind power plant. Power supply and energy saving in agriculture*. Moscow, 2003, Part 4, pp. 177 - 185.

11 Nobuhiro Murakami A.c. RU № 2330988. A *wind power generator based on the Magnus effect ITO Dzun*; Published: 27.03.2012. Bull. No. 25, 4, p.

12 Bychkov N.M .; A.C. RU № 2118699. *A wind turbine and the method of its operation*. Published: 18.06.1996. Bull. No. 45, 3, p.

13 Gorshenin D.S. *A guide to practical training in the aerodynamic laboratory*. Moscow, Mechanical Engineering. 1997, 224, p.

14 Sakipova S.E., Kambarova Zh., Turgunov M.M., Kussaiynov Ye.K. Study of the aerodynamic characteristics of a three-blade wind turbine with rotating cylinders of various cross-sections in the flow of air. *Proc. of the 9th Intern. Conf. «Chaos and structures in nonlinear systems. Theory and experiment »,* Karaganda, 2015, pp. 319 - 323.

Article accepted for publication 02.12. 2016

SUMMARIES ТҮСІНІКТЕМЕЛЕР АННОТАЦИИ

Потапов А.А.
Ионосферадағы найзағай электр разрядтардың фракталдық өлшемдер спектрінің жаңа түрлері туралы: эльф, джет мен спрайт.
XX ғасырдың ортасында 90-шы жылдан бастап физиктер назарына жаңа феномен пайда болды - ол абсолюттік көпшілік бұлттардын жоғарыда болатын, 20-дан бастап 100 км-ге дейін биіктіктердегі орта атмосферада найзағай электр разряды. Бұл разряд құбылыстардың бірнеше мүлдем жаңа класс разрядтық түрлеріне әкеледі. Бұл жұмыста эльф, джет пен спрайттың физикалық сипаттамалары мен ионосферадағы биік разрядтары ең қызықты түрлері қарастырылған. Фракталдық сипаттамаларын зерттеу нәтижелері көрсетілген. Бұл нәтижелер атмосфералық процестер мен радиожүйелердің жұмыс істеуіне осы түрдегі табиғи бұзылуын әсерін толық түсіну үшін негіздерді береді.

Потапов А.А. **О спектре фрактальных размерностей новых видов грозовых электрических разрядов в ионосфере: эльфы, джеты и спрайты**.
Начиная с середины 90-х годов XX века в центре внимания физиков новое явление – грозовой электрический разряд в средней атмосфере на высотах от 20 до 100 км, лежащих выше абсолютного большинства облаков. Это приводит к возникновению нескольких абсолютно новых классов разрядных явлений. В работе рассмотрены физические характеристики эльфов, джетов и спрайтов – наиболее интересных типов высотных разрядов в ионосфере. Приведены результаты исследований их фрактальных характеристик. Полученные результаты дают основу для более глубокого понимания таких атмосферных процессов и учета действия такого рода естественных помех на функционирование радиосистем.

Потапов А.А.
Радиолокациялық және статистикалық шешімдері теориясы жаңа саласы ретінде қарқынды шу аясында төмен контрастты мақсаттарға топологиялық радиолокациялық детекторларды талдау және синтездеу.
Жаңа, атап айтқанда, фракталдық-масштабтау немесе салмақтық-масштабтық-инвариантты және қазіргі кезіндегі радиолокациялық әдістерінің түрлері берілген. Жаңа топологиялық радиолокациялық детекторлар төмен контраст объектілерін синтездеу негіздегі көзқарас пен стратегиялық бағыты қарастырылған. Нысанды анықтау жер, теңіз және жаңбырдан қарқынды бейне аясында жүзеге асырылады. Кейбір жаңа мүмкіндіктер мен қарқынды шу аясында төмен контраст заттарды анықтау үшін топологиялық әдістері көрсетілген. Бұл әдіс құрылымды және фракталдық талдау, сондай-ақ детерминделген хаос теориясы нәтижесінде негізделеді. Жұмыстың негізгі мақсаты - радиофизика, радиотехника және радиолокациялық мәселердің негізгі бағыттарын «фракталдық» тілінде түсіндіру жаңа жолдарын жасау және болашақ перспективті радиосистеманы қорытындылау үшін.

Потапов А.А. **Анализ и синтез топологических радиолокационных обнаружителей малоконтрастных целей на фоне интенсивных помех как новая ветвь радиолокации и теории статистических решений**.
Предложен новый вид и новый метод современной радиолокации, а именно, фрактально-скейлинговая или масштабно-инвариантная радиолокация. Рассмотрены основные идеи и стратегические направления в синтезе новых топологических радиолокационных обнаружителей малоконтрастных объектов. Обнаружение объектов производится на фоне интенсивных отражений от земли, моря и осадков. Представлены новые топологические признаки и методы обнаружения малоконтрастных объектов на фоне интенсивных помех. Методы основаны на текстурном и фрактальном анализе, а также на теории детерминированного хаоса. Основная цель работы - истолкование основных направлений радиофизики, радиотехники и радиолокации на “фрактальном” языке, что создает новые пути и обобщения на будущие перспективные радиосистемы.

Домрачев А.Н., Говорухин Ю.М., Криволапов В.Г., Палеев Д.Ю.
Жерасты тау-кен қазбаларын ыдырағаннан тәуекелдерді бағалау әдістемесін талдау.
Бұл мақалада тау-кен куйреу тәуекелдерді бағалау өзектілігін дәлелдейді. Негіздеу қайта пайдалану әзірлемелерді мүмкіндігін болжау тұрғысынан және көмір бағаналардың тұрақтылықты сақтау, екі атқарылған, және жабық желдетилмеген көлемінің тәуекел жарылғыш газ-ауа қосындысын сөзсіз жинақтаушы болып табылады. Тау-кен куйреу ең көп тараған шетелдік тәуекелдерді бағалау әдістері карастырылган. Осы әдістердің ішінде, төбесі коллапс индексі (RFRI) және Жаңа Оңтүстік Уэльс университетінің (UNSW) тірегі тұрақтылықты бағалау әдісін тәуекел деңгейін есептеу үшін алгоритмі. Нақты мысалда, Оңтүстік Кузбасс шахталарында тау-кен жұмыстарын тиімділігін және қауіпсіздігін арттыру, тәуекелдерді бағалау әдістерін қазбаларының коллапс пайдалану мүмкіндігін тексерілді.

Домрачев А.Н., Говорухин Ю.М., Криволапов В.Г., Палеев Д.Ю.

Анализ методологии оценки риска обрушения подземных горных выработок.

В данной статье обоснована актуальность оценки риска обрушения горных выработок. Обоснование выполнено как с точки зрения прогнозирования возможности повторного использования выработок и сохранения устойчивости угольных целиков, так и опасности возникновения замкнутых непроветриваемых объёмов, в которых неизбежно накопление взрывоопасных газовоздушных смесей. Рассмотрены наиболее распространенные зарубежные методы оценки риска обрушения горных выработок.Среди данных методов алгоритм вычисления индекса уровня риска обрушения кровли (RFRI) и метод оценки устойчивости целиков университета Нового Южного Уэльса (UNSW). На конкретном примере проверена возможность использования методов оценки риска обрушения выработок для повышения уровня эффективности и промышленной безопасности ведения горных работ на шахтах юга Кузбасса.

Жумаев М.Р., Шарипов М.З.

Диэлектрлік көпқабатты наноқұрылымдардағы Фарадей әсері резонанстық диссипативті моделі.

Диэлектрлік ортада поляризация жазықтығы айналу бұрышыннын теориясы қарастырылды. Бұл мақалада диэлектрлік көпқабатты наноқұрылымдардағы моделі диссипативті резонансты Фарадей әсерін ұсынылады. Көп қабатты наноқұрылымдардағы Фарадей әсерін күшейту жағдайы табылды. Сыртқы магнит өрісінің әсерінен Фарадей айналу бұрышын резонанстық арттыру мүмкіндігі корсетілген. Оң және сол поляризацияланған жарық сыну көрсеткіштерінің жиілік тәуелділігі талданылды.

Жумаев М.Р., Шарипов М.З. **Резонансная диссипативная модель эффекта Фарадея в диэлектрических многослойных наноструктурах.** Рассмотрена теория угла вращения плоскости поляризации в диэлектрических средах. В работе предложена модель диссипативной резонансного эффекта Фарадея в диэлектрических многослойных наноструктур. Найдено условие усиления эффекта Фарадея в многослойных наноструктурах. Показана возможность резонансного усиления угла вращения Фарадея под действием внешнего магнитного поля. Проанализирована частотная зависимость показателей преломления для право и лево поляризованного света.

Ивщенко Л.И., Прибора Т.И., Комочкин Н.С., Саханюк Н.В.

Газ - турбиналы қозғалтқыштағы таңғыш сөрелер қалақтарының тозуын зерттеу әдістемесі туралы.

Газ - турбиналы қозғалтқыштағы турбинаның таңғыш сөрелер қалақтарының тозу проблемасы қарастырылған. Осы мәселені шешуге әдістеме таңғыш сөрелердегі процестерін анықтау арқылы ұсынылады. Нысан үлгісі сынау әдісі және авиациялық қозғалтқыштардағы турбина бөлшектерінің байланыс тербеліс жүйесін заңдарын зерттеу әдістемесі сипатталды. Ротор қалақтардың тозуының зерттеу үшін түпнұсқа жабдық ұсынылды.

Ивщенко Л.И., Прибора Т.И., Комочкин Н.С., Саханюк Н.В.

К методологии исследования изнашивания бандажных полок лопаток турбины газотурбинного двигателя.

Рассматривается проблема изнашивания бандажных полок лопаток газотурбинных двигателей турбины. Предлагается методология решения этой проблемы путем определения процессов, которые происходят в бандажных полках. Описываются методы испытаний модели объекта и методика изучения закономерностей системы связанных колебаний деталей турбины авиационного двигателя. Представлена оригинальная установка для исследования изнашивания рабочих лопаток.

Хейфец М.Л., Витязь П.А., Сенють В.Т.,Колмаков А.Г., Клименко С.А.

Наноалмаздар негізделген поликристалды материалдарды қалыптастыру процестерді физика-химиялық талдау.

Физико-химиялық талдау негізінде фазалық диаграмма көміртекті күйінде қалыптастыру алмаздардын термодинамикалық жағдайлар зерттелген. Тепе-тең емес жағдайында наноқұрылымды материалдар алмаздық синтездеу әр түрлі тетіктер мүмкіндігі және ықтималдығы қарастырылған. Наноалмаздар каталитикалық қасиеттерге ие және жоғары температурада мен қысым астында алмаз ішіне графит фазалық айналдыру активатора ретінде әрекет мүмкін екендігі көрсетілген. Детонациондық наноалмаз ұнтақтарынан жасалынған поликристалл алмаздық материалдарды өндіру технологиялық параметрлері анықталған.

Хейфец М.Л., Витязь П.А., Сенють В.Т.,Колмаков А.Г., Клименко С.А.

Физико-химический анализ процессов формирования поликристаллических материалов на основе наноалмазов. На основе физико-химического анализа фазовой диаграммы состояния углерода исследованы термодинамические условия образования алмазов. Рассмотрена возможность и вероятность различных механизмов синтеза алмазных наноструктурных материалов в неравновесных условиях. Показано, что наноалмазы обладают каталитическскми свойствами и могут выступать в роли активатора фазового превращения графита в алмаз в условиях высоких давлений и температур. Определены технологические параметры получения алмазных поликристаллических материалов из порошков детонационных наноалмазов.

Ибраев Н.Х., Сериков Т.М., Зейниденов А.К., Кутербеков К.А., Бекмырза К.Ж.
TiO_2 наноқұрылымды қабыршақтарды температуралық күйдірудің фотофизикалық қасиетіне әсері.
Титан диоксиді қабыршақтарының фотолюминесценциясының спектрлі және кинетикалық қасиеттері зерттелді. Қабыршақтарды ультракүлгінмен қоздырғанда анатаз құрылымына сәйкес люминесценциялық спектр байқалады. Рутилдың кристалдық құрылымының пайда болуын үлгілерді термиялық өңдеуде 1273 К фотолюминесценция жолағы максимум ұзынтолқынды 850 нм жылжуға алып келуі куәландырады. Титан диоксиді қабыршақтарының вольт-амперлық сипаттамалар өлшенді. Анатаз құрылымды қабыршақтар, рутил құрылымды қабыршақтарға қарағанда аса жоғары фототокқа ие екені анықталды. Титан диоксиді қабыршақтарының фотокаталитикалық қасиеттері зетрттелді. Анатаз құрылымды титан диоксидінің қабыршақтары ең үлкен фотокаталитикалық белсенділікке ие екені көрсетілді.

Ибраев Н.Х., Сериков Т.М., Зейниденов А.К., Кутербеков К.А., Бекмырза К.Ж.
Влияние температуры отжига на фотофизические свойства наноструктурных пленок TiO_2.
Исследованы спектральные и кинетические свойства фотолюминесценции пленок диоксида титана. При ультрафиолетовым возбуждении пленок наблюдается спектр люминесценции характерный для анатазной структуры. Термическая обработка образцов при 1273 К приводит к длинноволновому сдвигу полосы фотолюминесценции с максимумом на длине волны 850 нм, что свидетельствует об образовании кристаллической структуры рутила. Измерены вольт-амперные характеристики пленок диоксида титана. Установлено, что пленки со структурой анатаза имеют более высокое значение фототока, чем пленки с рутильной структурой. Изучены фотокаталитические свойства пленок диоксида титана. Показано, что наибольшей фотокаталитической активностью обладают пленки диоксида титана с анатазной структурой.

Павлов А.М., Агельменев М.Е., Жилкашинова А.М., Павлов А.В., Сатбаева З.А.
Созу барысында 20гл болатының физикалық моделінің сипаттамасын зерттеу және ультрадыбыстық бақылау. Сыртқы энергетикалық әсерлерде металдардың физикалық сипаттамаларының жаңа заңдылықтарын іздеу мәселесі – қатты дене физикасындағы негізгі мәселе болып табылады. Бұл жұмыс құйма металдарының пластикалық сипаттамаларын ультрадыбыстық бақылауға арналған, яғни серпімділік модулінің ультрадыбыс жылдамдығының байланысына және 20ГЛ маркалы болат мысалындағы кернеудің деформацияға тәуелділік көрсеткішіне негізделген. Созу барысында алынған нәтижелер бойынша металдың физикалық моделінің жаңа теориялық негізі ұсынылады. Бұрындары ұсынылған параболалық функцияның көрсеткіші деформацияның максимумына жету үшін жеткіліксіз болып орнатылды. Көрсеткіш функциясы үшін аналитикалық сызба алынды. Көрсеткіш функциясы ретінде эллипс түрінде болатын функция көрсетілген. Осы функция тәжірибелік нәтижелерді қанағаттандырды.

Павлов А.М., Агельменев М.Е., Жилкашинова А.М., Павлов А.В., Сатбаева З.А.
Ультразвуковой контроль и исследование физической модели поведения стали 20гл при растяжении.
Проблема поиска новых закономерностей в поведении физических характеристик металлов при внешнем энергетическом воздействии на них – одна из важнейших в физике твердого тела. Настоящая работа посвящена ультразвуковому контролю пластических характеристик литого металла, основанному на связи скорости ультразвука с модулем упругости и анализу зависимости напряжения от деформации на примере стали марки 20ГЛ. По результатам эксперимента выдвигается новое теоретическое обоснование физической модели поведения металла при растяжении. Установлено, что ранее предложенная параболическая функция отклика оказалась не применима при достижении максимума деформации. Получено аналитическое выражение для функции отклика. Показано, что в качестве функции отклика подходит функция, отображающаяся в виде эллипса. Установлено, что именно эта функция удовлетворительно описывает опытные данные.

Аймуханов А.К., Ибраев Н.Х., Есимбек А.М.
Родамин С бояғышының жұтылу және люминесценттік қасиеттеріне Au нанобөлшектерінің әсері
Au нанобөлшектері этанол спіртінде қаттыденелі екінші гермоникалы LQ 215 лазерімен алтын нысананы абляциялау әдісімен алынды. 30 минут абляциялау кезінде Au нанобөлшектерінің (НБ) концентрациясы алтын нысан массасының өзгеруі бойынша анықталды (абляциялауға дейін және кейін). Жүргізілген зерттеулерде бояғыш ерітіндісіне $C= 5*10^{-6}$ моль/л Au нанобөлшектерін енгізгенде бояғыш ерітіндісінің оптикалық тығыздығының максимумы арттыратының көрсетеді. Флуоресценция қарқындылық максимумы 1.2 есе артты. Жолақтың максимумы және олардың жартылай ендері өзгермейді.

Аймуханов А.К., Ибраев Н.Х., Есимбек А.М.

Влияние наночастиц Au на поглощение и люминесцентные свойства родамина С в этаноле

Наночастицы Au были получены абляцией золотой мишени в этаноле второй гармоникой твердотельного лазера LQ 215. Концентрация наночастиц (НЧ) Au определялась по изменению массы мишени до и после абляции в течение 30 минут аблирования. Проведенные исследования показали, что при добавлении наноцастицы Au C= $5*10^{-6}$ моль/л в раствор красителя величина оптической плотности в максимуме поглощения увеличивается. Интенсивность флуоресценции в максимуме увеличивается в 1.2 раза. При этом положения максимумов полос и их полуширины не меняются.

Көмеков С.Е., Саитова Н.К., Сырғалиев Е.О.

Наноқұрылымды көміртекті объектілердің фотолюминесценция спектрлері

Көміртекті кванттық нүктелер, сутектендірілген көміртегі пленкасы және табиғи биополимер – нативті коллаген сияқты объектілердегі фотолюминесценцияның мүмкін болатын механизмі қарстырылған. Соңғы кезде көміртекті кванттық нүктелерде фотолюминесценцияның қызықты ерекшеліктері бақыланып жүр. Ерекшеліктер, аморфты сутектендірілген көміртегі пленкасы мен табиғи биополимер – нативті коллагендегі фотолюминесценцияны салыстырғанда анықталды. Осы мақалада заманауи өлшеу құралдарын пайдалана отырып, коллагендегі жұту, қоздыру және фотолюминесценция спектрлерін зерттеудің тәжірибелік әдістемесі сипатталаған. Фотолюминесценция қозуы аргонды лазер арқылы жүргізілді.Азотты лазер импульстік қоздыру үшін пайдаланылды. Егер коллаген фотолюминесценциясының табиғатын ескерсек, онда люминесценценттік сәуле шығарудың кейбір қасиеттерін түсіндіруге болады.

Кумеков С.Е., Саитова Н.К., Сыргалиев Е.О.

Спектры фотолюминесценции углеродсодержащих наноструктурированных объектов.

Обсуждается возможный механизм фотолюминесценции таких объектов, как углеродные квантовые точки, слои аморфного гидрогенизированного углерода и природного биополимера – нативного коллагена. В последнее время в некоторых исследованиях наблюдались интересные особенности фотолюминесценции углеродных квантовых точек. Особенности были обнаружены при сравнении фотолюминесценции в слоях аморфного гидрогенизированного углерода и в природном биополимере - нативном коллагене. В данной статье описана методика экспериментального исследования спектров поглощения, возбуждения и фотолюминесценции коллагена с использованием современных устройств измерения. Возбуждение фотолюминесценции проводилось аргоновым лазером. Азотный лазер использовался для импульсного возбуждения. Установлено, что некоторые свойства люминесцентного излучения можно объяснить, учитывая природу фотолюминесценции коллагена.

Сәулебеков А.О., Камбарова Ж.Т.

Зарядталған бөлшектер шоқтарының құрамдасқан энергия талдағышының аппараттық функциясын есептеу.

Жұмыста электрстатикалық айналық өрістерден құрамдасқан энергия талдағышының моделі сандық есептеулер көмегімен зерттелген. Берілген электронды-оптикалық жүйеде зарядталған бөлшектер қозғалысының траекториялық талдауы жүргізілген. Энергия талдағышының шығыс диафрагмалар мен өткізуші терезешелердің өлшемдерін оптимизациялау мақсатында алғаш рет нүктелік көз үшін аспаптың аппараттық функциясы тұрғызылды, бұл өз кезекте аспаптың энергиялық ажыратуын бағалауға мүмкіндік берді. Спектрометр көзден 90^0-қа жақын бұрыштармен шығатын зарядталған бөлшектер шоқтарын 2 % инструменталдық энергиялық ажыратуымен талдауға мүмкіндік береді.

Саулебеков А.О., Камбарова Ж.Т.

Расчет аппаратной функции комбинированного энергоанализатора пучка заряженных частиц.

В работе исследована модель комбинированного энергоанализатора из электростатических зеркальных полей посредством численных расчетов. Проведен траекторный анализ движения заряженных частиц в данной электронно-оптической системе. С целью оптимизации размеров выходных диафрагм и пропускных окон энергоанализатора впервые построена аппаратная функция прибора в случае точечного источника, что позволило оценить энергетическое разрешение прибора. Спектрометр дает возможность анализировать пучки заряженных частиц, выходящих из источника под углами близкими 90^0 с инструментальным энергетическим разрешением 2 %.

Платонова Е.С., Юров В.М., Еремин Е.Н., Бучинкас В., Гученко С.А., Лауринас В.Ч.

Тотығу теориясы мен практикасының кейбір аспектілері және металдық жабындылар мен металдардың термиялық бұзылулары.

Жабынды немесе "ақаулық" метал бетінен тотығу дақтар аумағында логарифмдік тәуелділікті көрсететін, статистикалық тәсіл негізінде тотығу дақтары біліміне коррозиялық дақтар өрнегі алынған. Жабынды және олардың балқу температурасы, металл үстінен тартумен, термодинамикалық модел негізінде тотығу жылдамдығы арасындағы байланыс алынған. Бойлай және кесе-көлденең өлшенген үлгідегі, микроқаттылық эксперименталдық мәндердің негізінде, термосерпімді кернеу жабуды айқындау әдісі ұсынылды. Термодинамикалық моделі негізінде ыстыққа төзімді жабындар арасындағы байланыс пен олардың беттік энергиясы алынған. Термиялық және деформациялық әсерлер кезінде жабындар мен металдың бұзылу жылдамдығын болжау және сапалы талдау үшін жарамды теңдеу алынған.

Платонова Е.С., Юров В.М., Еремин Е.Н., Бучинкас В., Гученко С.А., Лауринас В.Ч.

Некоторые аспекты теории и практики коррозии и термического разрушения металлов и металлических покрытий.

На основе статистического подхода к образованию коррозионного пятна получено выражение, которое показывает логарифмическую зависимость площади коррозионного пятна от «дефектности» поверхности металла или покрытия. На основе термодинамической модели получена связь между скоростью коррозии, поверхностным натяжением металла, покрытия и их температурой плавления. Предложен метод определения термоупругих напряжений в покрытии на основе экспериментальных значений микротвердости, измеренных вдоль и поперек образца. На основе термодинамической модели получена связь между жаростойкостью покрытий и их поверхностной энергией. Получена формула, которая пригодна для качественного анализа и прогнозирования скорости разрушения металла и покрытий при деформационных и термических воздействиях.

Супрун Т.Т. **Тербелмелі цилиндр туындаған өтпелі аймағы бар жылу алмасу.**

Ламинарлы - турбуленттік аусу тәртібі барысында тегіс пластинада қозғалмайтын және тербелмелі цилиндрлірдің ізімен индуцияланған жылу алмасуы заңдылықтары тәжірибе ретінде зерттелінген. Жергілікті жылуалмасу коэффициенттерінің, температурасы және жылдамдық профильдері, олардың ауытқуы және ұзындығы, шекаралық қабаттарының өзге де сипаттамаларынын бөліп талдауы із - көшуін анықтау үшін талданды. Сыртқы ағындағы іздерінің алдын ала көшуінің сипаттамаларын зерттеу негізінде шекаралық қабаттағы жылуалмасу қарқындату себебтері анықталды. Период түрде қайталанған стационарлық емес іздерінің әсерінен аусу аймағы тіркелген тректің жағдайына қарағанда жоғарғы жағына қарай қозғалғаны байқалды.

Супрун Т.Т.

Теплообмен при наличии перехода, индуцированного колеблющимся цилиндром.

Проведены экспериментальные исследования теплообмена плоской пластины при наличии ламинарно-турбулентного перехода, индуцированного следами за неподвижным и колеблющимся цилиндром. Анализ распределений локальных коэффициентов теплоотдачи, профилей температуры и скорости, их флуктуаций и других характеристик пограничных слоев позволяет определить длину и расположение следового перехода.

На основе исследования характеристик следов во внешнем потоке определена причина интенсификации теплообмена в пограничном слое, предшествующем переходу. Под воздействием периодически нестационарных следов область перехода сдвигалась вверх по потоку по сравнению со случаем неподвижного следа.

Ершина А.К., Борибаева М.А., Нурсадыкова Ж.К.

Қазақстан жел электр құрылғыларының талдау.

Мақалада желэнергетикасы жөнінде баяндалады. Бүкіл әлемдегі жел электр қондырғылары көмегімен өндірілетін электр энергиясының қуаты келтірілген. Қазақстан Республикасы жаңарып тұратын энергия көздерін қолдаузаңы және жел электр қондырғылары арқылы энергияны электр энергиясына айналдыру жөнінде жекелей қарастырылып өтіледі. Дарье жел агрегаты туралы нақтырақ сипатталынды. Басқаша айтқанда Бидарье жел турбинасына толық мәлімет келтірілді.

Ершина А.К., Борибаева М.А., Нурсадыкова Ж.К.

Анализ казахстанских ветроэнергетических устройств

Статья посвящена проблемам ветроэнергетики. Показаны данные темпа роста установленной мощности ветроэнергетических установок в мире. Проведен анализ технико-экономических показателей ветроэнергетических систем, разработанных казахстанскими учеными. Описаны технические характеристики ветровых турбин типа Дарье. Показаны преимущества ветротурбины Бидарье.

Шуюшбаева Н.Н., Стоев М., Ахмадиев Б., Алтаева Г.

Влияние импульсных электрических разрядов на микроструктуру электродной системы бура.

Работа посвящена практическием аспектам электрогидравлического бурения скважин. Основой данного метода является уникальное явление – способ прямого преобразования электрической энергии в механическую энергию ударных волн, сопровождающих электрические разряды в условиях ограниченного пространственного объема воды в забое скважины. Мощность озникающих вударных волн позволяет эффективно разрушать не только твердые горные породы, но также влияет на состояние самой бурильной системы. Изучены структура и качество поверхности электродной системы бура, и характер изменений после электрогидроимпульсной обработки. Проведен спектральный анализ микроструктуры расплавленных участков поверхности электродов бура, полученных в результате воздействия подводных искровых разрядов. Экспериментально установлены закономерности процесса эрозийного износа металла электрода от энергетических параметров и количества электрогидравлических импульсов.

Шуюшбаева Н.Н., Стоев М., Ахмадиев Б., Алтаева Г.

Бұрғының электродтық жүйесі микроқұрылымына импульстік электр разрядтарының әсері.

Жұмыс ұңғымаларды электрогидравликалық жолмен бұрғылаудың тәжірибелік аспектілеріне арналған. Берілген әдістің негізі айрықша құбылыс - электр энергиясын соққы толқындарының механикалық энергиясына тура түрлендіру әдісіне негізделген, яғни бұл шектелген кеңістік аймағында ұңғыманың төменгі бөліктеріндегі сұйықта жүретін электр разрядтары әсерінен болатындығын көрсетеді. Соққы толқындары тудыратын қуат тек қана қатты тау жыныстарын ғана емес, сонымен қатар бұрғы жүйесінің өзіне де біршама әсерін тигізеді. Бұрғының электродтық жүйесінің беткі бөлігінің сапасы мен өзгерісі зерттеліп, электрогидравликалық өңдеулерден кейінгі өзгерістері сипатталған. Суасты ұшқын разрядтарының әсерінен алынған нәтижелер бойынша, бұрғы электродтарының бетіндегі балқыған бөліктеріндің микроқұрылымдарына спектрлік талдаулар жасалды. Электрод металының желіну үдерісі заңдылықтарының энергетикалық параметрлер мен электрогидравликалық импульстер санына тәуелділіктері тәжірибе жүзінде келтірілген.

Сақыпова С.Е., Танашева Н.К., Киврин В.И., Құсайынова А.К.

Айналмалы цилиндрлері бар жел турбинасы макетінің аэродинамикалық сипаттамаларын зерттеу.

Мақала баламалы энергия көздерін бір түрі жел энергиясының мәселелеріне арналған. Магнус әсері негізінде жел турбиналары аэродинамикасын эксперименттік зерттеу нәтижелері қарастырылынған. Аэродинамикалық сынау үшін ауыспалы қимасы мен айналмалы цилиндрлері бар үш қалақты жел турбинасының макеті жасалынды. Әр түрлі ауа ағының тәртіптерінде жел турбинасының макетіне аэродинамикалық тестілеу жүргізілді. Ауа ағының әр түрлі жылдамдықтары мен бұрыштар үшін мандайлық кедергі күшінің, тарту күштін және жел дөнгелегінің айналу жылдамдығының тәуілділіктері анықталды. Бұл кедір (өрескел) беті айнымалы қимасы айналмалы цилиндрлер пайдалану Магнус әсерінен, генерацияланатын қосымша қозғаушы күш қолдануды мүмкіндікті беретіні көрсетілген.

Сакипова С.Е., Танашева Н.К., Киврин В.И., Кусаиынова А.К.

Изучение аэродинамических характеристик макета ветротурбины с вращающимися цилиндрами

Статья посвящена проблемам использования альтернативных источников энергии, в частности, энергии ветра. Рассматриваются результаты экспериментального изучения аэродинамики ветротурбины с использованием эффекта Магнуса. Для проведения испытаний изготовлен макет трехлопастной ветротурбины с вращающимися цилиндрами переменного сечения. Проведены аэродинамические испытания данного макета ветротурбины при различных условиях обтекания воздушным потоком. Получены зависимости силы лобового сопротивления, силы тяги и частоты вращения ветроколеса от скорости при разных углах скоса потока. Показано, что применение вращающихся цилиндров переменного сечения с шероховатой поверхностью позволяют использовать дополнительную движущую силу, возникающую за счет эффекта Магнуса.

INFORMATION ABOUT AUTHORS | АВТОРЛАР ТУРАЛЫ МӘЛІМЕТТЕР | СВЕДЕНИЯ ОБ АВТОРАХ

Agelmenev, M.E. – Doctor of chem. sciences, Professor, Head of National Laboratory, S.Amanzholov East Kazakhstan State University, Ust-Kamenogorsk, Kazakhstan

Aimukhanov, A.K. - Candidate of phys.-math. sciences, Docent, Physical-Technical faculty, Karaganda State University named after E.A.Buketov, Karaganda, Kazakhstan

Akhmadiev, B. - Master, Senior lecturer, Physical-Technical Faculty, Karaganda State University named after E.A.Buketov, Karaganda, Kazakhstan

Altayeva, G. - Master, Lecturer, Department of Physics and Mathematics, Kokshetau State University named after Sh. Ualikhanov, Kokshetau, Kazakhstan Master of physics

Bekmyrza, K.Zh. - PhD, Docent, Department of Technical Physics, L.N. Gumilyov Eurasian National University, Astana, Kazakhstan

Borybaeva, M.A. – master student, Kazakh State Women’s Teacher Training University, Almaty, Kazakhstan

Buchinskas, V. – PhD, Vilnyussky Technical University named after Gediminas, Vilnius, Lithuania

Domrachev, A.N. - Doctor of of techn. sciences, professor, Senior Researcher, National Mine Rescue Centre, Novokuznetsk, Kemerovo region, Russia.

Eremin, E.N. - Doctor of techn. sciences, Professor, Head of the Department «Equipment and Technology of Welding Engineering», Omsk State Technical University, Omsk, Russia

Esimbek, A.M. – master student, Physical-Technical faculty, Karaganda State University named after E.A.Buketov, Karaganda, Kazakhstan

Govorukhin, Yu.M. **-** Candidate of techn. sciences, Leading Researcher, National Mine Rescue Centre, Novokuznetsk, Kemerovo region, Russia.

Guchenko, S.A. - Master, Junior Researcher, Karaganda State University named after E.A.Buketov, Karaganda, Kazakhstan

Ibrayev, N.Kh. - Doctor of phys.-math. sciences, Professor, Director of the Molecular Nanophotonics Institute, E.A.Buketov Karaganda State University, Karaganda, Kazakhstan

Ivshchenko, L.I. – Doctor of techn. sciences, Academician of the Ukrainian Academy of tribotechnology, Professor, Department of «Metal-cutting machines and tools», Zaporizhzhya National Technical University, Zaporozhie, Ukraine.

Kambarova, Zh.T. – PhD, Docent, Physical-Technical faculty, Karaganda State University named after E.A.Buketov, Karaganda, Kazakhstan

Kheyfetz, M.L. - Doctor of techn. sciences, Professor, «Center» SSPA, NAS of Belarus, Minsk, Belarus.

Kivrin, V.I. - master student, Physical-Technical Faculty, Karaganda State University named after E.A.Buketov, Karaganda, Kazakhstan

Klimenko, S.A. - Doctor of techn. sciences, Professor**,** V.N. Bakul Institute for Superhard Materials, NAS of Ukraine, Kiev, Ukraine

Kolmakov, A.G. - Doctor of phys.-math. sciences, Professor, A.A. Baykov Institute of Metallurgy and Materials Science, Russian Academy of Sciences, Moscow, Russia

Komochkin, N.S. – Senior Lecturer, Department of «Metal-cutting machines and tools», Zaporizhzhya National Technical University, Zaporozhie, Ukraine.

Krivolapov, V.G. - Candidate of techn. sciences, Leading Researcher, National Mine Rescue Centre, Novokuznetsk, Kemerovo region, Russia.

Kumekov, S. E. - Doctor of phys.-math. sciences, Professor, Director of the Hi-Tech Engineering Institute, Kazakh National Research Technical University named after K.I.Satpaev, Almaty, Kazakhstan

Kussaiynova A.K. - master student, Physical-Technical Faculty, Karaganda State University named after E.A.Buketov, Karaganda, Kazakhstan

Kuterbekov, K.A. - Doctor of phys.-math. sciences, Professor, Department of Nuclear Physics, New Materials and Technologies, L.N. Gumilyov Eurasian National University, Astana, Kazakhstan

Laurynas, V.Ch. - Candidate of phys.- math. sciences, Professor, Physical-Technical Faculty, Karaganda State University named after E.A.Buketov, Karaganda, Kazakhstan

Nursadykova, Zh.K. – master student, Kazakh State Women's Teacher Training University, Almaty, Kazakhstan

Paleev, D.Yu. - Doctor of tech. sciences, Head of Scientific Research dept., National Mine Rescue Centre, Novokuznetsk, Kemerovo region, Russia.

Pavlov, A.M. – Ph.D., Docent, Professor, Department of Physics and Technology, S.Amanzholov East Kazakhstan State University, Ust-Kamenogorsk, Kazakhstan

Pavlov, A.V. – Master, Junior Researcher, S.Amanzholov East Kazakhstan State University, Ust-Kamenogorsk, Kazakhstan

Platonova, E.S. - PhD student, Karaganda StateTechnical University, Karaganda, Kazakhstan

Potapov, A.A. - Doctor of phys.-math. sciences, Professor, Academician, Head of the Chinese-Russian laboratory of informational technologies and signals fractal processing of JNU-IREE RAS, JiNan University (JNU), Guangzhou, China, V.A. Kotelnikov Intstitute of Radio Engineering and Electronics of RAS, Moscow, Russia.

Pribora, T.I. – Senior Lecturer, Department of «Technology of aircraft engines», Zaporizhzhya National Technical University, Zaporozhie, Ukraine.

Saitova, N. K. - PhD student, Department of General and Theoretical Physics, Kazakh National Research Technical University named after K.I.Satpaev, Almaty, Kazakhstan

Sakhnyuk, N.V. – Ph.D., Associate Professor, Department of «Technology of aircraft engines», Zaporizhzhya National Technical University, Zaporozhie, Ukraine.

Sakipova, S.E. - Candidate of phys.-math. sciences, Professor, Physical-Technical Faculty, Karaganda State University named after E.A.Buketov, Karaganda, Kazakhstan

Satbaeva Z.A. - Master, Researcher, S.Amanzholov East Kazakhstan State University, Ust-Kamenogorsk, Kazakhstan

Saulebekov A.O. - Doctor of phys.-math. sciences, Professor, M.V. Lomonosov Moscow State University, Kazakhstan branch, Astana, Kazakhstan

Senyut, V.T. - Candidate of techn. sciences, Leading Researcher, Joint Institute of Mechanical Engineering of NAS of Belarus, Minsk, Belarus.

Serikov, T.M. - PhD, Junior Researcher Electron Microscopy Laboratory, Institute of Molecular Nanophotonics, Karaganda State University named after E.A.Buketov, Karaganda, Kazakhstan

Sharipov M.Z. – Candidate of phys.-math. sciences, Docent, Bukhara Engineering-Technologies Institute, Bukhara, Uzbekistan

Shuyushbayeva, N.N. - PhD, Senior Lecturer, Department of Physics and Mathematics, Kokshetau State University named after Sh. Ualikhanov, Kokshetau, Kazakhstan

Stoev Mitko - Ph.D, Associate Professor, Director of the Solar Energy Center, Head of the Laboratory of Biotechnology, South West University of “Neofit Rilski”, Blagoevgrad, Bulgaria

Suprun, T.T. - Candidate of techn. sciences, Seniour Scientific Researcher, Institute of Engineering Thermophysics National Academy of Sciences of Ukraine, Kiev, Ukraine

Syrgaliyev, E. O. - Candidate of phys.-math. sciences, Professor, Rector of the Almaty University of Energy and Communication, Almaty, Kazakhstan

Tanasheva, N.K. - Ph.D, Physical-Technical Faculty, Karaganda State University named after E.A.Buketov, Karaganda, Kazakhstan

Vityaz, P.A. – Doctor of techn. sciences, Professor, Member of the National Academy of Sciences of Belarus, Presidium of the National Academy of Sciences of Belarus, Minsk, Belarus.

Yershina, A.K. - Doctor of phys.-math. sciences, Professor, Kazakh State Women’s Teacher Training University, Almaty, Kazakhstan

Yurov, V.M. - Candidate of phys.-math. sciences, Docent, Director of Scientifically Research Center «Ion-Plasma Technologies and Modern Instrument-Making», Karaganda State University named after E.A.Buketov, Karaganda, Kazakhstan

Zeinidenov, A.К. **-** PhD, Docent, Department of Radio Physics and Electronics, Karaganda State University named after E.A.Buketov, Karaganda, Kazakhstan

Zhilkashinova, A.M. – Ph.D, Head of Laboratory of Energy Conservation and Alternative Energy National Science Laboratory, S.Amanzholov East Kazakhstan State University, Ust-Kamenogorsk, Kazakhstan

Zhumaev, M.R. – Doctor of phys.-math. sciences, Docent, Bukhara Engineering-Technologies Institute, Bukhara, Uzbekistan

About «Eurasian Physical Technical Journal»

ISSN 1811-1165 Key title: Eurasian physical technical journal (Print)
Abbreviated key title: Eurasian phys. tech. j. (Print)

ISSN 2413-2179 Key title: Eurasian physical technical journal (Online)
Abbreviated key title: Eurasian phys. tech. j. (Online)

"Eurasian Physical Technical Journal" (Eurasian phys. tech. j.) is a peer-reviewed open access international scientific journal publishing original research results on actual problems of Physic, Technology and Engineering.

Since 2004 "Eurasian phys. tech. j." is publishing in English. Periodicity is 2 issues per year.

The E.A. Buketov Karaganda State University is the main organizer and financial sponsor of EAPhTJ. The efforts of the international highly qualified Editorial Board consisting prominent physicists from 12 countries allow provide EAPhTJ international level.

Since 2004 more than 200 scientific papers written by physicists representing 23 countries were published. Among the authors there are full members and corresponding members of National Academies of Sciences of several countries and scientists with high H-index.

Since 2008 EAPhTJ has been included in the list of publications recommended by the Ministry of Science Education and Science of the Republic of Kazakhstan for the publication of the main results of the master's and PhD doctoral dissertations on the physical and mathematical sciences.

Publication Ethics and Malpractice Statement

Submission of an article to the Eurasian phys. tech. j. implies that the paper described has not been published previously, that it is not under consideration for publication elsewhere, that its publication is approved by all authors and tacitly or explicitly by the responsible authorities where the paper was carried out, and that, if accepted, it will not be published elsewhere in the same form, in English or in any other language, including electronically without the written consent of the copyright holder. In particular, translations into English of papers already published in another language are not accepted.

For information on Ethics in publishing and Ethical guidelines for journal publication see http://www.elsevier.com/publishingethics and http://www.elsevier.com/journal-authors/ethics.

The Eurasian phys. tech. j. follows the Code of Conduct of the Committee on Publication Ethics (COPE), and follows the COPE Flowcharts for Resolving Cases of Suspected Misconduct (http://publicationethics.org/files/u2/New_Code.pdf).

To verify originality, your article may be checked by the originality detection service Cross Check http://www.elsevier.com/editors/plagdetect.

Authors are responsible for the content of their publications. No other forms of scientific misconduct are allowed, such as plagiarism, falsification, fraudu-lent data, incorrect interpretation of other works, incorrect citations, etc. Authors are obliged to participate in peer review process and be ready to provide corrections, clarifications, retractions and apologies when needed. All authors of a paper should have significantly contributed to the research.

Reviewers should provide objective judgments and should point out relevant published works which are not yet cited. Reviewed articles should be treated confidentially. The reviewers will be chosen in such a way that there is no conflict of interests with respect to the research, the authors and/or the research funders.

Editors have complete responsibility and authority to reject or accept a paper, and they will only accept a paper when reasonably certain. They will preserve anonymity of reviewers and promote publication of corrections, clarifications, retractions and apologies when needed.

All submitted papers will the sent for reviewing to leading experts in the given area.
The Editorial Board of the Eurasian phys. tech. j. will monitor and safeguard publishing ethics.
The editors reserve the right to accept or reject manuscripts.

GUIDELINES FOR AUTHORS

Research articles, survey papers and short notes are accepted for exclusive publication in the «**Eurasian phys. tech. j.** » in English

The manuscripts and short notes must contain original results of investigation in the following scientific areas of Physics:

Non-linear Physics
Modeling of the nonlinear physical - technical processes
Termophysics, Hydrodynamics, Energetics
Material Sciences
Technology of the creation new material
Ecological Aspects of New Technologies
Engineering
Devices and methods of experiment

All publishing manuscripts and short notes must have been recommended by a member of the editor board or by the organization (University), where the work was performed. The author who submitted an article for publication will be considered as a corresponding author.

The paper, short note or review paper shall include an abstract of the contents, not exceeding 200 words and keywords (no more than 10). The abstract must not coincide with the introduction or conclusive part of the work and must not contain references, abbreviations and other unknown words.

All articles should have list of keywords or terms (3 to 10) for indexing purposes.

The text of a paper must not exceed 8-12 pages including tables, figures (no more than 6) and references. A short note must not exceed 4-5 pages including no more than 2 figures. A review paper must not be more than 20 pages (including no more than 10 figures).

The text should be divided on structural parts: **Introduction, Theoretical part, Experimental technique, Results and Discussion, Conclusion,** etc.

Printed copies shall be on good quality paper of International size A4. All texts must be printed in Microsoft Word. It is preferable to use the Times fonts. The text must be printed in 12 point letters, 1.5 intervals. There shall be a margin of 30 mm at the left-hand edge, of 15 mm at the fore edge, of 30 mm at the head of the page and of 30 mm at the tail. All pages must be numbered.

Acknowledgments may be shown at the end of the article text, before **REFERENCES**.

All references must be numbered in the text (for example, [1], [2-4]) and listed in numerical order.

Equations in your paper have to be written using the Microsoft Equation Editor or the MathType (http://www.mathtype.com) for (Insert | Object | Create New | Microsoft Equation or MathType Equation).

Tables must be inserted into the text.

Figures should be prepared in a digital form suitable for direct reproduction. Figures shall be submitted on the separate sheets and not included into the text.

The following files must be submitted via e-mail:

- Article text (*.doc);
- Figures (fig1.jpg, fig2.pcx);
- Figure captions (*.txt, *.doc).

The text file containing all Authors’ names, organizations, postal code, postal address, telephone, fax, E-mail, scientific topic of the paper.

It is possible to use **rar** or **zip** compressors and to transmit the files as an attachment.

Title page (specimen)

UDC

TITLE

Smith J.H., Cooper H.J.

Karaganda State University , Universitetskaya Str. 28, Karaganda, 100028, Kazakhstan, email@for_correspondence.kz

Abstract

Keywords:

Introduction

Article text. Article text. Article text. Article text. Article text. Article text. Article text. Article text. Article text. Article text Article text. Article text. Article text. Article text. Article text Article text. Article text. Article text. Article text. Article text Article text. Article text. Article text. Article text. Article text Article text. Article text. Article text. Article text. Article text…

Reference Format (specimen)

1. Nahar J., Wahedra M. Elastic scattering of positrons and electrons by argon. *Physical Rewiew A*, 1987, Vol. 35, No. 5, pp. 2051 – 2064.
2. Rivoalen H. Electrotubular heat exchanger in chemical industry. *Proc. 12th International Congress on Electricity Applications*. Birmingham, 1996, pp. 29 – 39.
3. Conrad H., Muhlbauer A., Thomas R. *Elektrothermische Verfahrenstechnik*. Vulkan-Verlag, Essen Publ., 1993, 240 p.

The authors should represent References according to the requirements of international journals on physics, but should to consult preliminarily for standard abbrevi-ations of journal's names.

For more information on references guidelines for journal publication you see Harvard reference system: http://www.emeraldgrouppublishing.com/authors/guides/write/harvard.htm?part=2